ABSTRACT

The Springshed and Potential Recharge Areas for the Downtown Salado Spring Complex, Salado, Texas

Clara P. Smith-Salgado, M.S.

Mentor: Joe C. Yelderman, Jr., Ph.D.

The Northern Segment of the Edwards (BFZ) Aquifer is a complex, karst system experiencing increases in groundwater demand and environmental stresses in response to a growing population. This study delineated the Salado Springshed under baseflow conditions and identified significant recharge zones by analyzing synoptic water-level maps under different aquifer conditions, collecting groundwater samples for ionic chemistry and isotopic composition analyses, and statistically correlating precipitation to changes in baseflow at Salado Springs. The geochemical samples and statistical correlations generally confirm the springshed interpretation. Apparent groundwater ages indicate the youngest groundwater occurs below the Edwards outcrop and the oldest groundwater in the deeper confined portion of the aquifer. The geochemical signature of the groundwater supports the interpretation that the deeper flow system does not flow to Salado Springs under natural flow conditions. The statistical analyses support recharge in the delineated springshed, but also possibly in an upgradient losing stream segment.

The Springshed and Potential Recharge Areas for the Downtown Salado Spring Complex, Salado, Texas

by

Clara P. Smith-Salgado, B.S.

A Thesis

Approved by the Department of Geosciences

_____

Joe C. Yelderman Jr., Ph.D., Chairperson

Submitted to the Graduate Faculty of
Baylor University in Partial Fulfillment of the
Requirements for the Degree
of

Master of Science

Approved by the Thesis Committee

_____

Joe C. Yelderman Jr., Ph.D., Chairperson

_____

Steve Dworkin, Ph.D.

_____

Jane L. Harvill, Ph.D.

Accepted by the Graduate School

August 2021

_____

J. Larry Lyon, Ph.D., Dean

Page bearing signatures is kept on file in the Graduate School.

TABLE OF CONTENTS

LIST OF FIGURES

LIST OF TABLES

LIST OF ABBREVIATIONS

BFZ –	Balcones Fault Zone
CoCoRaHS –	Community Collaborative Rain, Hail, and Snow Network
CUWCD –	Clearwater Underground Water Conservation District
DOR –	Drought of Record
DSSC –	Downtown Salado Spring Complex
GIS –	Geographical Information System
LCRA –	Lower Colorado River Authority
LiDAR –	Light Detection and Ranging
LMWL –	Local Meteoric Water Line
NEXRAD –	Next Generation Weather Radar
NWS –	National Weather Service
PPS –	Precipitation Processing System
TWDB –	Texas Water Development Board
USGS –	United States Geological Survey
WHAT –	Web based Hydrograph Analysis Tool
WSR-88D –	Weather Surveillance Radar-1988 Doppler

ACKNOWLEDGMENTS

I would like to acknowledge many individuals and organizations who gave their support throughout the writing of this thesis. To Dr. Joe C. Yelderman Jr., my mentor and thesis advisor, I am sincerely grateful for your constant guidance, encouragement, and for continuing to inspire my growth within the field of hydrogeology. Thank you to my committee, Dr. Dworkin and Dr. Harvill, for being a part of this process.

I would like to thank the Clearwater Underground Water Conservation District, Baylor University, and the Texas Water Development Board for supplying the generous funding needed to conduct this project. And thank you to all the landowners who allowed me to access their property to sample their wells.

Special thank you to Dr. Jane L. Harvill and Jerry Ma of the Statistics Department at Baylor University for your collaboration and for creating the statistical model to analyze our hydrologic data. I greatly appreciated your efforts and insights.

To my colleagues in the hydrogeology team, thank you for your moral support and for field assistance. Special thank you to Stephanie Wong for your constant help and collaboration, and for providing data from your previous work within the Northern Segment.

Last but not least, thank you to my loving parents, Brian and Sandra, for your constant support and encouragement, and for showing me the values of education. None of this would have been possible without you.

CHAPTER ONE

Introduction

Background

The Edwards Balcones Fault Zone (BFZ) Aquifer in central Texas is a karstic aquifer that parallels and lies within the Balcones Fault Zone. The aquifer is characterized by water yielding units of carbonate rocks and sandstones and extends an area of about 4,350 square miles (Schwartz and Zhang, 2003). Much of the groundwater pumped from the Edwards is used for public water supplies and for irrigation in central Texas. The Edwards (BFZ) Aquifer is a heterogenous and anisotropic aquifer, which contributes to a wide variation on orders of magnitude in transmissivity, storativity and permeability. This study focuses on the Northern Segment of the Edwards (BFZ) Aquifer, which serves as a groundwater resource for municipalities such as Georgetown, Pflugerville, Round Rock, and Salado. Research for this study was conducted at the Salado Springs complex in downtown Salado and within the Salado Creek basin located in Bell County. The Edwards (BFZ) Aquifer is the source of the Salado Springs complex and serves as the main water supply for the Village of Salado. Rapid population growth and development taking place in the region highlight the importance for proper groundwater management to avoid the heavy exploitation of the Edwards (BFZ) Aquifer. In addition to the dependance on groundwater from the Northern Segment, the Salado Spring complex provides habitat to the Salado Salamander (*Eurycea chisholmensis*). Federally listed as “threatened”, these

salamanders are important to the Northern Segment of the Edwards (BFZ) Aquifer because they may serve as indicator species for changes in aquifer conditions.

Historically, Salado Springs served as a concentration area for Paleo-Indian culture when the Tawakoni Indians recognized the attraction of large herds to the bountiful groundwater resource. In 1732, the Spaniard Bustillo y Ceballos stopped in this area on his journey west and named the town *Salado* for the "salty" taste of the water at Sulphur Springs, which is located east-northeast of Salado (Brune, 1981). Later in 1851, the area was settled by Archibald Willingham who built a well-known stage stand known today as Stage Coach Inn. From 1851 to 1868, the Salado Creek and Springs' power were utilized for flour, grist, saw, cotton-gin, and wool-carding mills, which demonstrated the dependable spring discharge as baseflow (Brune, 1981). Today, Salado has become a local landmark for tourist attractions with antique and art stores, cafes, and a swimming hole. The spring-fed creek is an iconic feature that is important to tourism and to communities and rural residents within the Salado Creek basin who depend on the Northern Segment of the Edwards (BFZ) Aquifer as a source of water supply.

The recent population growth and urban development along the Interstate Highway 35 (I-35) corridor will continue to stress the aquifer supply as demand increases. The population in the counties along this corridor is projected to increase from 11.3 million to 17 million between 2010 and 2040, an increase of more than 50 percent (I-35 CAC, 2011). More specifically, Bell County has experienced a population increase from 310,000 to 363,000 between 2010 and 2019, about a 17 percent increase (United States Census Bureau, 2021). Total pumping from the Northern Segment of the Edwards (BFZ) Aquifer from 1980 to 2015 has increased from about 16,000 acre-feet per year to about 50,000 acre-

feet per year. Municipal and domestic use are the dominant sources of groundwater pumping, with irrigation, mining, and manufacturing pumpage accounting for 10 percent (Jones, 2020).

The Edwards (BFZ) Aquifer is one of nine major aquifers in Texas. This karst aquifer spans an outcrop area of 1,566 square miles through Central Texas and is composed of three hydrogeological segments shown in Figure 1: The Northern Segment, the Barton Springs Segment, and the San Antonio Segment (Jones, 2020). The state of Texas manages groundwater through Groundwater Conservation Districts (GCD) or Underground Water Conservation Districts (UWCD) created under Texas Constitution, Article III, Section 52 or Article XVI, Section 59. Districts' roles are to protect, enhance, and regulate the production of groundwater resources under their jurisdiction (TWDB, 2021). The northernmost portion of the Northern Segment of the Edwards (BFZ) Aquifer is the focus of this study and lies within the Clearwater Underground Water Conservation District (CUWCD) jurisdiction and encompasses all territory located within Bell County, Texas (Figure 2).

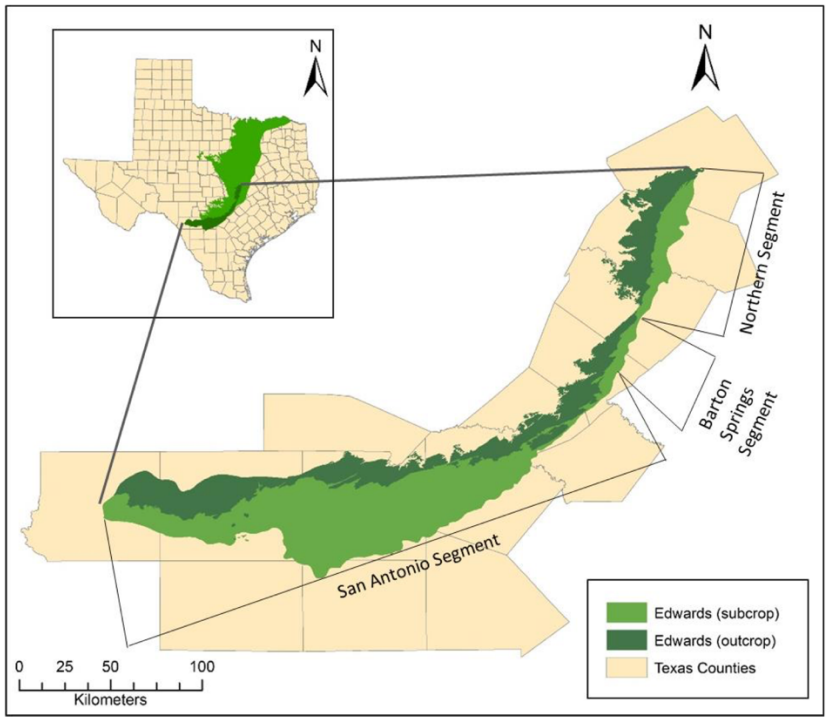

Figure 1. Location of the Edwards (BFZ) Aquifer and the three hydrogeological segments (Map from Eckhoff, 2016).

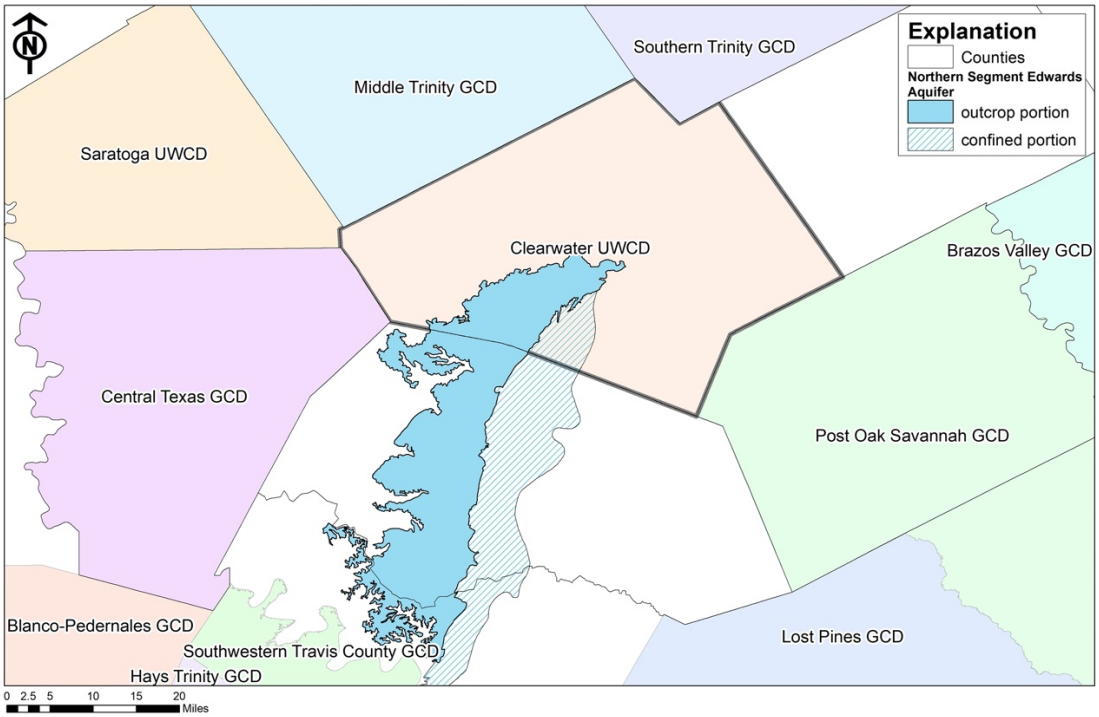

Figure 2. Map of Clearwater Underground Water Conservation District and surrounding groundwater conservation districts.

Purpose and Objectives

A majority of the communities and rural residents within the Salado Creek basin depend on groundwater from the Northern Segment of the Edwards (BFZ) Aquifer for municipal use, manufacturing, mining, and rural domestic use. An improved understanding of the dynamics of the aquifer is important for supporting groundwater management and further protecting the aquifer and the federally listed threatened Salado Salamander. The continual population growth within the study area will correspondingly increase groundwater demand and environmental stresses on the aquifer, leading to concerns on the quantity and quality of the groundwater resource. This research aims to provide assistance in groundwater management by delineating the Salado Springshed and identifying significant recharge zones to determine areas that require high concern and protection through the following objectives:

Objective 1: Develop potentiometric maps to visualize how different aquifer conditions could affect a springshed boundary. A hypothesized springshed boundary will serve as a guide into key areas of study and to better understand groundwater flow dynamics and recharge.

Objective 2: Spatially and statistically correlate precipitation data in the basin to spring-flow response to evaluate potential contributing recharge areas. Using gridded precipitation data serves as a tool to spatially characterize recharge locations in the karstic Edwards (BFZ) Aquifer.

Objective 3: Assess flow paths throughout the basin geochemically using the ionic chemistry and isotopic composition of the groundwater under different aquifer conditions.

Sampling water wells and springs throughout the study area would act as a natural tracer method.

Location

The Northern Segment of the Edwards (BFZ) Aquifer is located in central Texas and runs along Interstate 35 underlying Bell, Williamson, and northern Travis counties. The subject of this study is the Downtown Salado Springs Complex (DSSC) and its contributing zone located within the Northern Segment of the Edwards (BFZ) Aquifer in southern Bell County (Figure 3). To analyze both the groundwater divides and surface-water divides, the study area includes the Salado Creek basin, the formations comprising the Edwards (BFZ) Aquifer, and their surrounding areas (Figure 3). The upper 1/3 of the basin largely serves as an area of recharge, while the lower portion of the basin (2/3) is an area of discharge into the creek with more than 20 springs present (Dahl, 1990). The DSSC is located at the center of downtown Salado, Texas and provides annual baseflow to Salado Creek. Eight different springs identified in previous studies (Figure 4) make up the DSSC and serve as an important management parameter for CUWCD.

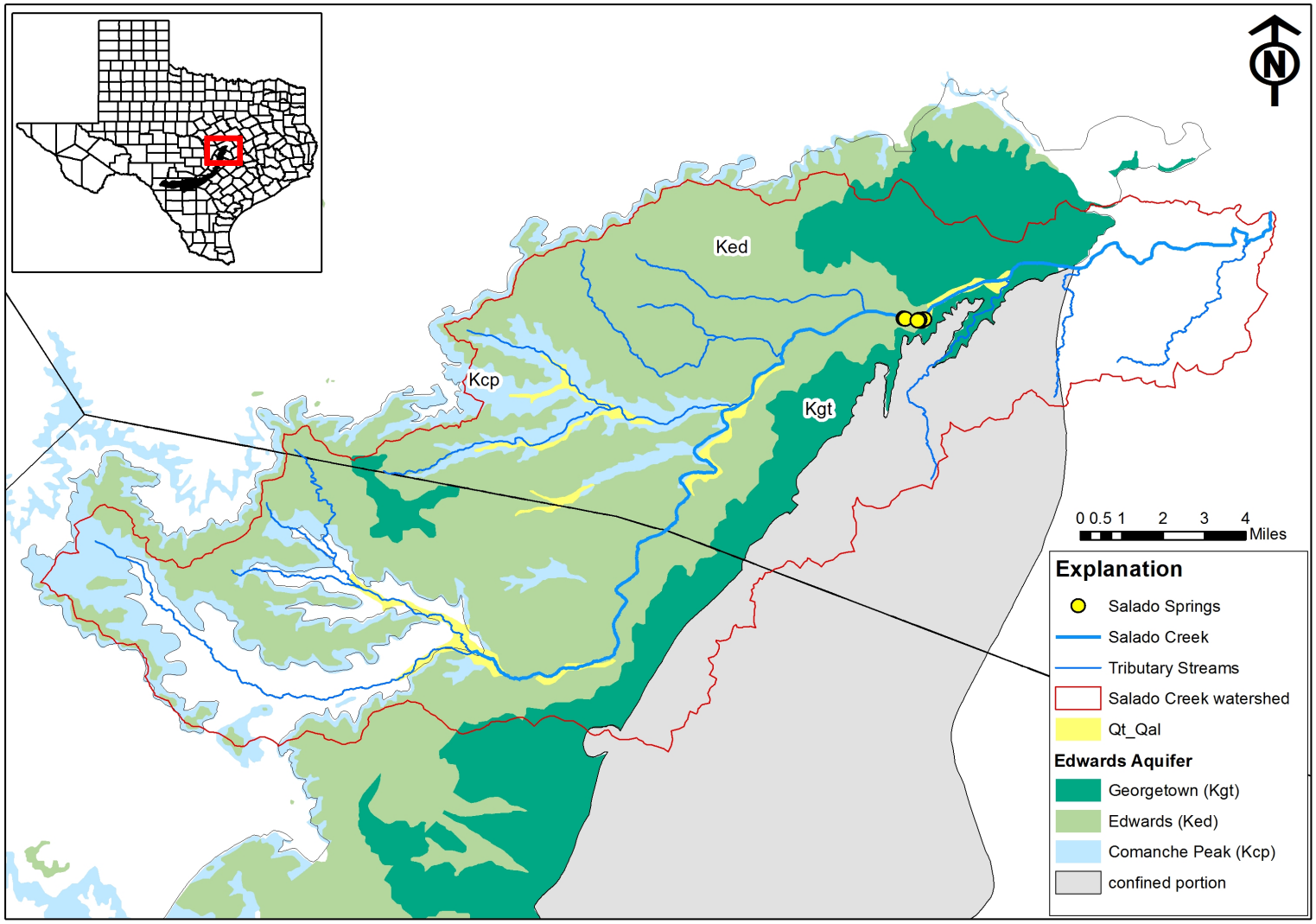

Figure 3. Location of the Salado Creek Watershed within the Northern Segment of the Edwards (BFZ) Aquifer in Central Texas.

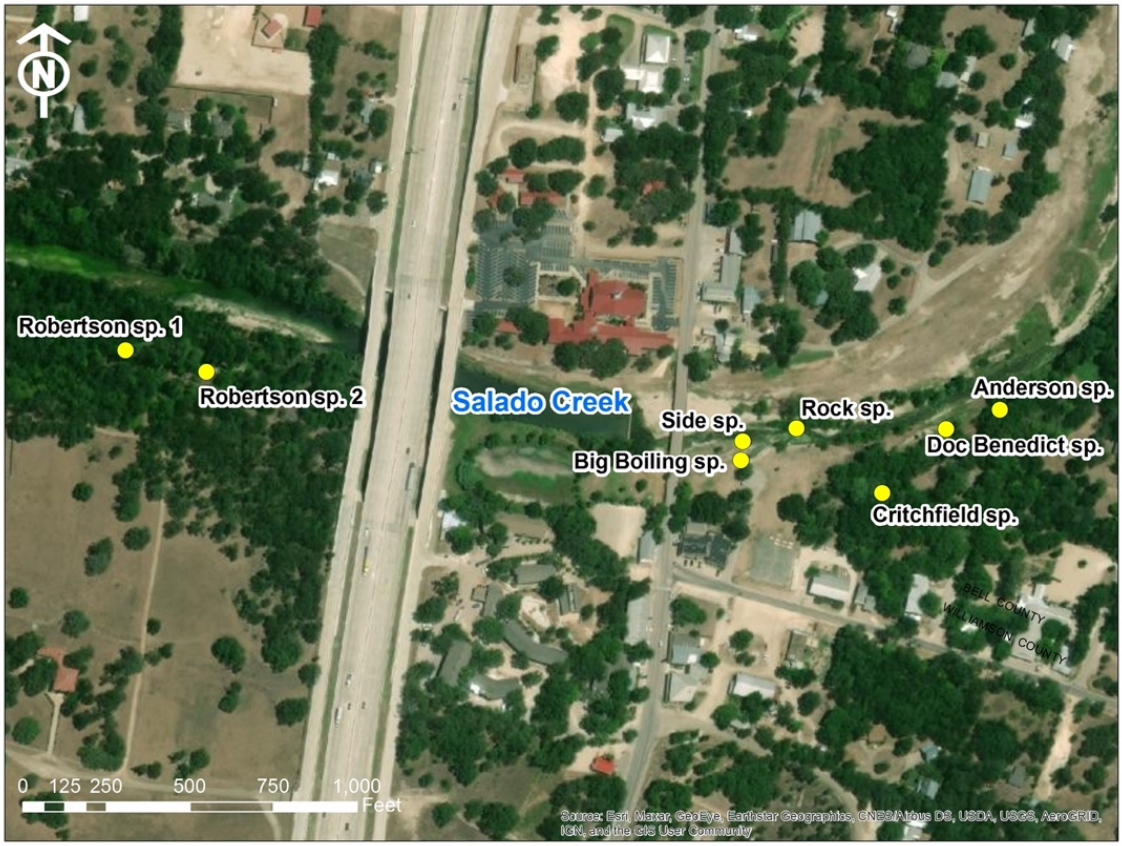

Figure 4. Map of the Downtown Salado Spring Complex and the location of the eight identified springs within the complex.

Previous Works

Early characterizations of the Northern Segment of the Edwards (BFZ) Aquifer were conducted by Tucker (1962) and Rose (1972), among others. The authors of these studies largely described the lithology and identified major and minor faults in the northern segment. Hydrogeologic studies on springs, stream discharge and wells are discussed in Brune (1981), Baker and others (1986), and Senger and others (1990). Lastly, guidebooks such as Woodruff and others (1985) and Yelderman and others (1987) summarize various components of the hydrogeology and geomorphology of the northern segment discussing topics such as transmissivity, pump tests, and water supply.

Dahl (1990) studied the porosity and permeability of the Northern Segment of the Edwards (BFZ) Aquifer and identified specific fault locations that provide significant recharge to the aquifer. Additionally, a water budget of the aquifer within the Salado Creek basin indicated that direct infiltration of precipitation in the basin contributes greater volumes of water to the aquifer than storm runoff (Dahl, 1990).

A sediment transport tracer test was conducted in 1995 and 1996 by Mahler and others (1998) to analyze the connection between Big Boiling Spring at the DSSC and a cave approximately 0.14 miles southwest of the spring. This study used Lanthanide-Labeled Clay, a particle tracer with extremely low detection limits and quick and automated sample analyses (Mahler and others, 1998). The sediment was injected into the cave under normal and low-flow conditions (Mahler and others, 1998). Results showed that under normal flow conditions, the particle tracer was detected at the springs. Under low-flow conditions, the particle tracer was not detected at the springs indicating that the sediment will settle out or go into storage during low-flow.

Jones (2003) developed a conceptual groundwater flow model of the Northern Segment of the Edwards (BFZ) Aquifer using steady-state and transient conditions for the period 1980-2000. As a follow up to earlier research, Jones (2020) developed an updated conceptual model with an extended calibration period of 1980-2015 and included the interaction with the underlying Trinity Aquifer. The purpose of these calibrated models is to predict future water-level changes that can result from changes in pumping rates and climate conditions.

Yelderman (2013) summarized current understandings of the karst hydrogeology in the Northern Segment of the Edwards (BFZ) Aquifer, discussed aquifer parameters

obtained from pumping tests conducted on four wells in Bell County in August 2012, and identified recharge features that require further investigations. This study also produced a preliminary springshed boundary based on water-level data from July 2010 (Yelderman, 2013).

Wong and Yelderman (2015, 2016, 2017) reported on various studies run by Baylor University for the Bell County Adaptive Management Coalition for the purpose of biological research on the Salado Salamander and geo-hydrologic research to better understand the structure and function of the aquifer. These studies were focused on the DSSC and Salado Creek basin and highlighted on synoptic water-level measurements, dye-trace tests, water quality and quantity, natural radon as an indicator of groundwater-surface water interaction, rainfall patterns and recharge response, and the use of LiDAR data to detect recharge features. The dye trace test confirmed the connection identified by Mahler and others (1998) between the nearby cave and Big Boiling Spring, but Wong and Yelderman (2015, 2016, 2017) also identified a connection between the cave and other springs that make up the DSSC. Overall, findings from Wong and Yelderman (2015, 2016, 2017) have accommodated growth and development in Salado, while simultaneously protecting the karst system.

A methodology for evaluating approaching drought conditions based on various hydrogeologic parameters such as creek flow, water levels, and precipitation, was determined by Keester and Konetchy (2017). This study used a multilinear analysis to develop a Salado Creek discharge model as a tool for predicting low flow during evolving climate conditions (Keester and Konetchy, 2017).

Along with these previous studies, this thesis research will enhance the understanding on the hydrogeology of the Salado Springshed and build upon previous precipitation, spring flow, and geochemical datasets for future research. Although various studies have been conducted over the years for the Northern Segment of the Edwards (BFZ) Aquifer, the ionic chemistry and isotopic composition of the groundwater have not yet been examined and the effects of precipitation on springflow have not yet been statistically analyzed for the Salado Springshed. These investigations will further refine the Salado Springshed boundary and define areas of varying concern for management purposes.

Springshed

A springshed is an area where all groundwater will flow to a spring discharge point. This is analogous to that of a watershed where all the precipitation and runoff in a certain area will collect and drain to a common outlet. Springsheds can include the aquifer recharge area or areas beyond the outcrop. It is possible for a springshed boundary to change over time as flow paths adapt to different aquifer conditions or to appear different based on the precision of the water-level data sets used. In general, it is important to protect and manage these springshed areas because the actions taken at the surface may eventually affect the quality and quantity of water flowing at the springs.

Previous studies have been conducted to delineate springsheds for aquifers using various methods. Budge (2008) conducted a spatial cross-correlation analysis using Next Generation Weather Radar (NEXRAD) rainfall data by correlating springflow to rainfall to estimate the springshed of Jacob's Well, a karst spring sourced from the Middle Trinity Aquifer in Wimberley, Texas, and Barton Springs, sourced from the Barton Springs Segment of the Edwards Aquifer in Austin, Texas. Gary and others (2019) used various

water-budget calculations for Jacob's Well and confirmed a similar springshed estimate as Budge (2008). In the karst lands of Southeastern Minnesota, Alexander and others (2008) applied detailed structural mapping of the aquifers to define the size and geometry of springsheds. Previous studies in this area have used dye-trace tests to delineate springsheds, but due to the time and expense of tracer testing, Alexander and others (2008) used well driller's records and gamma logs to enhance findings from previous dye-trace studies. Lastly, similar delineation methods have been applied to a lacustrine groundwater setting in northeastern Germany (Meinikmann and others, 2013). Meinikmann and others (2013) calculated groundwater recharge to the subsurface catchment (springshed) feeding a lake to quantify lacustrine groundwater discharge to understand nutrient budgets of a lake. This thesis study focuses on various methods using potentiometric data, hydrographs, and chemical and isotopic studies to further refine the springshed boundary of the DSSC.

CHAPTER TWO

Aquifer Setting

Geologic Setting

The surface geology in the study area consists of Cretaceous bedrock to Quaternary alluvium present along stream channels within the Salado Creek basin (Figure 3). Cretaceous rocks in the area formed largely as deposits on the shallow seafloor marked by major transgression events of the present-day Gulf of Mexico (Young and others, 1977). The Pre-Cretaceous units beneath the younger deposits dip between 10 to 70 degrees to the east and the Cretaceous units lie unconformably across them. The Cretaceous units in the study area dip toward the southeast with a slope of 10 to 300 feet per mile (Brune and Duffin, 1983; Duffin and Musick, 1991). The Edwards (BFZ) Aquifer lies along the normally-faulted Balcones Fault Zone (Brune and Duffin, 1983). This fault system cuts through Cretaceous-age rocks and extends from Waco to San Antonio positioned approximately parallel to Interstate Highway 35 (Figure 5). Faulting and fracturing associated with the Balcones Fault Zone strongly affect groundwater flow paths and hydraulic properties of the Edwards (BFZ) Aquifer. The faults and fractures provide natural pathways for groundwater to flow and aid in forming caves and sinkholes within the region as a result of carbonate dissolution, karstification.

The Northern Segment of the Edwards (BFZ) Aquifer is a confined and unconfined, karst aquifer comprising the Comanche Peak, Edwards, and Georgetown formations, in

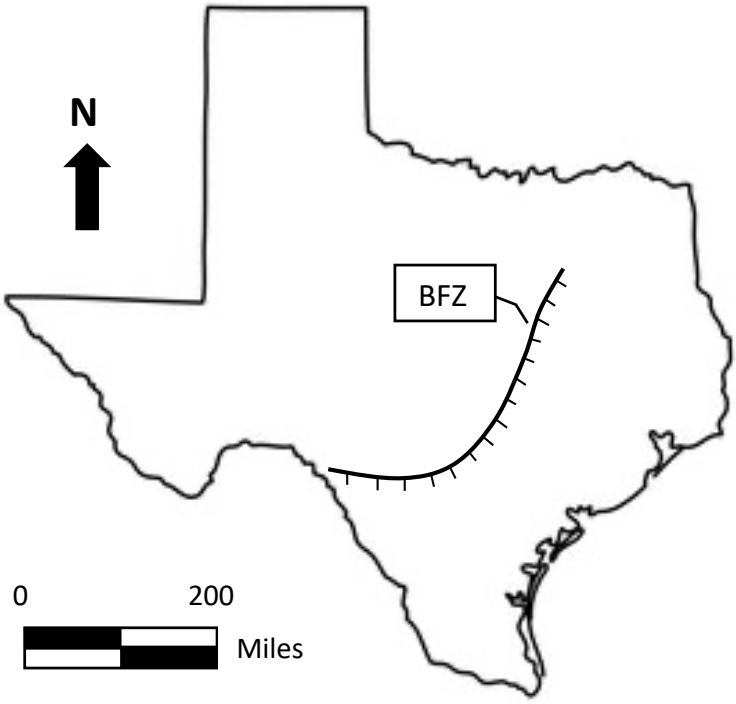

Figure 5. Map showing the Balcones Fault Zone location through central Texas.

ascending stratigraphic order. The aquifer is confined below and above by the clay-rich Walnut and Del Rio formations, respectively. The unconfined portion of the aquifer consists of outcropping Comanche Peak Limestone, Edwards Limestone, and Georgetown formations. Brune and Duffin (1983) describe the confined portion as the down-dip section of the aquifer where the hydraulically conductive Edwards Limestone and associated limestones are overlain by the confining Del Rio Clay (Figure 3). These Cretaceous-age formations include parts of the Fredericksburg and Washita Groups (Jones, 2003). The Fredericksburg Group is made up of the Walnut Formation, Comanche Peak Limestone, and the Edwards Limestone; the Washita Group is partially made up of the Georgetown Formation and Del Rio Clay (Figure 6).

System	Series	Group	Stratigraphic Unit	Hydrologic Unit	Approximate Maximum Thickness (feet)
Cretaceous	Comanche	Washita	Buda Limestone		50
			Del Rio Clay	Upper Confining Unit	65
			Georgetown Formation	Edwards (Balcones Fault Zone) Aquifer	98
		Fredericksburg	Edwards Limestone		196
			Comanche Peak Limestone		50
			Walnut Formation	Lower Confining Unit	165

Figure 6. Stratigraphic column for the Northern Segment of the Edwards (BFZ) Aquifer and the overlying and underlying formations (modified from Jones, 2019).

The Walnut Formation serves as the lower confining unit to Northern Segment of the Edwards (BFZ) Aquifer and yields little to no water (Duffin and Musick, 1991). This confining unit is described as a fine-grained limestone, marl formation with low permeability. More specifically, the Walnut Formation grades upward from a soft, fossiliferous marl, to a hard, nodular fossiliferous limestone, then to a soft fossiliferous marl in its uppermost member which is in contact with the Edwards (BFZ) Aquifer (Dahl, 1990). The Walnut has an estimated maximum thickness of 165 feet (Jones, 2019).

The Del Rio Clay is the upper confining unit to the Edwards (BFZ) Aquifer. It is of a calcareous, fossiliferous clay and does not yield water in the study area (Brune and Duffin, 1983). The Del Rio Clay has a maximum thickness of approximately 65 feet (Jones, 2019).

The Comanche Peak Limestone is a marly, fine-grained limestone unit that contains nodules and fossils. This unit is hydrologically connected with the Edwards Limestone directly above due to its moderate permeability[1] and existing fractures throughout. The Comanche Peak is present in the subsurface of the study area at a maximum thickness of about 50 feet but thins out to the south and is not present south of the Colorado River (Brune and Duffin, 1983).

Next, the Edwards Limestone is highly fractured and permeable and is visible in outcrops throughout the study area. This formation is described as a brittle, thick bedded to massive limestone and dolomite, with small beds of shale, clay, and siliceous limestone. Beds of chert are also present in the unit. The Edwards limestone has experienced significant gypsum dissolution, which has resulted in solution-collapse features that now serve as major water-bearing zones in the Edwards (BFZ) Aquifer (Brune and Duffin, 1983). The limestone formation has a maximum thickness of approximately 196 feet in the study area and begins to thin north of the study area (Jones, 2019).

Lastly, the Georgetown Formation, a nodular limestone interbedded with layers of marl, is the upper unit of the Edwards (BFZ) Aquifer and is hydrologically connected with the Edwards Limestone. It is fossiliferous and contains fewer and smaller solution features than the Edwards Limestone (Brune and Duffin, 1983). Maximum thickness of the formation in the study area is about 98 feet (Jones, 2019).

[1] Permeability and hydraulic conductivity are used interchangeably for this thesis.

Hydrogeologic Setting

The Edwards (BFZ) Aquifer is a karstic aquifer within the Balcones Fault Zone consisting of highly faulted and fractured carbonate rocks from the Cretaceous period (Brune and Duffin, 1983). Karst terrains form from the dissolution of soluble rock such as limestone and dolomite from meteoric water. This dissolution process allows for the formation of conduits along faults and fractures that easily transmit groundwater. Karstic aquifers are defined by the presence of springs, caves, and/or sinkholes. The Edwards (BFZ) Aquifer is characterized by water yielding units of carbonate rocks and sandstones and the Northern Segment extends an area of approximately 1,000 square miles (Schwartz and Zhang, 2003; Slade, 1985).

In the Northern Segment, the hydraulic gradient is generally towards the east-southeast, which is largely guided by the topography, but deflects northward toward Salado Springs along the Balcones Fault Zone in Bell County (Brune and Duffin, 1983; Dahl, 1990). Dahl (1990) reported that the average groundwater velocity in the outcrop portion is 0.94 feet per day and 9.06 feet per day towards the DSSC. The aquifer is classified as anisotropic due to preferential flow paths that follow the northeast-southwest positioned fractures associated with the Balcones Fault Zone (Jones, 2020). The aquifer and surrounding geologic units have an average slope of approximately 58 to 74 feet per mile to the east and groundwater flow is additionally facilitated by downdip faulting (Figure 7). Aquifer thickness ranges from 98 to 295 feet, with some sections being less than 98 feet thick as a result of stream erosion over the outcrop portion (Jones, 2019). Within the study area, regional groundwater flows towards the lowest head in the aquifer outcrop and to the

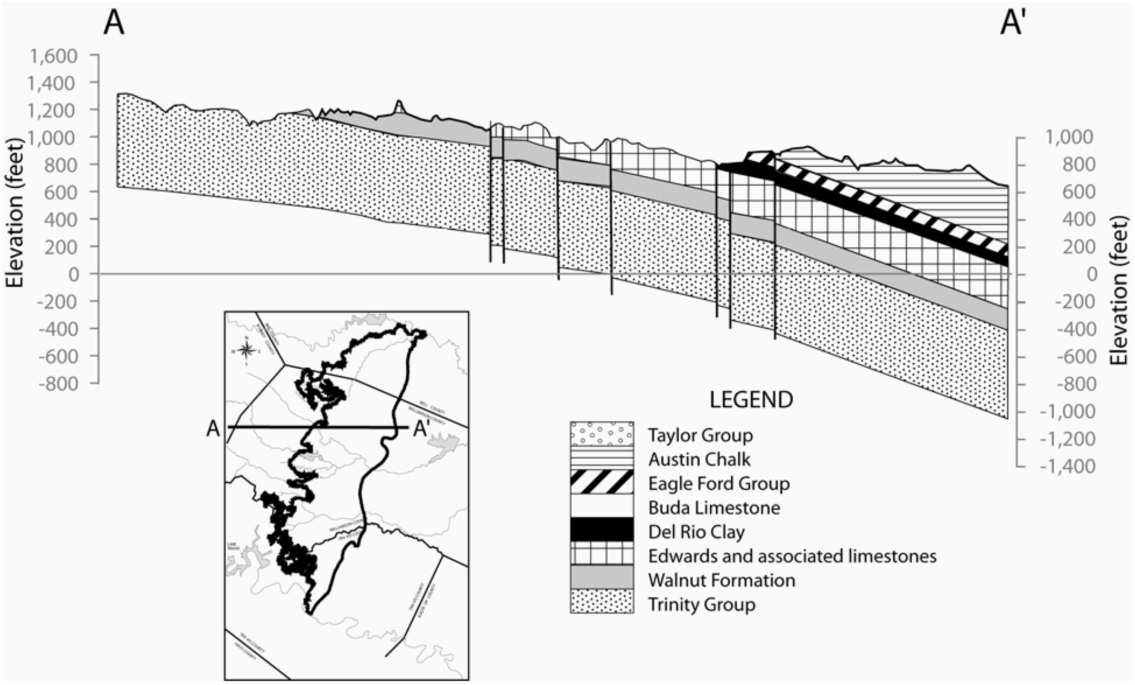

Figure 7. Cross section of the Northern Segment of the Edwards (BFZ) Aquifer (Jones, 2003).

main discharge point at the DSSC. The DSSC was created through the intrenchment process by Salado Creek into the Edwards (BFZ) Aquifer that locally intersected Balcones faults and caused the exposure of the springs at the surface (Dahl, 1990).

The climate in the study area is described as subtropical and sub-humid to semi-arid (Jones, 2020). Average annual temperature is 68 °F in central Texas. Summers are hot with mean maximum temperatures being 95 °F, and winters are typically mild with a mean minimum temperature of 41 °F. Precipitation records created by the U.S. National Weather Service from 1900 through 1976, indicate an average annual precipitation amount of 33.5 inches (Brune and Duffin, 1983). Peak rains typically occur in May and September each year and minimum rains occur in July and August. Additionally, the dominant moisture source for this region is the Gulf of Mexico, amplified by winter precipitation brought in

by storms from the west (Stamm and others, 2014). Recharge to the Northern Segment of the Edwards (BFZ) Aquifer is mainly sourced from precipitation as direct infiltration on the aquifer outcrop and runoff that infiltrates through losing stream sections within the creek basins (Yelderman, 2013). The limestone dissolution process characteristic of karst terrains allows for the formation of conduits along faults and fractures that easily transmit groundwater and facilitate recharge. A water budget analysis conducted for the Salado Creek basin by Dahl (1990) determined that of the total precipitation recharge, 90% is sourced from direct infiltration and 10% from losing streams. Previous studies indicate that recharge to the aquifer is estimated to be about 15–20% of annual precipitation (Dahl, 1990; Jones, 2003). The infiltrating water tends to settle within the Georgetown Formation due to the presence of interbedded layers of marl with low permeability that causes lateral flow to small seeps and springs. The remainder of the water will more rapidly recharge through the Edwards and Comanche Peak limestone outcrops, the more permeable units of the aquifer. Because the Georgetown Formation is a less permeable unit, surface water sourced from the Salado Creek tributaries will flow until the streams merge with the Edwards Formation allowing for direct percolation through the karstic limestone (Dahl, 1990).

The Northern Segment of the Edwards (BFZ) Aquifer is a highly variable fractured carbonate aquifer. The dominant limestone lithology contributes to the matrix porosity, but the largest contributor to groundwater flow comes from the resulting faults and fracture porosity continuously enhanced by dissolution (Abbot, 1975; Kreitler and others, 1987). To describe groundwater flow through an aquifer, hydraulic properties such as porosity, hydraulic conductivity, transmissivity and specific capacity are measured and calculated.

The ranges of each hydraulic property determined from previous studies on the northern segment are described below and listed in Table 1. Porosity is defined as the volume of void space in a volume of rock and it is expressed as a percentage. Within the Edwards Aquifer, the more significant porosity is secondary porosity, void space that has developed as a result of dissolution or fractures after a rock is formed (Yelderman, 2013). Fractures and karst features within the northern segment account for 1% – 3% of the outcrop area and generally lie near faults (Hovorka and others, 1998). Dahl (1990) measured fracture porosity from aquifer outcrops that represented all aquifer formations in the study area based on the methods described in Kovacs (1983). This method multiplied the width of a fracture by the representative length to get the area of a fracture and then divided the total area of the fractures by the total area of exposure (Kovacs, 1983). Measurements were taken near faults and away from faults, which resulted in greater porosity near faults than at further distances from faulting. The lowest porosity was measured within the Georgetown Formation due to the fine-grained lithology and marl beds characteristic of this unit. The Comanche Peak and Edwards Limestone had higher porosity ranges. Overall, Dahl (1990) calculated fracture porosity ranging from 0.41% to 2.45% away from faulting and 1.5% to 4.25% near faulting (Table 1).

Table 1. Summarized hydrogeologic data of the Northern Segment.

Aquifer Properties	Dahl (1990)	Yelderman (2013)	Jones (2020)
Hydraulic Conductivity (ft/day)	0.03 – 292	0.87 – 83.2	0.005 – 30,000
Specific Capacity ([gal/min]/ft)	–	–	0.01 – 20,000
Transmissivity (ft^2/day)	1 – 30,000 (De La Garza and Slade, 1987)	34.6 – 3300	0.5 – 4 × 10^6
Fracture Porosity (%)	0.41 – 4.25	–	–

Hydraulic conductivity is defined as the rate at which water can move through a permeable medium, which is largely controlled by fracturing and dissolution in a karst terrain (Fetter, 2001). Vertical and horizontal fractures are attributed to faulting and bedding planes, respectively. Units of hydraulic conductivity for this study are given in feet per day. Due to the limited number of pumping tests that have been conducted in the Northern Segment of the Edwards (BFZ) Aquifer, previous studies have determined hydraulic conductivity values based on transmissivity and saturated thickness data (Jones, 2020; Dahl 1990). These values are listed in Table 1. Aquifer pumping tests were conducted on four wells in August of 2012 by Bar W Groundwater Exploration and Clearwater Underground Water Conservation District to measure hydraulic characteristics of the Northern Segment of the Edwards (BFZ) Aquifer. Yelderman (2013) calculated hydraulic conductivity values from these tests ranging from 0.87 feet per day to 83.2 feet per day (Table 1). This variability of almost two orders of magnitude is due to fractures and dissolution of the heterogeneous medium. The lower range of hydraulic conductivity values are sourced from areas in the aquifer that are located further away from the significant faulting of the Balcones Fault Zone. Moving further west through the outcrop portion of the aquifer from the significant faulting causes fewer dissolution fractures to form from already created conduits and fractures. Groundwater circulation is enhanced along Balcones faulting resulting in higher hydraulic conductivity values as flow is diverted to the north (Dahl, 1990).

Transmissivity is the rate at which water of a given density and viscosity is transmitted through an aquifer under a hydraulic gradient. In other words, it is dependent on properties of the liquid, porous media, and saturated thickness and is the product of

hydraulic conductivity times the saturated thickness (Fetter, 2001). Units of transmissivity for this study are given in square feet per day. Like hydraulic conductivity, previous studies have used specific capacity measurements to estimate transmissivity of the Edwards Aquifer using the Cooper-Jacob solution drawdown in a pumping well (Cooper and Jacob, 1946). Jones (2020) calculated transmissivity using the Cooper-Jacob method and specific-capacity data sourced from the Texas Water Development Board (TWDB) well database. Transmissivity estimates vary within seven orders of magnitude ranging from 0.5 to 4×10^6 square feet per day (Table 1). Dahl (1990) calculated transmissivity values based on specific capacity of wells recorded in drillers' logs within the Northern Segment of the Edwards (BFZ) Aquifer ranging from 1 to 30,000 square feet per day (Table 1). Estimates from the pumping tests conducted by Bar W Groundwater Exploration and Clearwater Underground Water Conservation District ranged over two orders of magnitude from 34.6 to 3,300 square feet per day (Yelderman, 2013). Jones (2020), Dahl (1990), and Yelderman (2013) concluded that estimated transmissivity variability is due to fractures and karst dissolution characteristic of the Edwards Aquifer. Furthermore, areas with higher fracture density are where the highest transmissivity values occurred. This zone of higher fracture density is located along the major faults on the eastern boundary of the outcrop portion of the aquifer associated with the Balcones Fault Zone.

The water table in the outcrop portion of the Northern Segment of the Edwards (BFZ) Aquifer is generally located less than 100 feet below the ground surface. Water levels are closer to the ground surface in the confined portion of the aquifer and will tend to form artesian aquifer conditions (Senger and others, 1990). Water-level fluctuations are observed in the Edwards Aquifer primarily due to seasonal climatic changes that affect the

amount of groundwater storage in the aquifer (Brune and Duffin, 1983). These seasonal climatic changes are associated with infiltration from precipitation, the dominant source of recharge to the aquifer. Precipitation variability in central Texas is primarily driven by large-scale ocean and atmospheric circulation patterns, such as El Niño and La Niña. In other words, if precipitation serves as a function of recharge to groundwater resources in central Texas, then changes to these climate systems can determine groundwater supply replenishment, or scarcity, under extreme conditions. For example, El Niño and La Niña cycles have been linked to multiyear droughts, including that of the 1930s and the 1950s drought of record (DOR) in central Texas and other parts of the southwestern United States. Hydrologic records show the DOR resulted in the lowest total annual rainfall and water-levels reached a historic low in central Texas (Smith and Hunt, 2010). Overall, water levels recorded from wells throughout the Northern Segment of the Edwards (BFZ) Aquifer show seasonal variations closely correlated to precipitation amounts. Figures 8 and 9 display water-level measurements and average daily rainfall, respectively, for the outcrop portion of the aquifer in 2020. The water-level measurements correspond to the Rest Stop monitor well located south of Salado in the southern portion of Bell County. This well is 170 feet deep with a surface elevation of 735 feet and is screened in the Edwards Limestone. The Rest Stop monitor well provides the greatest indication of discharge rates at Salado Springs (Keester and Konetchy, 2017). Average daily rainfall amounts are sourced from the Weather Surveillance Radar-1988 Doppler (WSR-88D) data, a product of the National Weather Service obtained through their Next Generation Weather Radar (NEXRAD) program. Events that display a rapid water-level rise generally concur with significant rainfall events (Figures 8 and 9). These significant rain events took place in February-May

and September in 2020. Water-levels will begin to decline during periods of minimal recharge to the aquifer resulting in the de-watering of the aquifer. In essence, recharge to the aquifer is significantly dependent on precipitation therefore, recharge will vary seasonally and in response to changes in climate.

The Northern Segment of the Edwards (BFZ) Aquifer formed within the Cretaceous period carbonate rocks and is largely influenced by topography, faulting, and dissolution, resulting in highly variable hydraulic properties (Table 1). This study will serve to further investigate the influences on groundwater flow by defining the springshed boundary and identify areas of significant recharge to protect water quality in the DSSC.

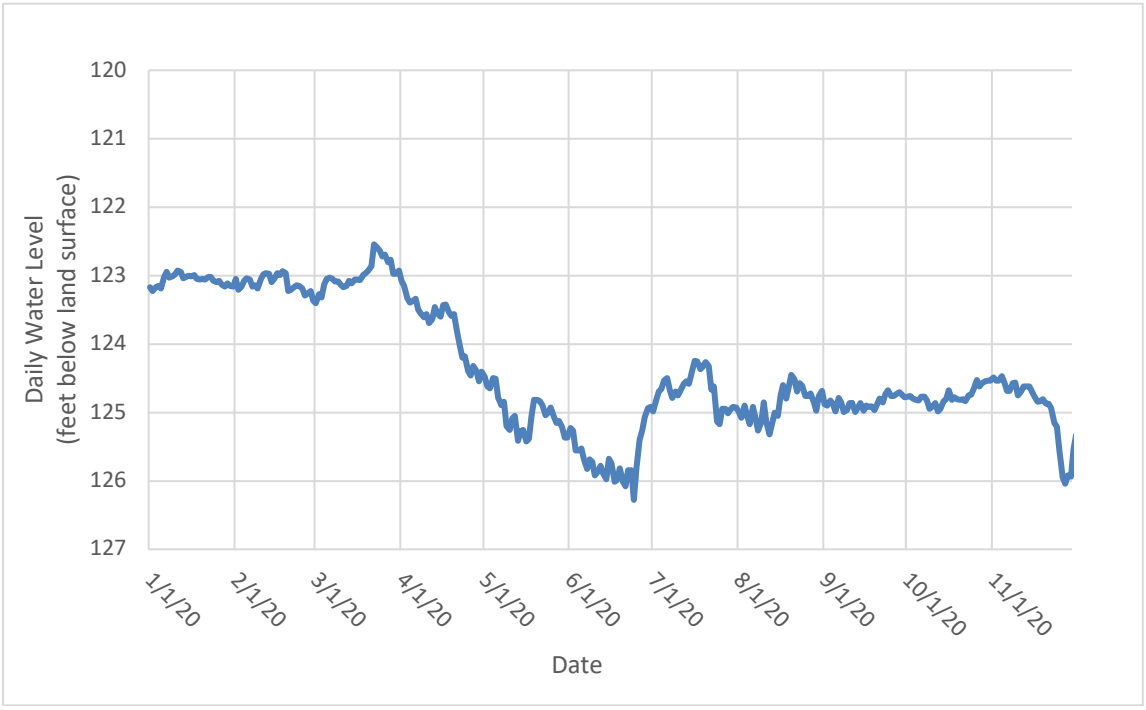

Figure 8. Hydrograph of the Rest Stop monitor well #5804816 during 2020.

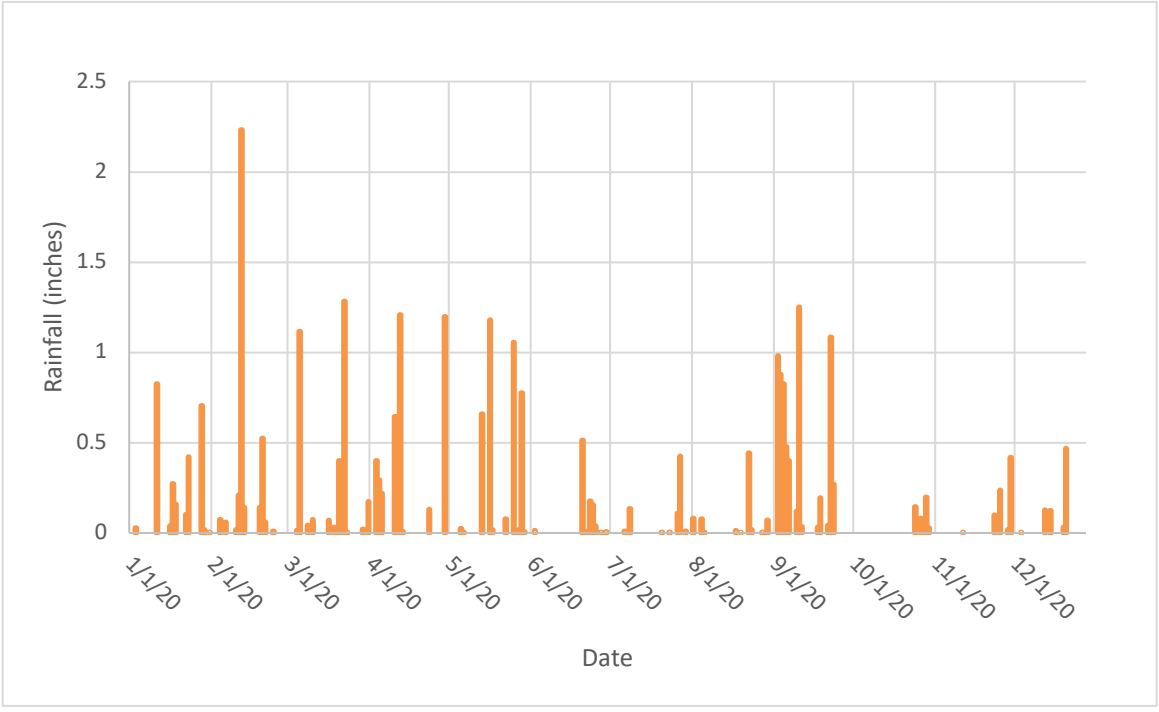

Figure 9. Daily precipitation record over the Northern Segment outcrop in 2020 from WSR-88D data.

CHAPTER THREE

Methodology

The various methods used for this study included estimating a springshed boundary using synoptic maps, a statistical correlation analysis of rainfall and springflow, an ionic chemistry and isotopic composition analysis during different aquifer conditions, and an isotopic analysis of specific precipitation events. These methods were used to delineate the Salado Springshed and to identify significant areas of recharge. Published streamflow and rainfall data were obtained from the United States Geological Survery (USGS) and the National Weather Service (NWS) database. Groundwater and spring water samples were analyzed at the Lower Colorado River Authority (LCRA) Environmental Laboratory Services, Beta Analytic Inc., and the Baylor University Stable Isotope Geochemistry Laboratory.

Springshed Boundary

Synoptic water-level maps produce a snapshot of general aquifer conditions for a given moment. These maps can be used to interpret groundwater flow direction and periodic snapshots can be used to monitor changes in aquifer conditions such as water volume and the effects from pumping. For this study, three synoptic water-level maps were used to generate an estimated springshed boundary based on potentiometric surfaces. Water-level measurements in Bell County were previously collected by the Clearwater Underground Water Conservation District (CUWCD) assisted by Randy Williams in 2010, and by Baylor University personnel in 2013 and 2019. Measurements were recorded from

wells over two consecutive days to capture a synoptic water level of the Edwards (BFZ) Aquifer across the outcrop and down-dip portions. Water levels were measured in feet-to-water below measuring point using a Sonic Water Level Meter or E-line and converted to water elevations in feet (Yelderman, 2013; Wong and Yelderman, 2015, 2016, 2017). Water-level points were plotted in ArcMap 10.5 for each year, then the potentiometric surfaces were contoured by hand and digitized in ArcMap using geoprocessing tools. The synoptic surfaces digitized in ArcMap were then used to estimate a springshed boundary for the DSSC in 2010, 2013, and 2019. The springshed boundaries were produced in ArcMap by drawing a path perpendicular to the equipotential lines from the DSSC to delineate the portion of groundwater that discharges at the spring complex. Figures 10, 11 and 12 show the well locations in 2010, 2013, and 2019, used for the synoptic maps, respectively.

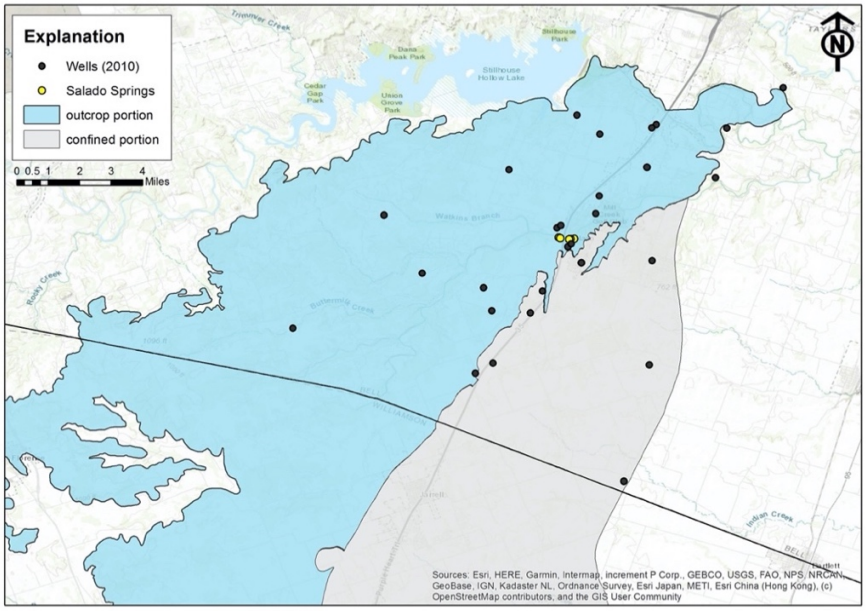

Figure 10. The 28 well locations for the 2010 synoptic map.

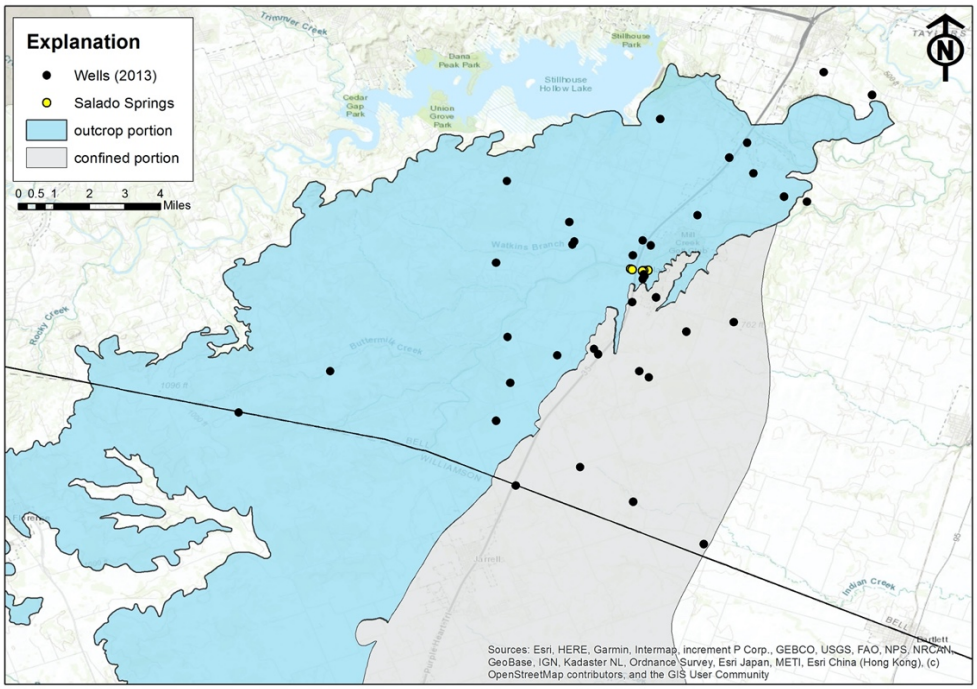

Figure 11. The 39 well locations for the 2013 synoptic map.

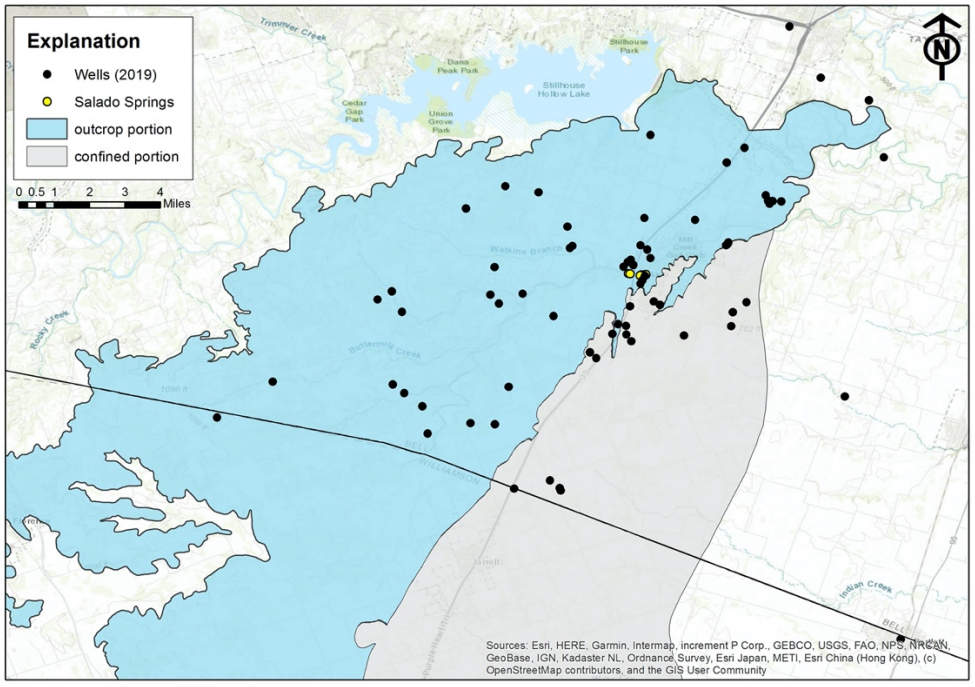

Figure 12. The 66 well locations for the 2019 synoptic map.

Rainfall and Springflow Statistical Analysis

A statistical analysis was conducted to correlate springflow and streamflow response along Salado Creek to the amount and location of precipitation that occurred in the basin during major rain events to identify key areas of recharge within and outside of the estimated springshed boundary. Precipitation data used for this project were sourced from the Weather Surveillance Radar-1988 Doppler (WSR-88D), a product of the National Weather Service obtained through their Next Generation Weather Radar (NEXRAD) program. The WSR-88D data are collected using 160 Doppler radar stations across the United States that have fully automated algorithms, called the Precipitation Processing System (PPS), to produce rainfall estimates. The PPS algorithms are validated with field data to produce 4-km gridded data sets of spatially distributed precipitation estimates (Fulton, 1998). The WSR-88D data for this study were obtained through the CUWCD data management dashboard for various precipitation events that took place between 2018 and 2020. The precipitation totals for each rain event were used from WSR-88D grid points that are located within the outcrop portion for the Northern Segment of the Edwards (BFZ) Aquifer in Bell County and northern Williamson County. A total of fifty WSR-88D stations were used for this analysis (Figure 13). The data for each rain event were exported from the CUWCD dashboard as Microsoft Excel spreadsheets and then the raw data were re-structured to conduct the statistical analysis (See Appendix A). Streamflow data from 2018 to 2020, were obtained through the USGS for stream gauge #08104300 in Salado, TX. The DSSC discharges upstream of the USGS gauge therefore, discharge measurements from the gauge account for streamflow and spring discharge. Baseflow separation was conducted to account for baseflow in the basin using the Web based Hydrograph Analysis

Tool (WHAT), a system by Lim and others (2005). WHAT utilizes digital filter methods and statistical components to separate high frequency signals (direct runoff) from low frequency signals (baseflow) using streamflow data directly from the USGS web server (Lim and others, 2005).

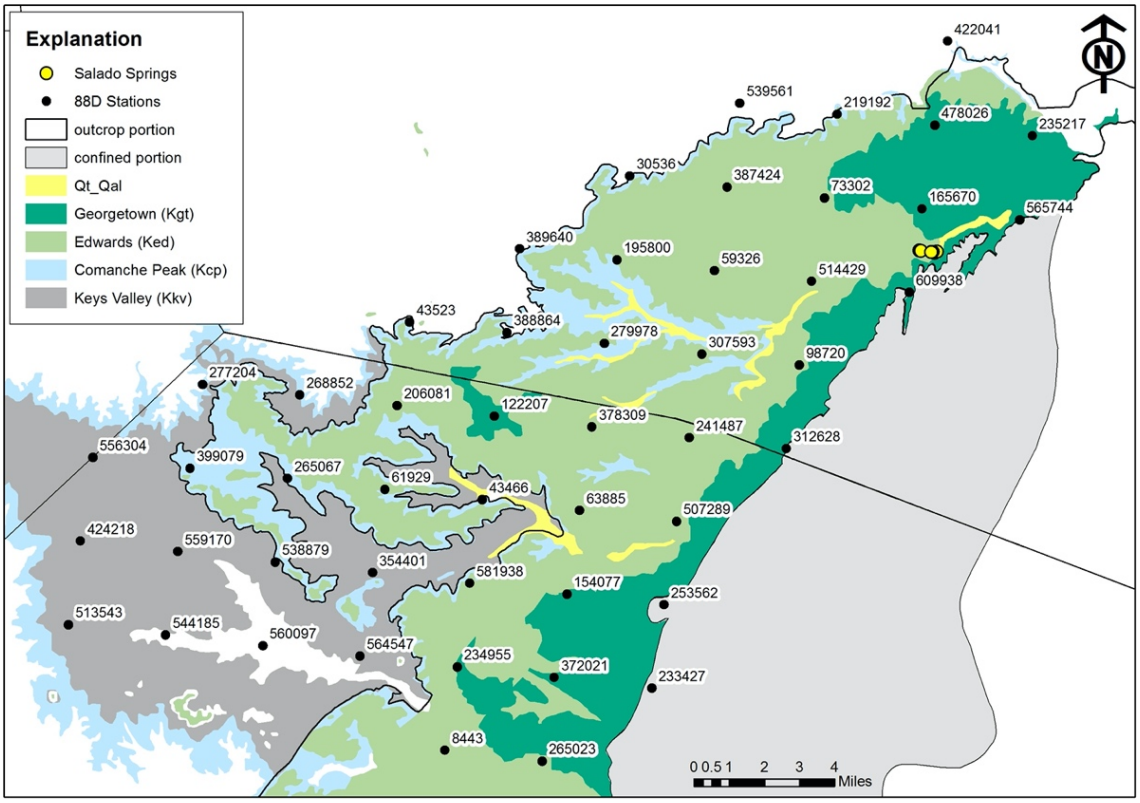

Figure 13. WSR-88D stations over the aquifer outcrop used for statistical analysis between rainfall and springflow.

The statistical model was created by Dr. Jane Harvill and Qida (Jerry) Ma, professor and Ph.D. graduate, respectively, from the Statistical Science Department at Baylor University, in collaboration with the author Clara P. Smith-Salgado and mentor Dr. Joe C. Yelderman Jr. A detailed methodology for the development of the statistical model can be found in appendix B.

Spring and Well Geochemistry

To analyze the groundwater flow system throughout the springshed boundary, groundwater and spring water samples were collected during two different aquifer conditions. These samples were used to analyze the ionic chemistry and isotopic composition of groundwater at specified locations to chemically assess their hydrogeologic connect. Samples were collected from three wells at varying distances and positions to the DSSC and two springs in the DSSC (Figure 14). Big Boiling Spring is located within the DSSC, the common discharge point for the springshed, and is representative of the eight springs identified at the spring complex. These springs are all part of an integrated fracture system as indicated from previous dye tracer studies (Wong and Yelderman, 2015, 2016, 2017). Robertson Springs is located about 0.3 miles upstream of Big Boiling. Big Boiling and Robertson Springs were sampled to determine their hydrogeologic connection and to determine the water chemistry at the discharge point for the springshed. Three wells were identified that can be used to help understand the flow system within the Salado springshed: 1) Young well 2) Bloomer well, and 3) Avila well (Figure 14).

Groundwater samples at the five sites were collected during two different aquifer conditions in the summer of 2020, to develop an understanding of the flow system within the springshed under varying conditions. Samples were collected on June 19, 2020 and August 21, 2020, when the daily flow average at Salado Creek was 10.0 cubic feet per second and 7.4 cubic feet per second, respectively (Figure 15).

Samples at each site were collected in accordance with the TWDB groundwater sampling guidelines (Boghici, 2003). The YSI Probe DSS was used prior to sampling to measure pH, temperature (°C), barometric pressure (mmHg), dissolved oxygen (mg/L),

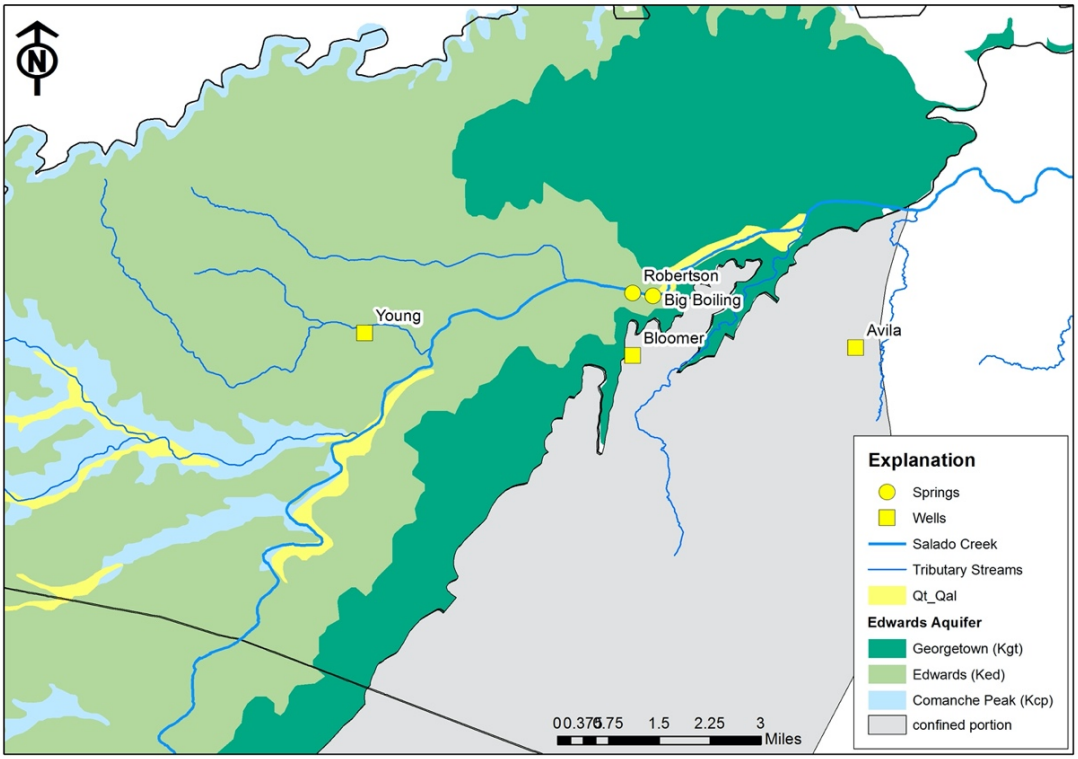

Figure 14. Sampling points for the ionic chemistry and isotope composition.

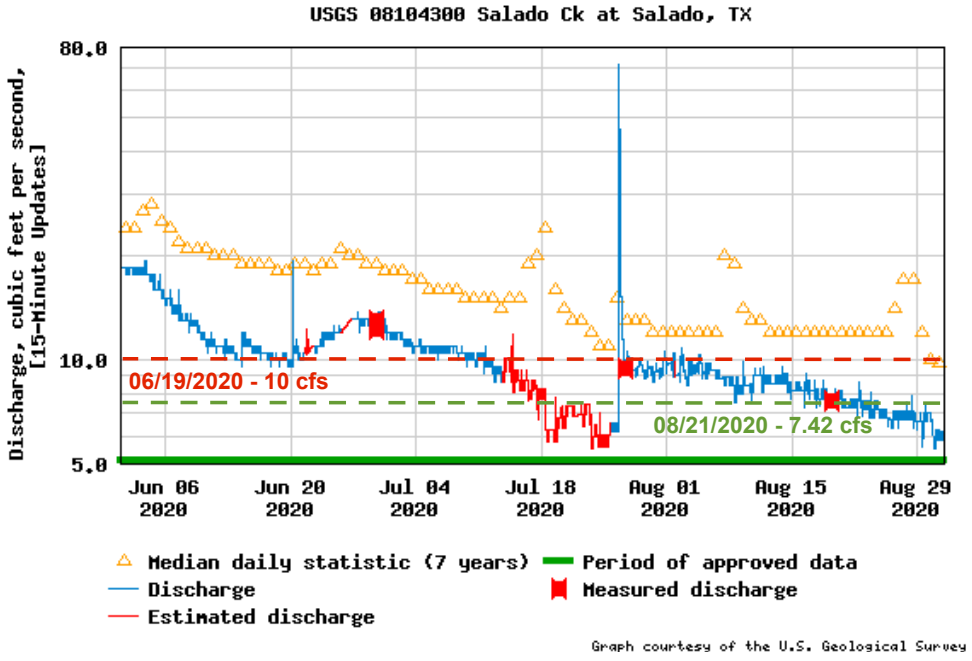

Figure 15. Daily discharge recorded at the USGS gauge on Salado Creek in the summer of 2020, marked by discharge comparison from when samples were taken (10 cfs and 7.42 cfs).

and specific conductance (µS/cm). At the springs (Big Boiling and Robertson), these parameters were recorded after thirty-seconds of submerging the probe in the water to allow for the equipment to equilibrate. The wells were purged and stabilized prior to collecting groundwater samples by taking field parameter readings at 3- to 5-minute intervals until the readings were steady.

To obtain the ionic chemistry and isotopic composition of the groundwater, samples were collected from the spring outlet or wellhead at the five sites for the concentration of cations, anions, and nitrates, in addition to the isotope values of tritium, deuterium, carbon-14, and oxygen-18. Seven bottles were used at each site to collect samples for the necessary analyses (Figure 16). To determine the concentration of dissolved constituents in the water, the ionic samples were filtered during collection. The filtration unit consisted of an unused 0.45-micron filter attached to the end of an unused bailer. The isotope samples did not need to be filtered; therefore, the water was collected directly from the spring outlet or wellhead. All the bottles were then filled completely, capped tightly, placed on ice, and delivered to the LCRA lab on the same day sampling took place.

Figure 16. Set of sample bottles used at each site.

Isotopic Analysis of Precipitation Events

To further investigate the flow system within the springshed boundary, spring, creek, and rain samples were collected during significant precipitation events that occurred within the creek basin to determine the isotopic composition of the waters. The stable isotopes analyzed were hydrogen and oxygen, which serve as natural chemical tracers for studying how recharge may affect discharge at the DSSC. The precipitation events that were sampled took place from July of 2020 to January of 2021. For this isotopic approach, water samples were collected in a plastic 50 mL vial along Salado Creek downstream of the DSSC and from the outlet of Big Boiling Spring within 7 days before and after the rain event being analyzed. The samples were collected within 7 days before and after each precipitation event to ensure that the creek had returned to baseflow conditions (Dahl, 1990). During the precipitation event, rainwater was collected in Salado, Texas in a Community Collaborative Rain, Hail, and Snow Network (CoCoRaHS) gauge and then transferred into a plastic 50 mL vial for analysis. The pre- and post-rain event samples from Salado Creek and Big Boiling Spring, in addition to the rainwater samples, were analyzed at the Baylor University Stable Isotope Geochemistry Laboratory for hydrogen and oxygen isotopic compositions using a gas source isotope ratio mass spectrometer. Samples are reported as per mil differences from the Vienna Standard Mean Ocean Water (VSMOW). VSMOW is an international reference standard for water used to generate a precise comparison of isotopic compositions. The resulting $\delta^{2}H$ and $\delta^{18}O$ values were plotted against the local meteoric water line (LMWL) as well as overtime to assess aquifer response to recharge in the study area.

CHAPTER FOUR

Results and Discussion

Springshed Boundary

The initial steps to understanding groundwater flow dynamics in the Salado Creek basin towards the DSSC were analyzed by creating synoptic water-level maps. The potentiometric surface in Figure 17 represents the water-table elevation with a 25-foot interval for the measurements taken in 2019. Overlying the 2019 potentiometric surface are the estimated springshed boundaries based on the 2010, 2013, and 2019 datasets. Each springshed boundary is slightly different from the others, but each boundary follows a consistent pattern. The limbs of each boundary enclose the tributary streams to Salado Creek that lie west to east, and the eastern portion of the boundaries extend into part of the confined portion of the aquifer. In general, the groundwater flowing within the springshed should discharge at the DSSC, whereas the groundwater located outside of the boundary would not flow to the DSSC.

The delineation of a springshed is strongly dependent on the density and quality of the groundwater-level dataset. The 2010 synoptic dataset is the most limited with 28 wells measured (Figure 10). In 2013, 39 wells were measured and in 2019, 66 wells were measured, which increased the density of the synoptic dataset (Figures 11 and 12). The 2010 and 2013 springshed boundaries both cover a smaller contributing area in comparison to the 2019 springshed boundary perhaps due to the smaller datasets. The larger data set may contribute to a larger springshed but increased pumping in the more developed area

near the Village of Salado may also affect the boundary, especially in the downdip, confined area of the aquifer. In addition, water levels could change under different aquifer conditions caused by periods of extreme drought or periods of greater than average precipitation. Rainfall at the Stillhouse Hollow Dam Station, located about 6.4 miles north of the DSSC, is presented in Figure 18 as 24-month running totals to demonstrate cumulative rainfall changes over time. The period shown is from 1990 to 2021, and the synoptic events measured in 2010, 2013, and 2019, are identified on the graph. The average 24-month total for the period shown in Figure 18 is 69.2 inches. The 2010 and 2013 synoptics both lie below the average, indicating there were drier than average conditions when measurements were collected. These synoptics took place before and after the epic drought of 2011, which could have caused the 2010 and 2013 springshed boundaries to cover a smaller contributing area from lower water-level measurements (Figure 17). Wong and Yelderman (2015, 2016, 2017) compared water-level changes in the aquifer from 2010 to 2013 and determined that no significant change took place as a result of groundwater usage in the area during the epic drought of 2011 and low amounts of recharge in 2012. The 2019 estimated springshed boundary covers a larger contributing area because of the denser dataset used. Furthermore, the 2019 synoptic water-level measurements were collected during a wetter than average period (Figure 18).

Results from the 2019 potentiometric surface generated from the synoptic water-level measurements show the dominant flow direction around the study area is east-southeast with flow deflecting northeast towards the DSSC along the confined and unconfined transition boundary (Figure 17). The anisotropic flow towards the DSSC is affected by the Balcones Fault Zone that increases the frequency of fractures and

heterogeneity in the aquifer (Dahl, 1990). Localized pumping by the Downtown Salado area may also affect the potentiometric surface and groundwater flow. The eastern portion of each estimated springshed boundary extends further east overtime, which correlates to the increase in groundwater use from the Northern Segment of the Edwards (BFZ) Aquifer over time. For example, total pumping from the Northern Segment of the aquifer has increased from 16,000 acre-feet per year to 50,000 acre-feet per year from 1980 to 2015 (Jones, 2020). Further sections of this study will cover findings that support interpretations from the estimated springshed boundaries discussed above through various hydrogeologic methods.

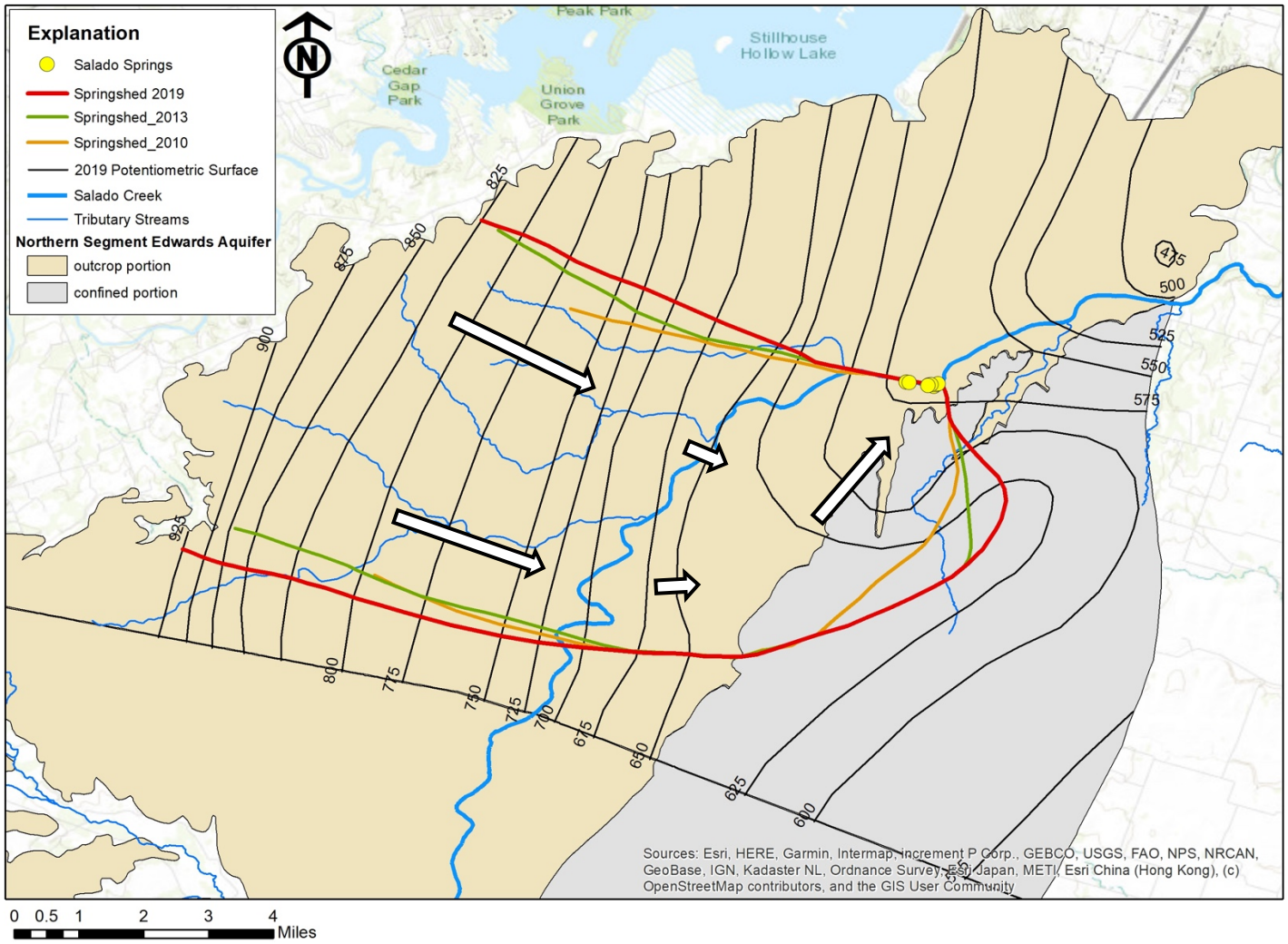

Figure 17. Estimated springshed boundaries based on water-level measurements collected throughout the Salado watershed in 2010, 2013, and 2019. White arrows mark the general flow paths.

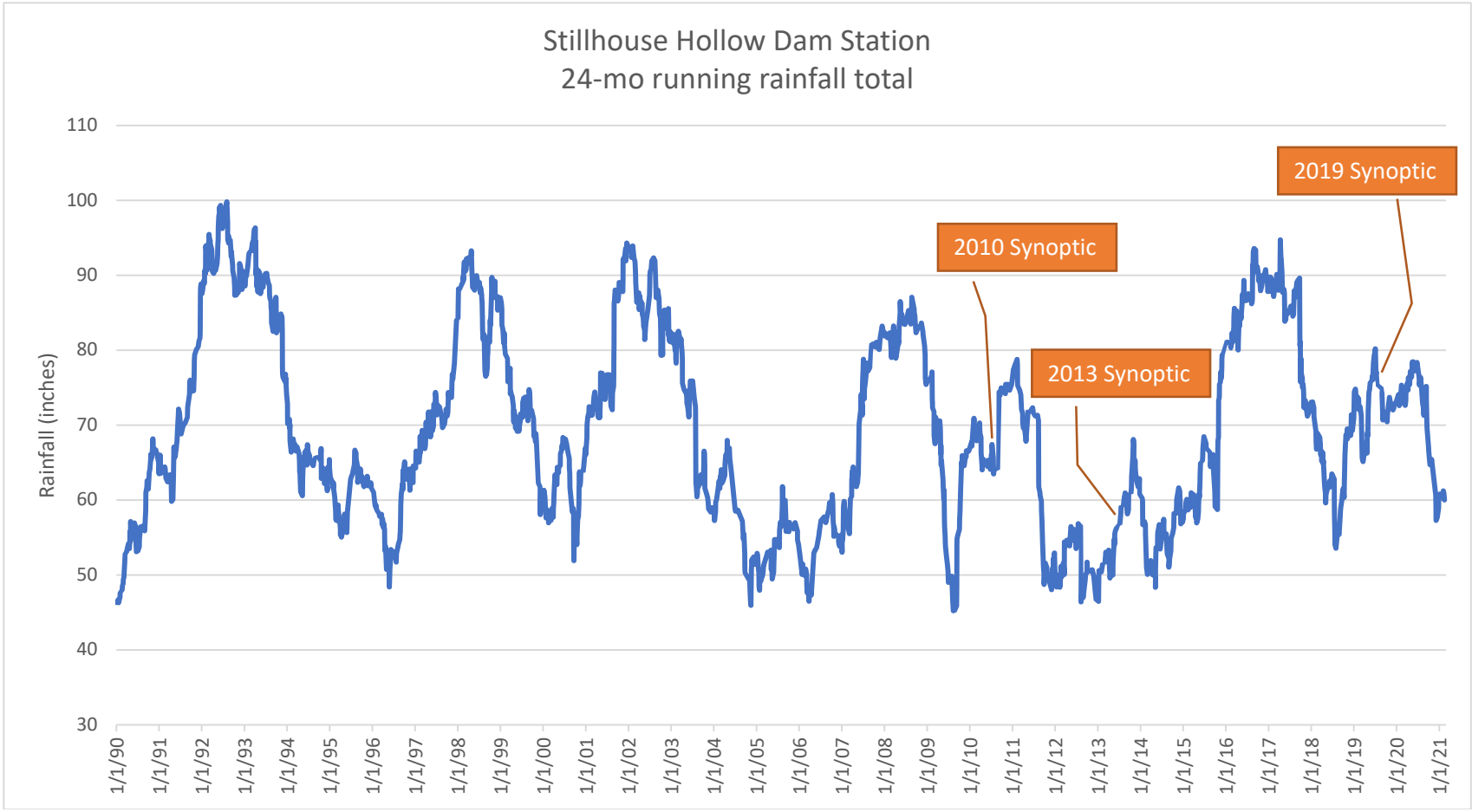

Figure 18. Record of meteorological data from the Stillhouse Hollow Dam Station (1990-2021) marked by when groundwater synoptics were collected by CUWCD and Baylor team.

Rainfall and Springflow Statistical Analysis

Recharge to the Northern Segment of the Edwards (BFZ) Aquifer is sourced from precipitation directly on the limestone outcrop as well as losing stream sections along Salado Creek that allow for the input of runoff and baseflow through fractured and faulted limestone (Dahl, 1990). To further investigate where significant recharge may be occurring on the Salado Springshed and the northernmost portion of the Edwards (BFZ) Aquifer, a statistical model was constructed by Dr. Jane Harvill and Qida (Jerry) Ma, professor and Ph.D. graduate, respectively, from the Statistical Science Department at Baylor University, to correlate the amount and location of precipitation to baseflow in Salado Creek. More specifically, this statistical model was used to quantify the effect of rainfall over the aquifer outcrop on streamflow and baseflow along Salado Creek based on significant rain events from 2018 to 2020. Baseflow accounts for the groundwater contribution to Salado Creek within the Salado Creek basin that is recorded at the USGS stream gauge.

The relationship between average rainfall from 50 WSR-88D stations over the Northern Segment was analyzed qualitatively with streamflow and baseflow recorded at the Salado Creek USGS gauge, by superimposing the hydrographs of the three hydrologic parameters from February 1, 2020 through May 6, 2020 (Figure 19). These hydrographs made it evident that the amount of precipitation that took place during a given event does not control the magnitude of the streamflow and baseflow response or the lag time between when rainfall took place and when an increase in flow initially becomes present. This inconsistency in the response magnitude and time lag of flow recorded at the USGS Salado Creek gauge is explained by antecedent moisture conditions and by where most of the rainfall is concentrated during a single event. For example, rainfall that took place on

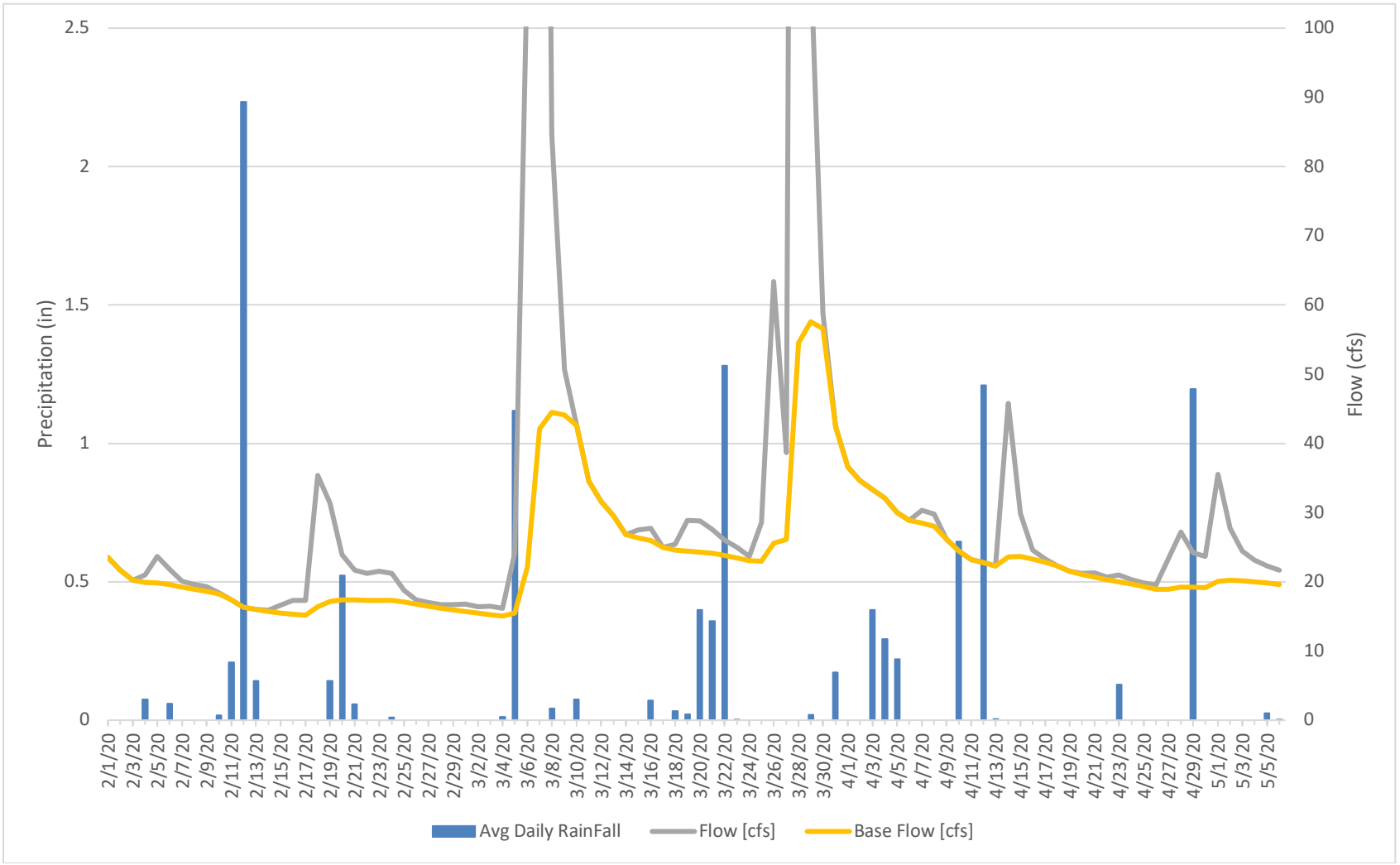

Figure 19. Average rainfall over the unconfined portion of the Northern Segment of the Edwards (BFZ) Aquifer and the streamflow and baseflow measurements recorded at the USGS gauge on Salado Creek near the DSSC.

February 10-13, 2020, produced nearly 2.5 inches of rain, but streamflow and baseflow did not begin to increase until 5 days after rainfall ceased, and flow did not increase above 35 cubic feet per second (cfs) (Figure 19). The 5-day lag time and limited increase of flow from the February 10-13 rain event was likely a result of limited antecedent moisture content. If soils were dry prior to rainfall, then less water will be able to infiltrate the soil and recharge the aquifer. Rainfall that took place on March 4-5, 2020, produced less than 1.5 inches of rain, but caused a large and immediate response in streamflow and baseflow at the USGS gauge. Since precipitation had occurred in the month prior to the event on March 4-5, it is likely that soils were still wet, which allowed for recharge too occur quickly and in greater quantity. Interpolated rainfall surfaces were generated in ArcMap using WSR-88D data for four rainfall events to visualize any patterns causing the different recharge responses in the Northern Segment of the Edwards (BFZ) Aquifer (Figures 20.1-20.4). Rainfall on February 10-13, 2020 and March 22, 2020 were mostly concentrated on the upper and western boundary of the basin (Figures 20.1 and 20.3). The two rainfall events resulted in a streamflow and baseflow response time of 5 days at different magnitudes. Rainfall that took place on March 4-5, 2020 and April 10-12, 2020 had their highest rainfall total over a portion of Salado Creek, which resulted in an increase in streamflow and baseflow within 1 day (Figure 20.2 and 20.4).

Due to the large variability in flow response from different recharge events, a proxy measure was used in developing the statistical model to numerically account for antecedent moisture content. The surface elevation of Stillhouse Hollow Reservoir, located about 5 miles north-west of the DSSC, was used as the proxy because it can represent the amount

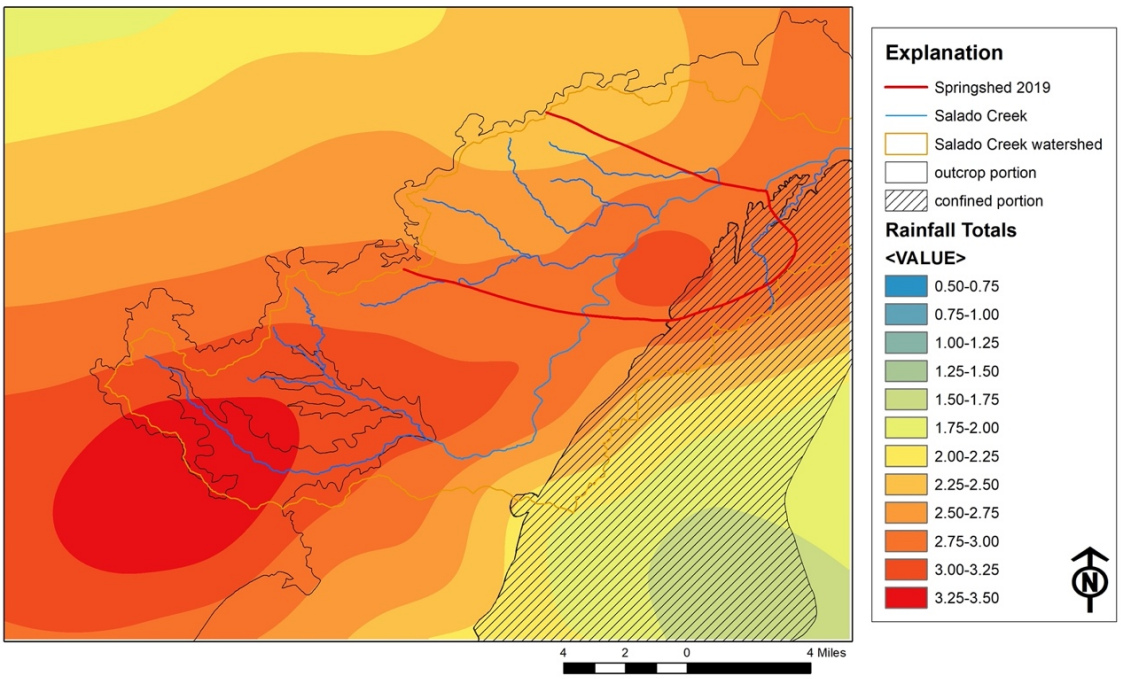

Figure 20.1. The precipitation pattern for rainfall that took place on February 10-13, 2020 over the Salado Springshed and Northern Segment of the Edwards (BFZ) Aquifer.

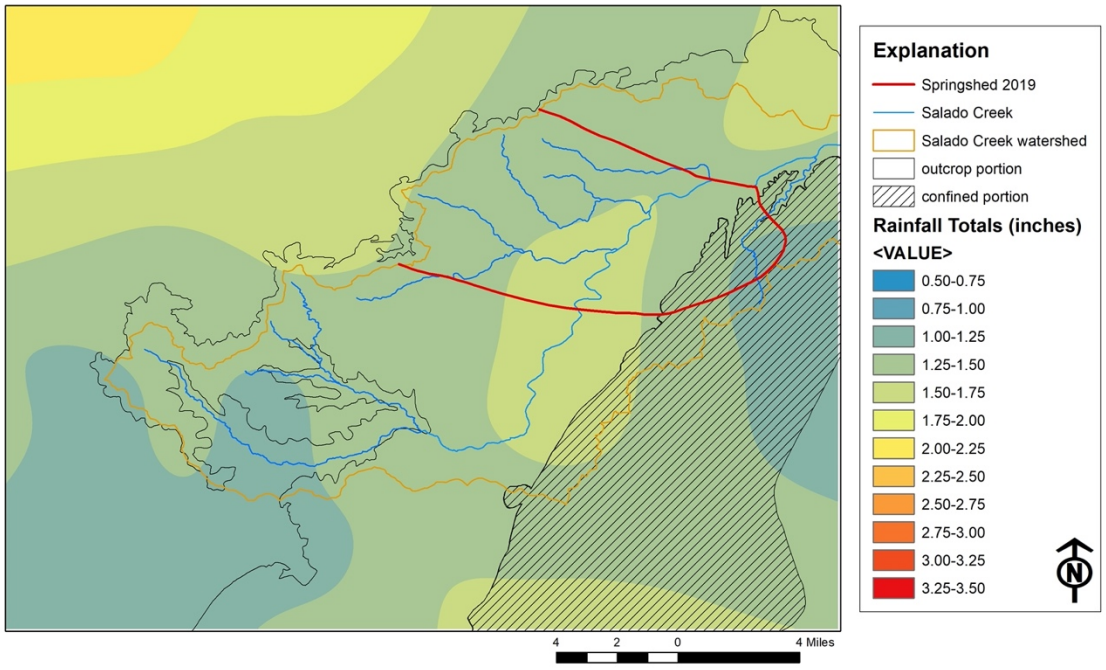

Figure 20.2. The precipitation pattern for rainfall that took place on March 4-5, 2020 over the Salado Springshed and Northern Segment of the Edwards (BFZ) Aquifer.

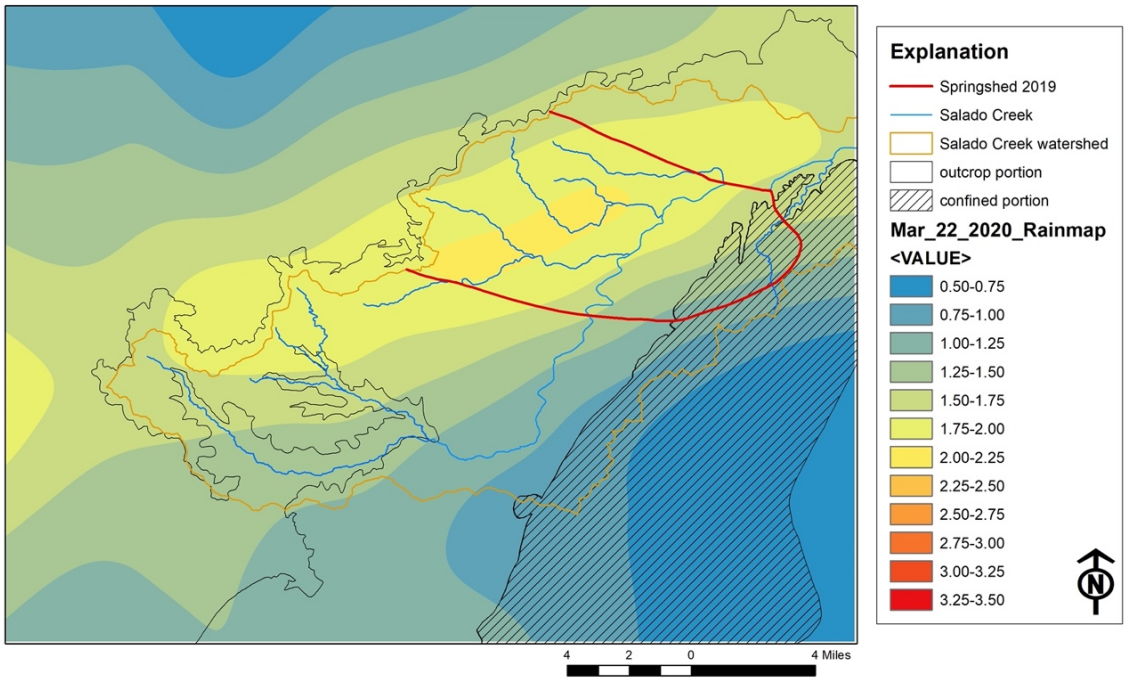

Figure 20.3. The precipitation pattern for rainfall that took place on March 22, 2020 over the Salado Springshed and Northern Segment of the Edwards (BFZ) Aquifer.

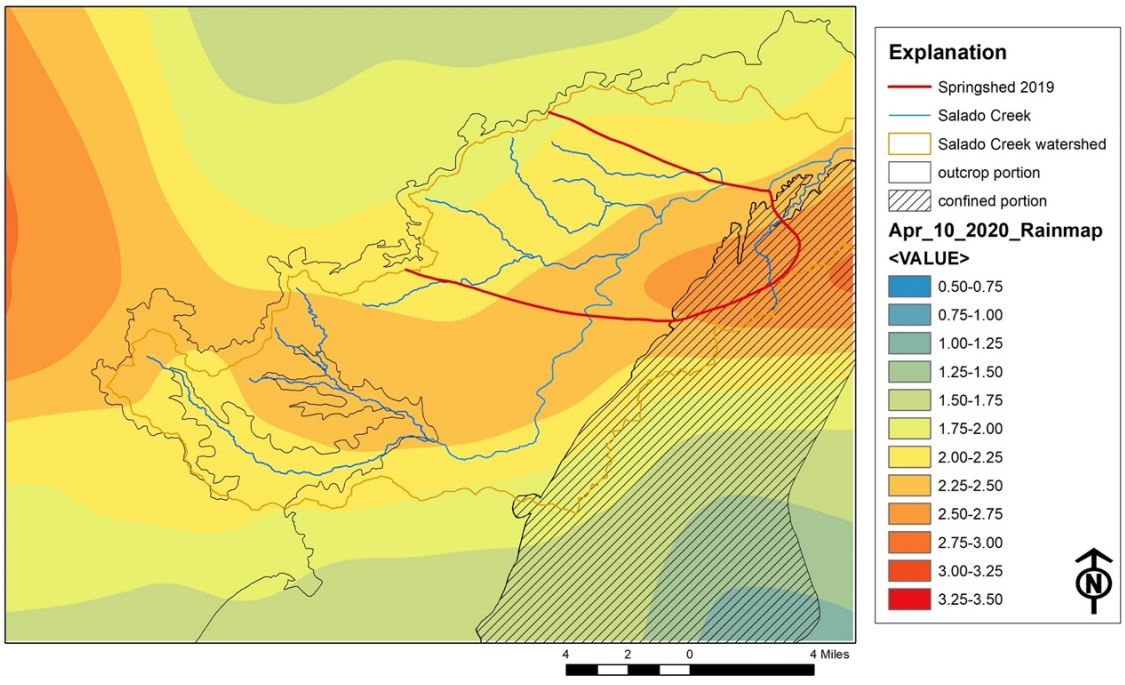

Figure 20.4. The precipitation pattern for rainfall that took place on April 10-12, 2020 over the Salado Springshed and Northern Segment of the Edwards (BFZ) Aquifer.

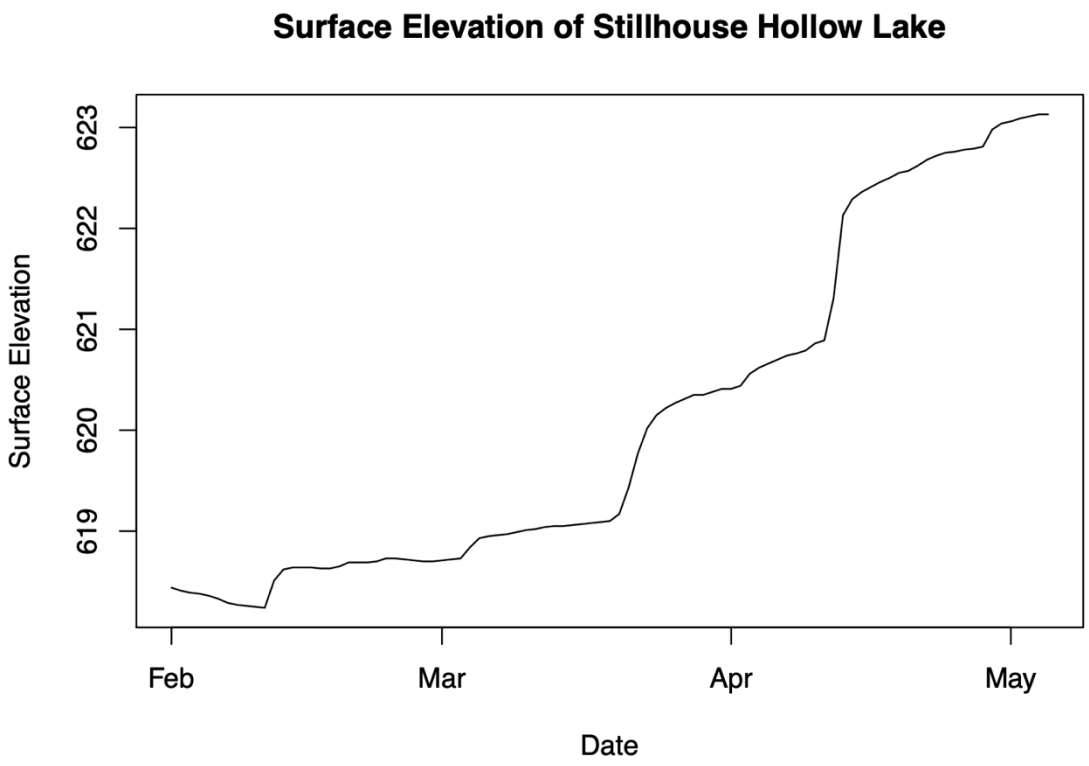

Figure 21. Daily surface elevation of Stillhouse Hollow Lake.

of precipitation that accumulates in the region (Figure 21). The relationship between surface elevation and baseflow (and streamflow) was first tested by conducting a linear regression between the two variables, which resulted in a correlation of 0.5927 for baseflow (0.5203 for streamflow). These values represent a moderately strong correlation between flow and reservoir surface elevation with respect to a natural karst system characterized by heterogenous and anisotropic groundwater flow. An extremely small p-value was also calculated through the regression analysis for surface elevation and both flow types (p-value = $< 2 \times 10^{-16}$) indicating a significant relationship between the two variables. Lastly, the correlation coefficient (R^2) value obtained from the linear regression suggested that 35.12% (27.07%) of the variation of baseflow (streamflow) is explained by the linear model of surface elevation at Stillhouse Hollow Reservoir.

In order to account for the effect of antecedent moisture content on flow and best quantify the effect of rainfall on the aquifer outcrop, the re-scaled residuals from the regression analysis for surface elevation were incorporated into the statistical model. Additionally, to compensate for the variable baseflow and streamflow response time after a given rain event, the residual rainfall at 1 day after the rainfall event, 2 days after, etc., up to 5 days after the event were also included in the model. This is referred to as the residual rainfall at "lagged" days (after the rainfall event). A stepwise regression was used for each of the 50 WSR-88D stations to determine the optimal subset model that described residual baseflow as a function of lagged values of residual rainfall (See Appendix B for stepwise regression equation and the lag days included in the final model). Lastly, the multiple correlation coefficient (R^2) was computed for each of the 50 stations based on the optimal fitted model for baseflow and streamflow. Figures 22 and 23 show the R^2 values for all 50 stations from largest to smallest based on baseflow and streamflow, respectively.

All stations show a positive correlation with flow at varying strengths. The ten stations with the largest multiple correlation coefficient to baseflow and streamflow are marked in Figures 24 and 25. Figure 24 shows that six of the ten stations with the largest multiple correlation coefficient values computed from the statistical model are concentrated within the springshed boundary. The multiple correlation coefficient for these six WSR-88D stations indicate that the stations concentrated within the springshed boundary produce the greatest changes in baseflow in Salado Creek after a given recharge event. These results produced from the statistical model support the estimated springshed boundary generated in ArcMap (Figure 17), where precipitation that falls over the outcrop portion of the Northern Segment of the Edwards (BFZ) Aquifer within the springshed

boundary is the primary source of recharge that contributes to discharge at the DSSC. The Edwards and Georgetown Limestone Formations are the main geologic units found at the surface within the springshed and both formations are more hydraulically conductive than the fine-grained Comanche Peak Formation. In addition, the Edwards Limestone consists of karst features that can easily facilitate recharge through fractures and conduits. A key finding from the rainfall and springflow statistical model shows that a WSR-88D station further south of the springshed boundary (#253562) and stations north of the springshed boundary (#73302, #539561, and #165670) are part of the top ten stations that most effect baseflow in Salado Creek (Figure 24). Station #253562, shown in Figure 24, is near a losing stream section found along the southern portion of Salado Creek, previously described by Dahl (1990) and hypothesized by Brune and Duffin (1983). The stream water at this section enters the aquifer through highly fractured and faulted limestone within the streambed (Woodruff and Abbott, 1979; Dahl 1990). Faults along this losing stream section shifted the Comanche Peak Formation causing the fractured, honeycombed Edwards Limestone to crop out at the surface (Brune and Duffin, 1983; Dahl, 1990). This section is not within the estimated springshed boundary because recharge through the stream occurs during significant rain events. When water-level data were taken for the synoptic measurements in July of 2010, 2013, and 2019, aquifer conditions were more stable and lower than after recent recharge events. New findings uncovered using the rainfall and springflow statistical model identified the section between Stillhouse Hollow Reservoir and the northern boundary of the estimated springshed to have relatively large correlation to baseflow in Salado Creek as well. The reservoir was not previously considered a contributing factor to

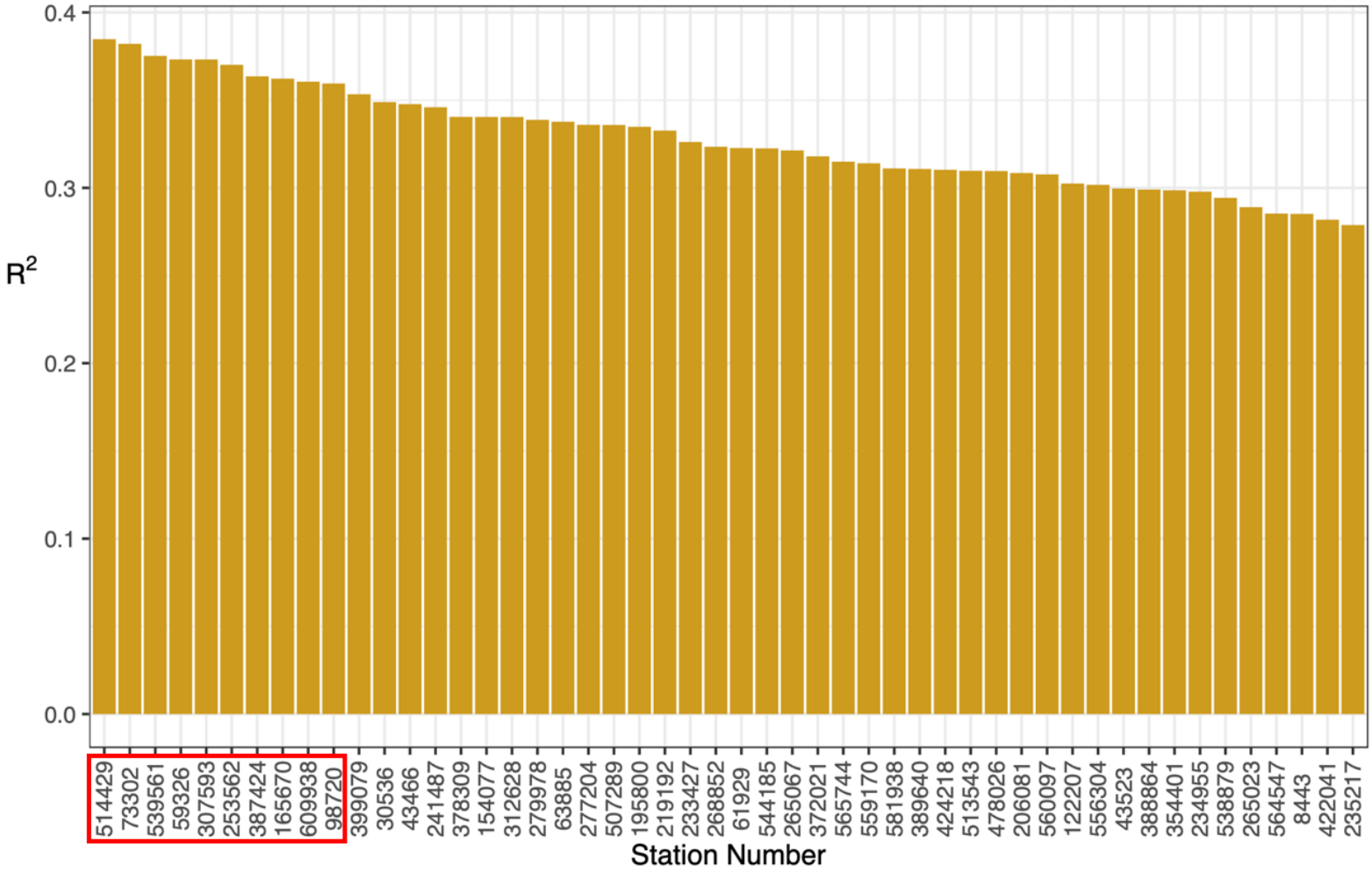

Figure 22. WSR-88D stations plotted by decreasing values of R^2 for regression of re-scaled residuals based on baseflow for optimal model of lagged days of residual rainfall at each station. The ten stations with the largest R^2 value are outlined in red.

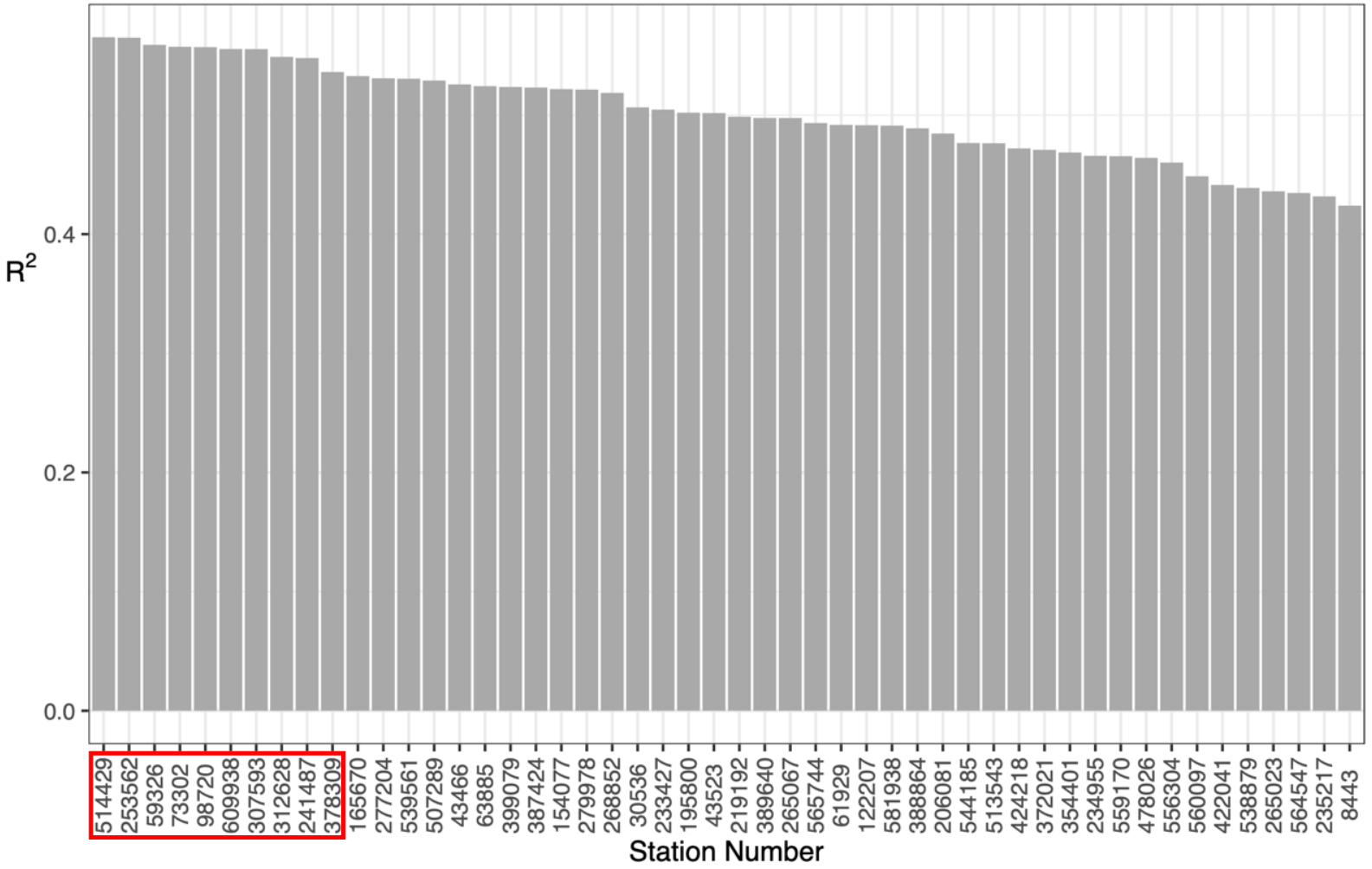

Figure 23. WSR-88D stations plotted by decreasing values of R^2 for regression of re-scaled residuals based on streamflow for optimal model of lagged days of residual rainfall at each station. The ten stations with the largest R^2 value are outlined in red.

aquifer recharge in the Salado Creek basin due to limited water-level data but resulting multiple correlation coefficients (R^2) values listed in Appendix B for baseflow, highlight their possible connection. This connection may occur after a precipitation event when a rise in hydraulic head in the reservoir causes diffuse groundwater flow towards Salado Creek. The surface elevation of the conservation pool at Stillhouse Hollow Reservoir is approximately 622 feet and the elevation of Salado Creek near the DSSC is approximately 560 feet. This natural topographic gradient could influence the groundwater flow paths from the reservoir towards the creek after significant recharge events.

Figure 25 marks the ten WSR-88D stations with the largest R^2 value in relation to streamflow. A majority of the top ten stations are also located within the estimated springshed boundary indicating precipitation enters Salado Creek as storm runoff and substantially contributes to streamflow at the USGS gauge. Station #73302, located directly north of the springshed boundary, correlated well with streamflow. In addition to diffuse groundwater flow from the reservoir, surface runoff may travel downdip and merge with the stream water and affect flow at the USGS gauge. Station #253562 near the losing stream section has a strong correlation to streamflow. This correlation is likely from surface water entering the losing stream segment and later entering Salado Creek as baseflow and contributing to streamflow recorded at the USGS gauge. Three of the top ten stations (#312628, #241487, and #378309) are located directly south of the estimated springshed. These stations are not within the springshed, but likely contribute to changes in streamflow because they are located adjacent to Salado Creek. Precipitation that falls near the creek will merge with the surface water as storm runoff and cause an increase in stream discharge at the USGS gauge.

Ultimately, the estimated springshed boundary generated through ArcMap is generally supported by the rainfall and springflow statistical model. A majority of the WSR-88D stations with the largest correlation coefficient to both baseflow and streamflow, were concentrated within the springshed boundary. Rainfall at the losing stream section and directly south of the Stillhouse Hollow Reservoir (Figures 24 and 25) also produced a significant relationship with groundwater and surface water discharging along Salado Creek. The springshed is a reasonable estimate but is biased towards equilibrated water-level data taken during baseflow, non-precipitating conditions. It is likely that precipitation events, such as the ones analyzed in the statistical model, produce a quick recharge pulse from the reservoir and losing stream section that do not appear during previously measured synoptics taken during dry, low flow conditions. Temporary mounds of concentrated recharge may build up within karst features of the losing stream section, but quickly dissipate as Salado Creek returns to baseflow conditions (Smith and others, 2012).

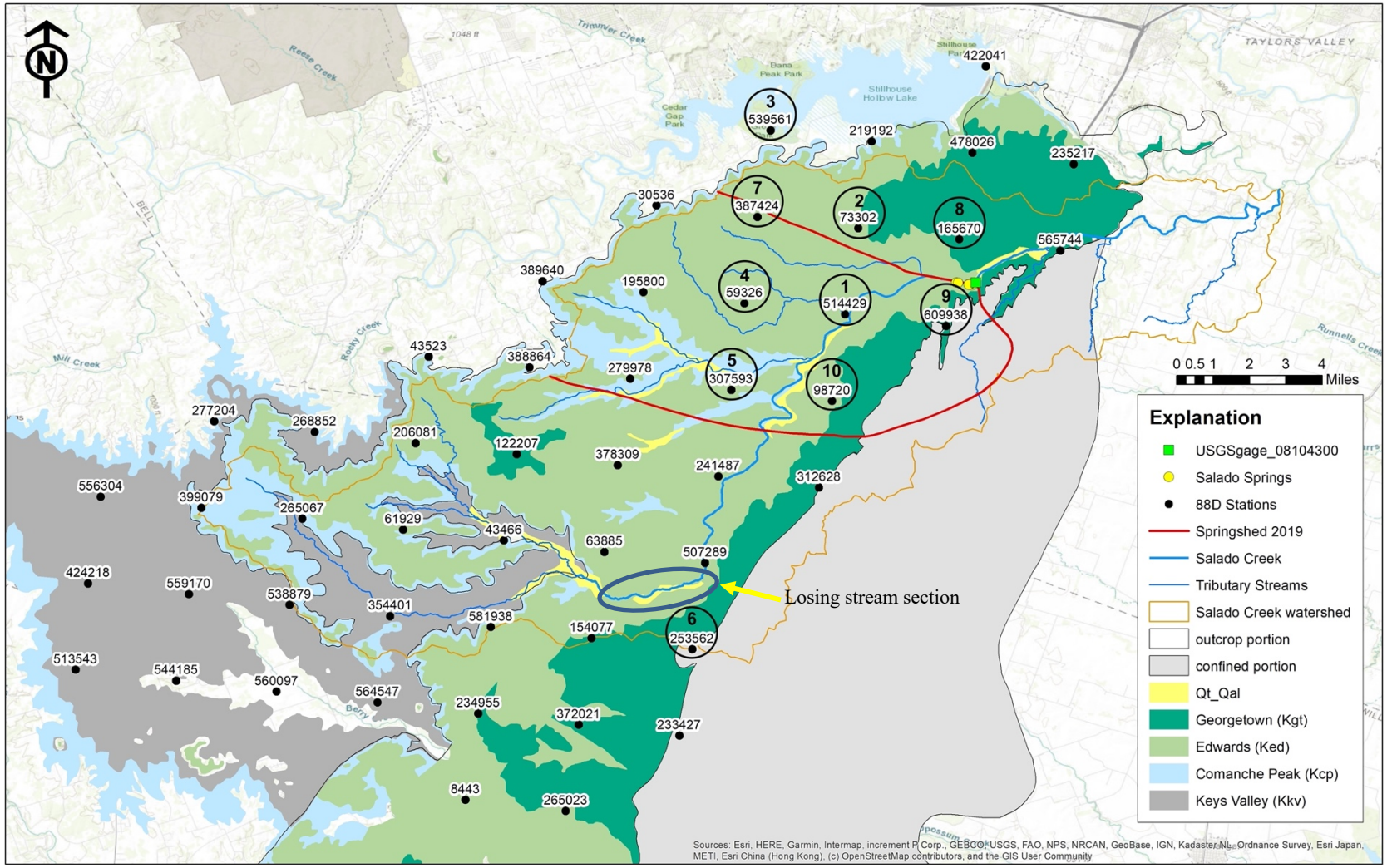

Figure 24. WSR-88D stations with the ten largest R^2 values for the rainfall and springflow statistical model based on baseflow. Map includes the estimated springshed boundary and losing stream section along Salado Creek.

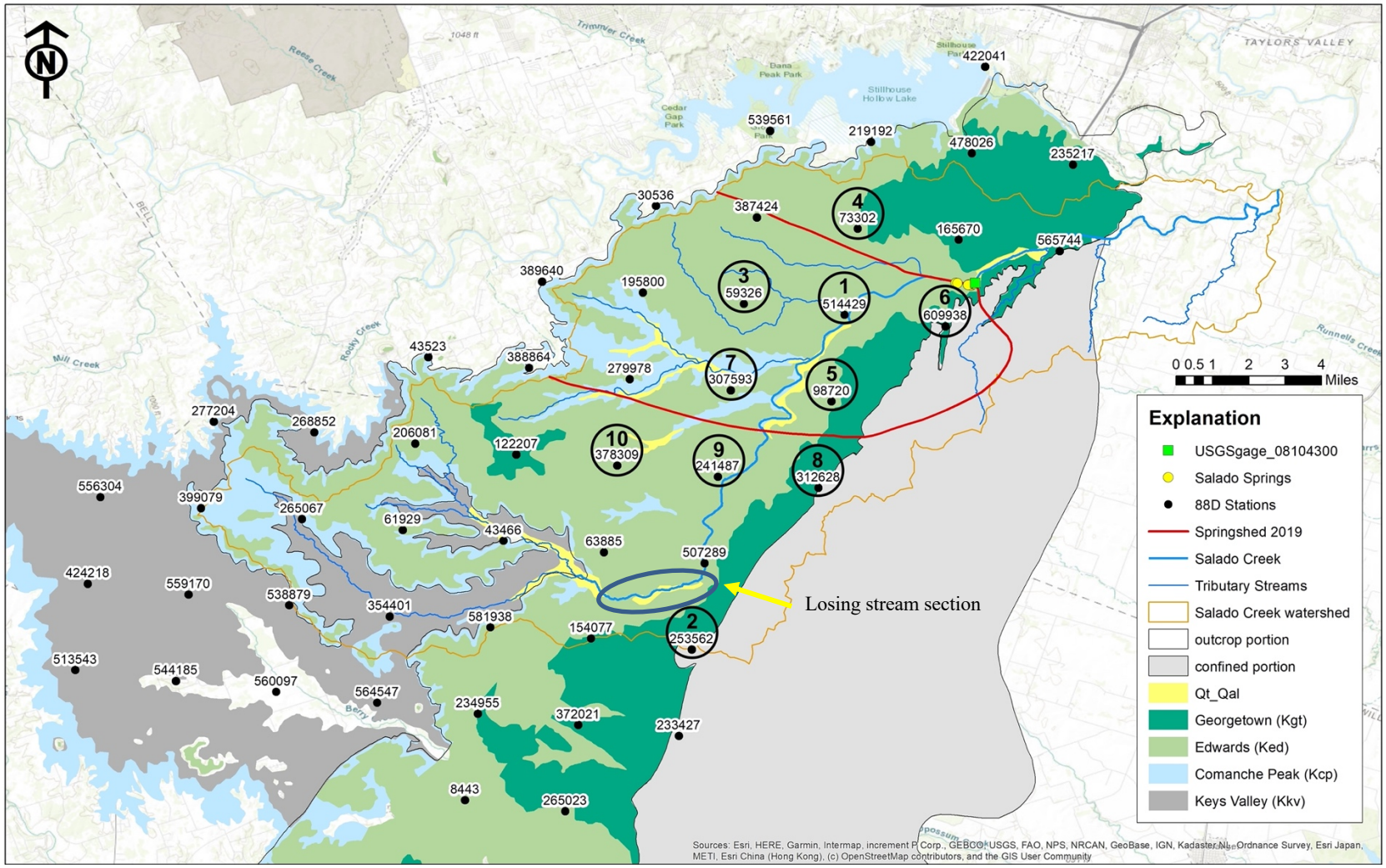

Figure 25. WSR-88D stations with the ten largest R^2 values for the rainfall and springflow statistical model based on streamflow. Map includes the estimated springshed boundary and losing stream section along Salado Creek.

Spring and Well Geochemistry

A suite of geochemical samples were collected on June 19, 2020 and August 21, 2020 to characterize groundwater flow paths in the Northern Segment of the Edwards (BFZ) Aquifer and further delineate the estimated springshed boundary for the DSSC. Hydrologic and geochemical processes within an aquifer can be better understood by analyzing how ionic and isotopic compositions of groundwater change along different flow paths. In June, samples were collected at two springs and three wells across the Northern Segment in Salado, Texas (Figure 14). The springs sampled, Big Boiling and Robertson Springs, are the main discharge points for the estimated springshed boundary, and they make up part of the DSSC. Of the three wells sampled, the Young well is located within the unconfined portion of the aquifer and the springshed boundary. Bloomer well is located over the Balcones Fault Zone at the transition zone between the confined and unconfined portions of the aquifer and is within the springshed boundary. Avila well is located in the confined portion of the aquifer outside of the springshed. Samples were collected at these sites to geochemically distinguish groundwater within and outside of the estimated springshed boundary. The same sites were sampled again in August except for Robertson Spring because groundwater was not flowing at the spring outlet due to dry conditions. Both sampling events were conducted during low-flow conditions when flow along Salado Creek was recorded at 10 cfs and 7.42 cfs (Figure 15). Median flow over the last 7 years on the days samples were taken for this study were approximately 19 cfs and 13 cfs, respectively. During the period of this study, flow remained below median conditions for all but a few brief periods (Figure 15).

The major ionic constituents at the five sites on June 19 and August 21, are listed in Tables 2 and 3, respectively. Results from both sampling events were consistent. In general, groundwater in the unconfined portion of the aquifer was a calcium-bicarbonate water, but groundwater in the deeper confined aquifer was a sodium-bicarbonate water. A higher concentration of most ions were found in the down-dip, confined portion of the aquifer. For example, maximum sodium, potassium, fluoride, chloride, and sulfate concentrations were found at the Avila well in both sampling efforts (Tables 2 and 3). These constituents generally increase along flow paths from the unconfined to confined portion of the aquifer due to longer groundwater residence time allowing for more rock-water interactions (Jones, 2020). The unconfined portion of the aquifer, where a majority of the estimated springshed is concentrated, has lower ionic concentrations because of the constant circulation of fresh groundwater from recharge (Senger and others, 1990). Piper trilinear and Stiff diagrams were used to display the hydrochemical facies of groundwater samples collected in the summer of 2020 (Figures 26 and 27). The diagrams highlight the similarities and differences in groundwater chemistry among the sample sites and the stark difference in the confined aquifer water. The springs, Young and Bloomer wells are clustered together on the Piper trilinear diagram, whereas the well in the confined portion is isolated in the sodium-bicarbonate hydrochemical facies. Big Boiling and Robertson Springs had similar ionic concentrations, which indicates these two springs may be hydraulically connected (Figures 26 and 27, Tables 2 and 3). Both the Young and Bloomer wells had similar ionic chemistry to the springs, while the Avila well does not. These results indicate the deeper flow system does not contribute directly to discharge at the DSSC.

Table 2. Ionic chemistry results for spring and well samples collected on June 19, 2020 in the Northern Segment of the Edwards (BFZ) Aquifer.

Parameter	Robertson Spring	Big Boiling Spring	Young (Unconfined)	Bloomer (BFZ)	Avila (Confined)
Calcium (mg/L)	93	92.6	101	84.2	24.6
Magnesium (mg/L)	15.4	15.3	31.4	24.8	15.5
Sodium (mg/L)	11.8	12.3	25.7	14.2	286
Potassium (mg/L)	1.19	1.22	1.16	1.3	7.26
Fluoride (mg/L)	0.227	0.242	0.281	1.6	5.57
Chloride (mg/L)	14.2	15	34.9	14.6	169
Sulfate (mg/L)	18.2	19.1	20.2	32.4	202
Bicarbonate (mg/L)	312.32	329.4	427	336.27	390.4
Specific Conductance (µS/cm)	602	604	802	629	1568
Water Type	Ca-HCO_3	Ca-HCO_3	Ca-HCO_3	Ca-HCO_3	Na-HCO_3

* Discharge at Salado Creek was 10 cfs on June 19, 2020.

Table 3. Ionic chemistry results for spring and well samples collected on August 21, 2020 in the Northern Segment of the Edwards (BFZ) Aquifer.

Parameter	Robertson Spring (not sampled)	Big Boiling Spring	Young (Unconfined)	Bloomer (BFZ)	Avila (Confined)
Calcium (mg/L)	–	93.3	103	85.5	24.7
Magnesium (mg/L)	–	14.7	29.1	22.6	14.1
Sodium (mg/L)	–	11.7	24.7	14.4	284
Potassium (mg/L)	–	1.18	1.38	1.33	7.52
Fluoride (mg/L)	–	0.251	0.281	1.56	5.27
Chloride (mg/L)	–	13.7	33.4	13.9	160
Sulfate (mg/L)	–	17.5	19.7	31.6	192
Bicarbonate (mg/L)	–	326.96	448.96	358.68	400.16
Specific Conductance (µS/cm)	–	594	796	623	1558
Water Type	–	$Ca\text{-}HCO_3$	$Ca\text{-}HCO_3$	$Ca\text{-}HCO_3$	$Na\text{-}HCO_3$

* Discharge at Salado Creek was 7.42 cfs on August 21, 2020.

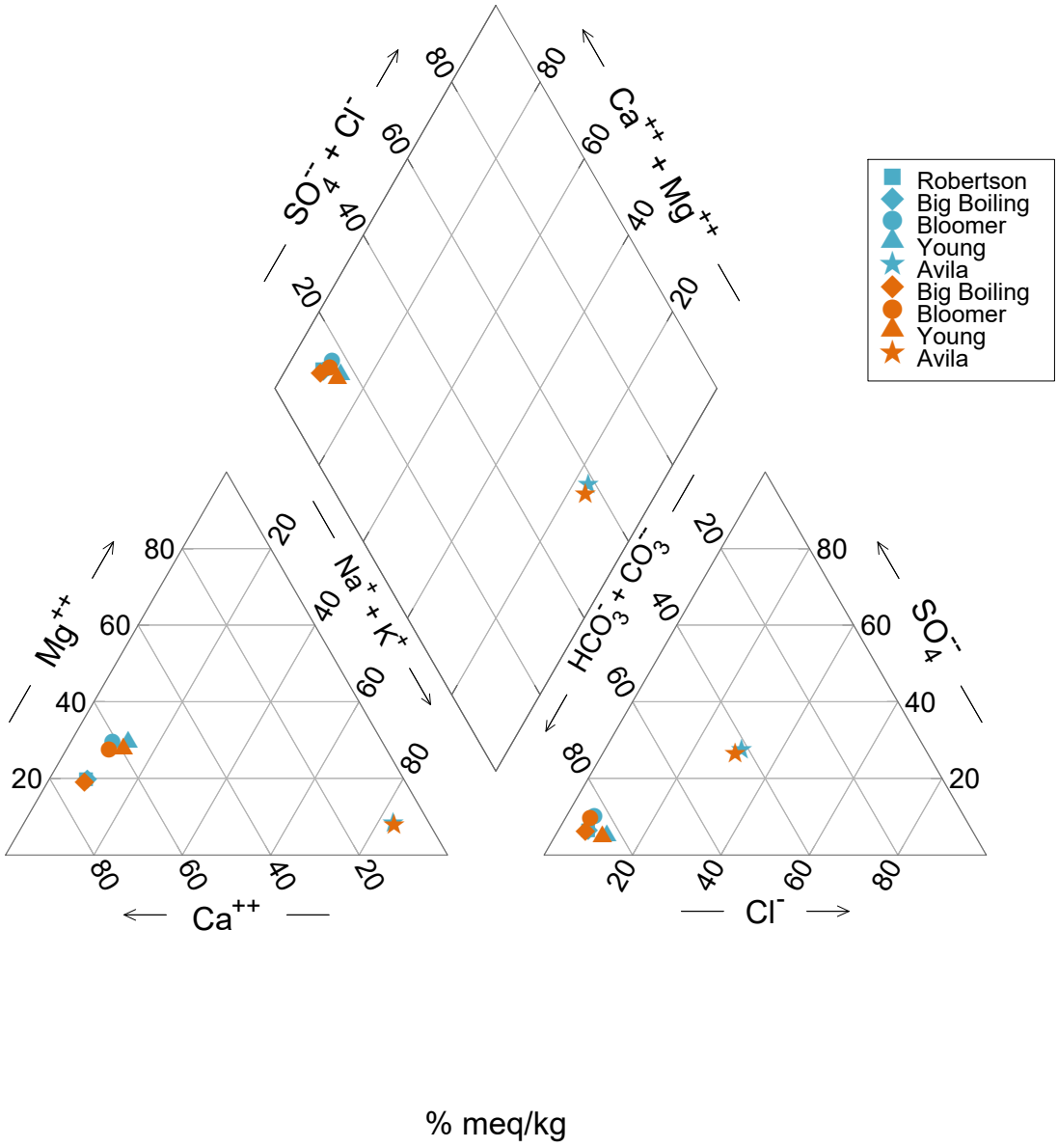

Figure 26. Piper trilinear plot of groundwater samples for wells and springs from sampling that took place on June 19, 2020 (blue symbols) and August 21, 2020 (orange symbols).

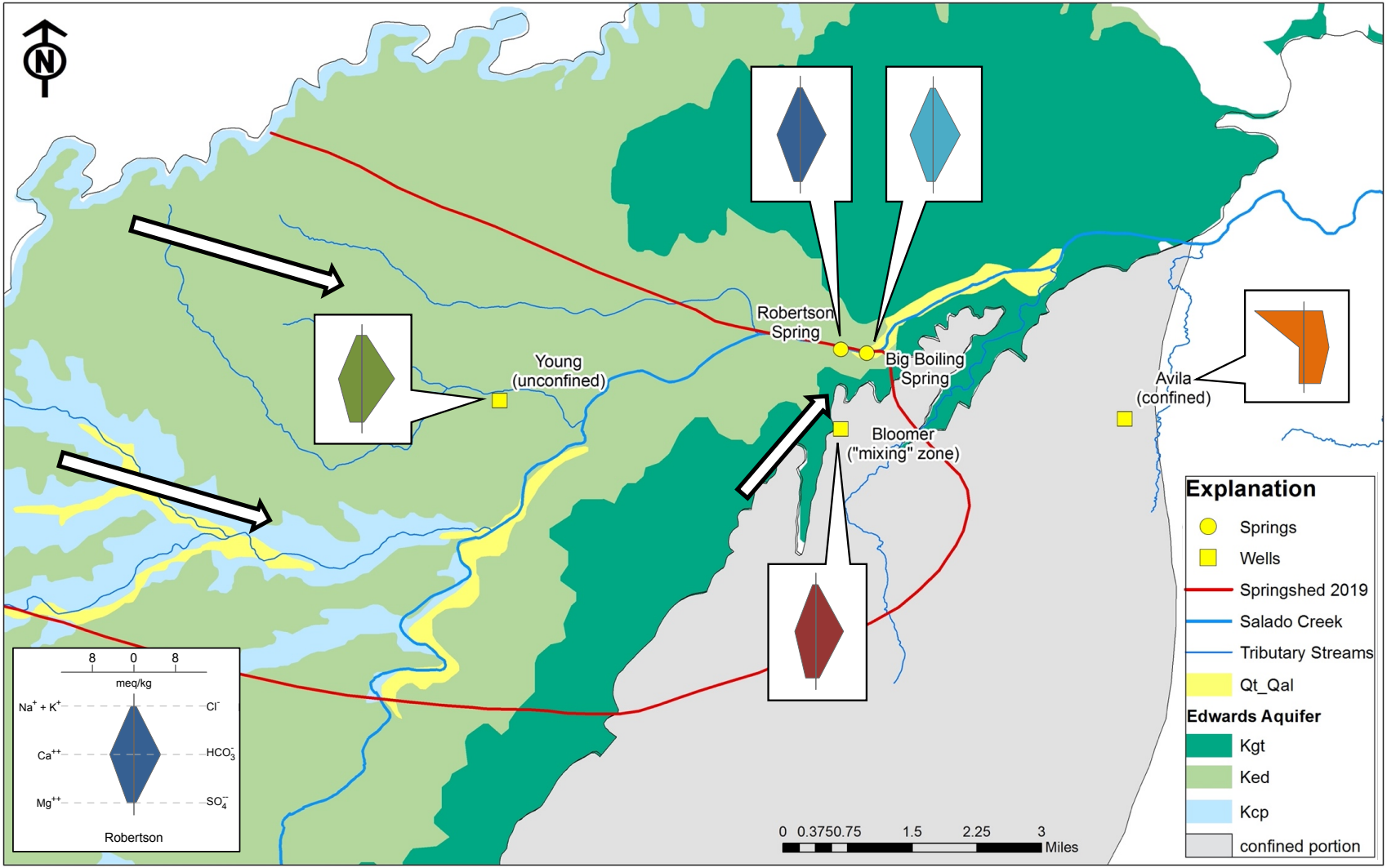

Figure 27. Stiff diagrams for sampling points on June 19, 2020. White arrows mark the general groundwater flow paths.

Tables 4 and 5 list the unstable isotopes analyzed on June 19, 2020 and August 21, 2020 from the springs and wells sampled. Results from the unstable isotopes from both sampling events were also consistent (Tables 4 and 5). Carbon-14 and tritium values were analyzed to determine groundwater ages throughout the Salado Springshed and into the confined portion of the Northern Segment. "Apparent" ages (uncorrected) estimated from the dissolved inorganic carbon content that were sampled in June were 1,110 years before present (BP) at Robertson Spring and 1,120 years BP at Big Boiling Spring. Young well, located in the upper, unconfined portion of the springshed boundary, had an "apparent" age of 690 years BP, while the Bloomer well located further downgradient had an "apparent" age of 3,490 years BP. Lastly, the Avila well in the confined portion had an "apparent" age of 31,260 years BP. The "apparent" ages (uncorrected) estimated from the carbon-14 values indicate that the groundwater becomes older as you move downgradient towards the springs and east towards the confining portion of the aquifer. The youngest signature was found at the Young well indicating recharge from precipitation occurs on the outcrop portion of the aquifer. The Bloomer well is in the transition zone from unconfined to confined portions of the aquifer and shows a possible mix of recent recharge and older water, which may be higher due to pumping that could be drawing water from both portions of the aquifer in this area. The percent modern carbon at the Young well was 91.81% due to recharge taking place in the shallow portion of the aquifer, in comparison to a percent modern carbon of 2.04% at the Avila well where most of the ^{14}C isotope had been decayed (Table 4). The carbon-14 dating method serves as a useful tool for determining flow rates and direction of groundwater flow (Mook and Rozanski, 2000). The carbon-14 activity will

decrease overtime as flow travels from the shallow, unconfined portion of the aquifer that receives recharge to the deep, confined portion where there is no recharge (Jones, 2020).

Tritium isotopic compositions at the five sites also showed the same pattern as carbon-14 (Tables 4 and 5). Tritium is the radioactive hydrogen isotope given in tritium units (TU). One TU represents one tritium atom to 10^{18} hydrogen atoms (Mook and Rozanski, 2000). The tritium isotopic composition was greatest at the Young well with 2.14 tritium units (TU) and the smallest composition was 0.09 TU at the Avila well (Table 4). These tritium results show that recent recharge occurs in the unconfined portion of the aquifer and older, slowly circulating groundwater is in the confined portion. Tritium values typically range from 0 to 3.0 TU in the Northern Segment of the Edwards (BFZ) Aquifer with tritium near 0 TU in the confined portion (Jones, 2020) as shown at the Avila well.

The resulting ionic chemistry and isotopic composition of the samples confirm interpretations made from the estimated springshed boundary. The calcium-bicarbonate water sourced from the wells upgradient in the springshed appears similar to the water chemistry at the springs. A sodium-bicarbonate water sourced from a well outside of the estimated springshed boundary provides evidence of a different flow path that does not contribute to discharge at the DSSC. Additionally, radiocarbon dating and tritium behavior of the samples present “apparent” age patterns and tritium values that support the general springshed boundary and the flow system interpretation.

Table 4. Radioactive isotope results for spring and well samples collected on June 19, 2020 in the Northern Segment of the Edwards (BFZ) Aquifer.

Parameter	June 19, 2020 – 10 cfs at Salado Creek Gauge				
	Robertson Spring	Big Boiling Spring	Young (Unconfined)	Bloomer (BFZ)	Avila (Confined)
Percent Modern Carbon	87.07 ± 0.31	86.96 ± 0.31	91.81 ± 0.33	64.74 ± 0.33	2.04 ± 0.04
"Apparent" Radiocarbon Age	1110	1120	690	3490	31260
Tritium (TU)	1.50	1.59	2.14	0.63	0.09

Table 5. Radioactive isotope results for spring and well samples collected on August 21, 2020 in the Northern Segment of the Edwards (BFZ) Aquifer.

Parameter	August 21, 2020 – 7.42 cfs at Salado Creek Gauge				
	Robertson Spring (not sampled)	Big Boiling Spring	Young (Unconfined)	Bloomer (BFZ)	Avila (Confined)
Percent Modern Carbon	–	85.98 ± 0.31	93.06 ± 0.34	64.64 ± 0.23	1.61 ± 0.04
"Apparent" Radiocarbon Age	–	1210	580	3510	33150
Tritium (TU)	–	1.43	1.53	0.64	0.45

Isotope Analysis of Precipitation Events

The stable isotope composition of groundwater can be used as a natural tracer to investigate recharge to the aquifer sourced from meteoric precipitation. The fractionation of hydrogen and oxygen isotopes (^{1}H, ^{2}H, ^{16}O, ^{18}O) are useful in understanding seasonal variations of meteoric precipitation caused by the ambient temperature during a precipitation event, the amount of precipitation, and the distance from a moisture source. The fractionation of hydrogen and oxygen are associated with phase changes from vapor to liquid, produced by evaporation and condensation. During evaporation, the lighter isotopologue has more vibrational energy and will be removed from a water body surface more easily than the heavier isotopologue. When an air mass begins to cool, it reaches supersaturation causing the heavier isotopologues to preferentially fractionate into the condensed phase (Sharp, 2017). The mean annual weighted oxygen isotopic composition of precipitation in central Texas is -4.03‰ $\delta^{18}O$ VSMOW (IAEA/WMO, 2021). Since precipitation is the main source of recharge to the Northern Segment of the Edwards (BFZ) Aquifer, hydrogen and oxygen isotopes were used to assess precipitation over the springshed and groundwater discharging at the DSSC to determine how specific recharge events may influence groundwater flow paths.

Over the course of this study, six rain events were sampled during the summer, fall, and winter of 2020. Samples were collected within 7 days before and after rainfall took place at the outlet of Big Boiling Spring and from Salado Creek. This 7-day lag period was used based on Dahl (1990), which states that Salado Creek will return to baseflow conditions on average 3 days after a precipitation event. This lag period was determined prior to analyzing the baseflow and streamflow response time for the statistical model

(Figure 19) that showed that flow at the DSSC will respond 1 to 5 days after a recharge event. The average 3-day equilibration period stated in Dahl (1990) is supported by the flow response shown in Figure 19. The purpose of collecting samples before and after a rain event was to determine if there were any changes to the isotopic composition of the groundwater discharging at Big Boiling Spring as a result of precipitation recharging the aquifer and mixing with the stored groundwater. Precipitation samples were also collected during each rain event. The isotopic composition of all samples can be found in Appendix C. The spring, creek, and precipitation samples will be discussed with reference to their oxygen isotopic composition since their hydrogen isotopic composition reflects the same trends. A bivariate plot of the hydrogen and oxygen isotopic composition of the samples collected for each rain event are shown in Figure 28 along with the LMWL. The LMWL is the long-term covariation of hydrogen and oxygen isotope ratios for Riesel, Texas and was generated from isotopic composition datasets of precipitation from 1961 to 1986 collected by the International Atomic Energy Agency (IAEA) Global Network of Isotopes in Precipitation (GNIP) program. Riesel is located about 50 miles northeast of Salado, Texas. The equation of this LMWL is $\delta D = 6.51\delta^{18}O + 4.58$ and the mean annual weighted oxygen isotopic composition based on the dataset is -4.03‰ $\delta^{18}O$ VSMOW (IAEA/WMO, 2021).

The spring and creek samples collected in 2020 before and after each of the six rain events fall along the LMWL (Figure 28). The creek samples show a slightly heavier isotopic signature than the spring samples due to the evaporation process of surface water. The creek samples lie within -4.46 ‰ and -2.82 ‰ $\delta^{18}O$ VSMOW, with an average of

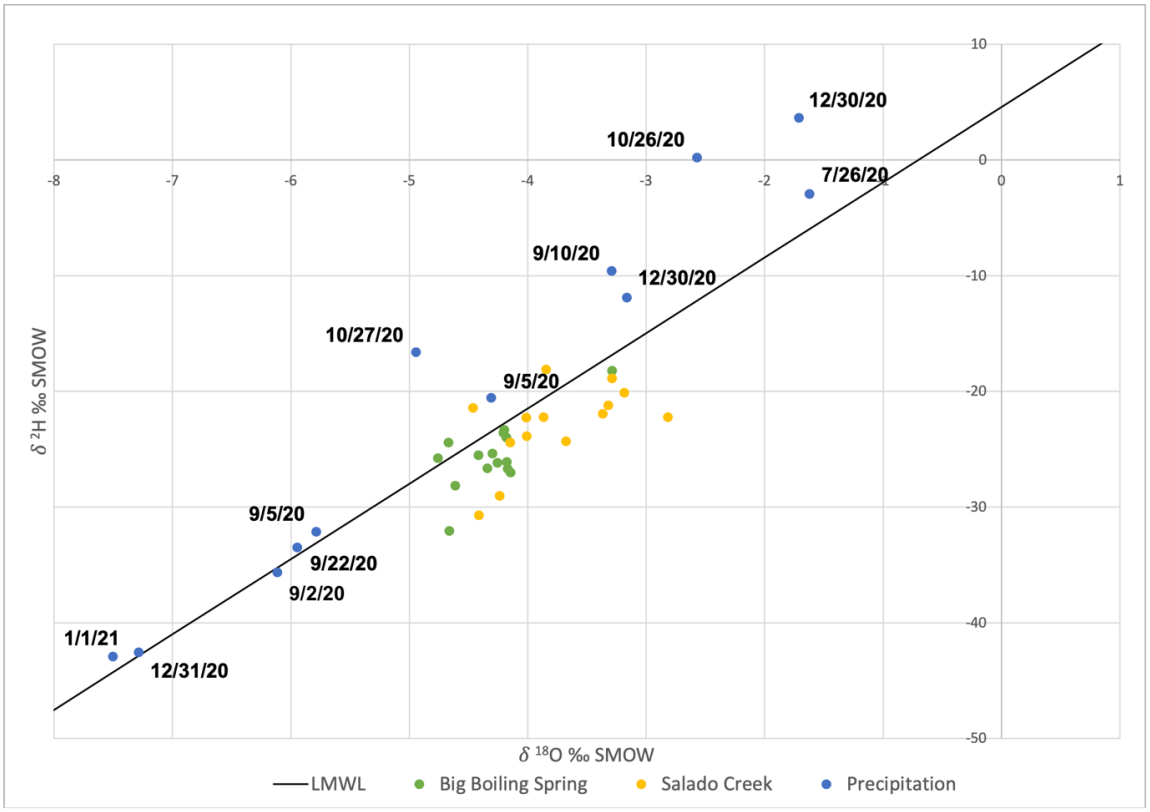

Figure 28. Bivariate plot of hydrogen versus oxygen isotopic composition of water samples and the Local Meteoric Water Line. Precipitation samples are labeled with the date they were taken.

-3.76 ‰ δ^{18}O VSMOW. Comparatively all but one of the spring samples lie within -4.76 ‰ and -4.14 ‰ δ^{18}O VSMOW, with an average of -4.29 ‰ δ^{18}O VSMOW. Overall, most of the spring and creek samples plot on or slightly below the LMWL indicating that the groundwater will experience evaporation prior to recharging the aquifer and prior to entering Salado Creek as runoff and creek samples (Dansgaard, 1964). The Northern Segment of the Edwards (BFZ) Aquifer is mainly recharged by precipitation therefore, the average isotopic composition of the spring (-4.29‰) is near the average isotopic composition of precipitation in central Texas (-4.03‰). The groundwater discharging at the spring represents a mixture of the local precipitation that enters the

aquifer, which will vary temporally depending on the ambient temperature and the precipitation amount (Dansgaard, 1964). Because of these factors, the precipitation samples cover a greater range of isotopic composition in comparison to the spring and creek samples (Figure 28). The mixing process of precipitation water in the aquifer matrix and within factures and conduits, as well as within the creek, corresponds to the narrow range of isotopic compositions for the samples taken at Big Boiling Spring and along Salado creek.

The precipitation samples ranged from -7.51 ‰ to -1.61 ‰ δ^{18}O VSMOW, with an average of -4.80 ‰ δ^{18}O VSMOW (Figure 28). The average oxygen isotopic composition calculated from the precipitation samples collected for this study is slightly lighter than the average composition obtained by the IAEA since the dataset in this study does not represent a long-term average (IAEA/WMO, 2021). The oxygen isotopic composition of precipitation was analyzed against the average temperature during each rain event to determine their relationship (Figure 29 and Table 6). The δ^{18}O values of precipitation decrease with decreasing temperature, representing a direct relationship between the two variables. Vapor masses that evolve under cold conditions experience greater depletion in ^{18}O and ^{2}H as isotope fractionation increases at colder temperatures (Dansgaard, 1964 and Ingraham, 1998). Even though a trend is visible between the oxygen isotopic fractionation of precipitation and the ambient temperature, the correlation shown in Figure 29 is not very significant (R^2 = 0.22) due to a small dataset used. Next, precipitation δ^{18}O values were compared with precipitation amounts that occurred each day rain samples were collected (Figure 30 and Table 6). Precipitation amounts also serve as a control on the oxygen isotope composition of the precipitation in that δ^{18}O values will

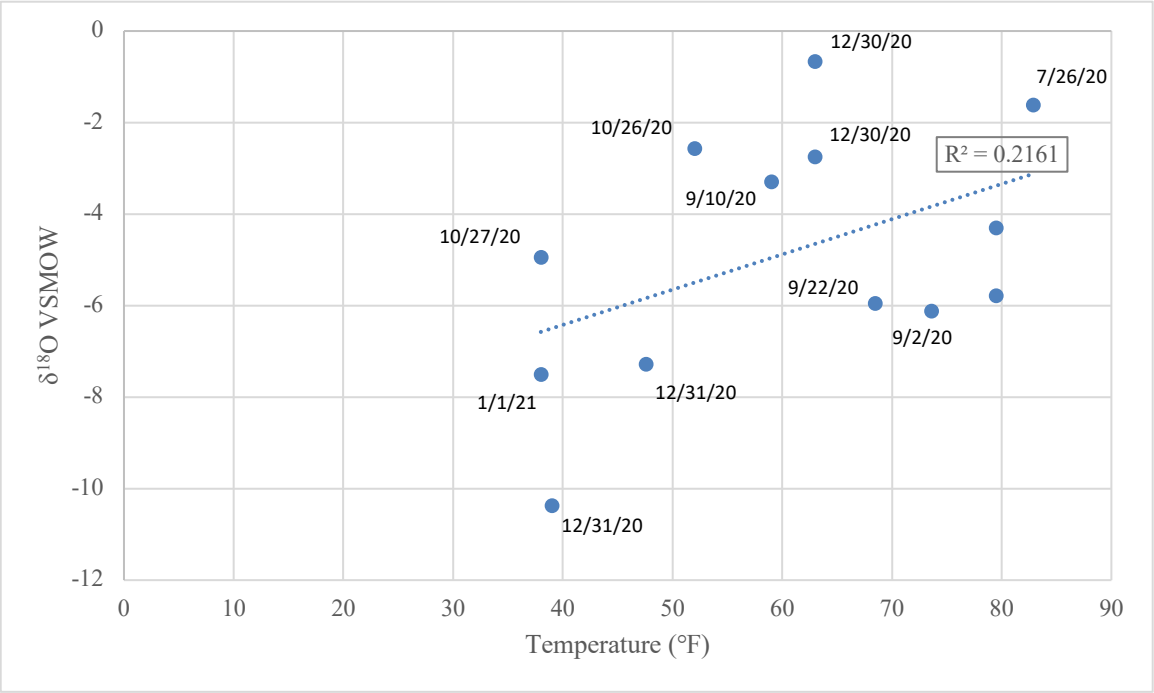

Figure 29. The $\delta^{18}O$ values for precipitation samples versus average air temperature during each rain event. Samples are labeled with the date they were taken.

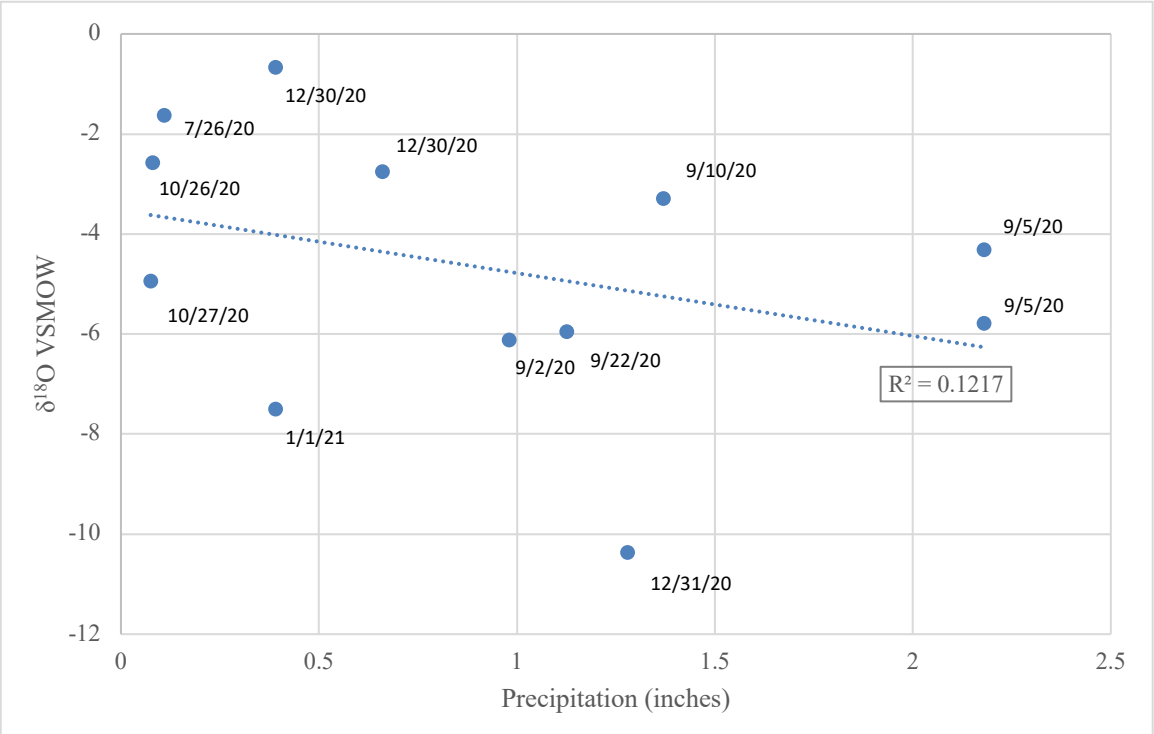

Figure 30. The $\delta^{18}O$ values for precipitation samples versus total rainfall amount of each rain event. Samples are labeled with the date they were taken.

Table 6. Total rainfall amount and mean air temperature of each rain event sampled.

Date	Rainfall Total (in)	Mean Temp Range (°F)
7/26/20	0.11	82.9
9/2/20	0.98	73.6
9/5/20	2.18	79.5
9/10/20	1.37	59
9/22/20	1.13	68.5
10/26/20	0.08	52
10/27/20	0.08	38
12/30/20	1.05	63
12/31/20	1.28	39
1/1/21	0.39	38

decrease with increasing rainfall amount. The more rain that falls during a given event, the more the precipitation becomes depleted in ^{18}O and ^{2}H (Dansgaard, 1964). This relationship is shown in Figure 30, but the correlation is also not very significant (R^2 = 0.12) because of the small dataset used.

To investigate how recharge to the Northern Segment of the Edwards (BFZ) Aquifer occurs, precipitation, spring, and creek oxygen isotope ratios were plotted over time to assess how individual rain events might influence the isotopic composition of groundwater and surface water (Figure 31). Of the rain events shown in Figure 31, three show a clear response at Big Boiling Spring and Salado Creek from the precipitation that entered the aquifer. Precipitation that occurred on July 26 had the highest $\delta^{18}O$ value of -1.62‰. The spring and creek samples collected within 6 days before and 2 days after

July 26 show a prominent shift towards a higher $\delta^{18}O$ value, which was influenced by precipitation. The spring and creek oxygen isotope composition increased by 0.74‰ and 0.41‰, respectively. Precipitation samples that were collected on September 2 and 5, had an average $\delta^{18}O$ value of -5.41‰, which caused the oxygen isotope composition of both the spring and creek to decrease slightly. The following rain event on September 10, had a much higher $\delta^{18}O$ value of -3.29‰ that caused values of the spring and creek to increase. On September 22, the precipitation sample had a low oxygen isotope composition of -5.95‰, but the spring and creek samples taken before and after this rain event continued to increase rather than shift towards the isotopic signature of the precipitation. It is possible that recharge from the previous rain event on September 10, was still passing through conduits in the aquifer and discharging at Big Boiling Spring and evaporation of surface water had taken place causing Salado Creek to become more enriched in ^{18}O. Rain events that took place on October 26-27 and December 30-January 1, produced precipitation samples with a wide range in oxygen isotope compositions (Figure 31). $\delta^{18}O$ values of the precipitation samples throughout each event decreased as a result of the temperature effect shown in Figure 29 (Dansgaard, 1964). Mean daily ambient temperatures during these events decreased from the first to the last day of rainfall by 14 °F and 25 °F, respectively, resulting in a depletion in ^{18}O on both occasions (Table 6). The $\delta^{18}O$ values of the precipitation samples collected throughout the rain events on October 26-27 and December 30-January 1 declined over time, but a corresponding signal of the oxygen isotope composition of groundwater and surface water sampled was not evident (Figure 31). More specifically, the oxygen isotope composition measured at Big Boiling Spring decreased from before to after the rain events, but not at the rate the isotope composition

dropped for the precipitation samples. The $\delta^{18}O$ values at Salado Creek increased from before to after the rain events. Overall, oxygen isotope compositions of the creek samples increased from before and after each of the six rain events sampled, likely due to evaporation expected for surface water. The oxygen isotope compositions of the spring samples remained around the average isotopic composition of precipitation in central Texas (-4.03‰), which greatly reduced the recharge response signal due to long-term mixing of rainwater within the aquifer matrix. These findings indicate that the isotope composition of a given recharge event may not always appear at the DSSC once the creek returns to baseflow conditions. A recharge signal at the DSSC is strongly dependent on where precipitation is concentrated within the creek basin or springshed. The recharging water may flow towards the springs through a direct conduit flow path or instead mix within the aquifer matrix and influence the long-term isotopic composition of the Edwards (BFZ) Aquifer.

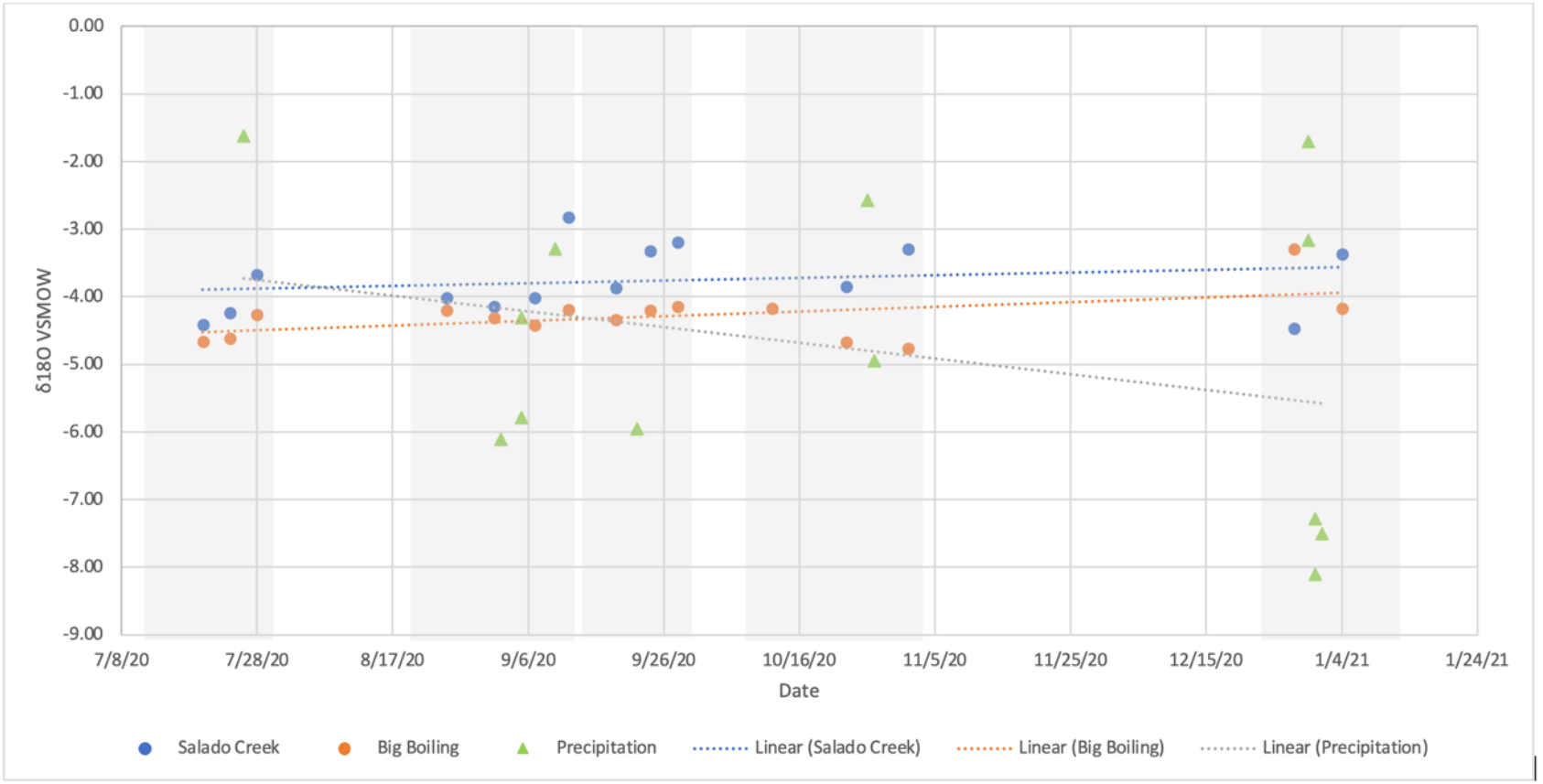

Figure 31. The $\delta^{18}O$ values for spring, creek, and precipitation samples over time with trendline shown for each sample type. Grey boxes mark separate rain events.

CHAPTER FIVE

Summary and Conclusions

The estimated Salado Springshed boundary is a representative model for groundwater flow paths that discharge at the DSSC based on geochemical sampling and statistical approaches using hydrologic data. Stillhouse Hollow Reservoir and the losing stream section on the southern portion of Salado Creek are located outside of the springshed boundary but may have a hydrogeologic connection to the DSSC or baseflow to Salado Creek based on the rainfall and springflow statistical model.

1a. The Salado Springshed boundary was estimated from synoptics maps generated using water-level data collected in 2010, 2013, and 2019 throughout the Salado Creek Basin. The estimated boundary encompassed a consistent area under each of the different flow conditions. A majority of the springshed is over the outcrop portion of the Northern Segment of the Edwards (BFZ) Aquifer, where precipitation can easily recharge through the highly fractured Edwards Limestone Formation.

1b. Total pumping from the aquifer in the area has increased since 1980, which has likely caused the Salado Springshed boundary to extend further east overtime.

2a. Hydrographs show that baseflow and streamflow will respond to precipitation over the Northern Segment of the Edwards (BFZ) Aquifer within 1 to 5 days and at varying magnitudes. This lagged response is dependent on where most of the rainfall is concentrated within the basin during a given event.

2b. The linear regression models highlight the moderately strong correlation between baseflow in Salado Creek and surface elevation at the Stillhouse Hollow Reservoir with correlation values of 0.59. The surface elevation of the reservoir served as a proxy to numerically account for antecedent moisture content in the basin.

2c. Based on the optimally fitted model for baseflow and streamflow, the WSR-88D stations that are concentrated within the estimated springshed boundary produce the greatest change in flow at the gauge. These results statistically model precipitation over the outcrop portion of the aquifer as a primary source of recharge. The rainfall and springflow statistical model also highlighted the losing stream section on the southern portion of Salado Creek and Stillhouse Hollow Reservoir as significant contributors to changes in flow along Salado Creek at the USGS gauge after a given rain event.

3a. Groundwater samples collected during low flow conditions on June 19, 2020 and August 21, 2020 produced consistent results. Ionic chemistry and isotopic compositions indicate young, calcium-bicarbonate water in the unconfined portion of the aquifer within the springshed boundary compared to older, sodium-bicarbonate water in the confined portion outside of the springshed. This stark difference points to a deeper groundwater flow system in the confined portion of the aquifer that does not contribute to the DSSC.

3b. Water samples from the Northern Segment of the Edwards (BFZ) Aquifer plot on or near the local meteoric water line and have an average isotopic composition near the mean annual weighted isotopic composition of precipitation in central Texas because groundwater represents long-term mixing of the local precipitation. Salado

Creek samples also plot on or near the local meteoric water line but show a slightly heavier isotopic signature than the groundwater samples due to evaporation. Precipitation samples cover a greater range of isotopic composition in comparison to spring and creek samples because of the temperature and amount effect (Dansgaard, 1964).

3c. The isotopic composition of a given recharge event may not always be present at the DSSC because the recharge response signal from groundwater is greatly reduced due to long-term mixing of rainwater within the aquifer matrix.

CHAPTER SIX

Recommendations

1. Water-level data need to be collected more frequently and with greater density to continue to refine the Salado Springshed and better understand how the aquifer may respond under different flow conditions.
2. Synoptic maps are biased towards equilibrated water-level data and therefore do not show quick recharge pulses from the losing stream section along Salado Creek and from Stillhouse Hollow Reservoir after a significant rain event as shown in the rainfall and springflow statistical model. Future work should strongly focus on studying these sites north and south of the estimated springshed boundary by collecting more detailed water-level data under different hydrologic conditions and conducting dye trace tests after recharge events to better understand groundwater flow paths contributing baseflow in Salado Creek and to the DSSC.
3. Larger and continuous data sets analyzed through groundwater models and machine learning could be used to quantify recharge to the aquifer more accurately.
4. Geochemical data need to be collected more frequently throughout the Salado Springshed to identify how flow may respond to different recharge events.
5. Research on the Northern Segment of the Edwards (BFZ) Aquifer needs to continue in order to further identify key areas of recharge and better understand groundwater flow paths in the area to aid in groundwater management decisions.

APPENDICES

APPENDIX A

WSR-88D Data for Statistical Correlation Analysis

Table A.1. Rain totals for the 88D grid points for the September 4-13, 2018 event.

GEO_ID	LAT	LON	9/4/18	9/5/18	9/6/18	9/7/18	9/8/18	9/9/18	9/10/18	9/11/18	9/12/18	9/13/18	TOTAL	UNITS
8443	30.7385	-97.7373	0.5315	0.0197	0.6732	0.563	0.9291	0.0551	1.6732	0.0433	0.1496	0.0118	4.6495	INCHES
30536	30.9752	-97.6612	0.8583	0.2677	0.9961	0.0748	0.4567	0.1102	0.626	0.0433	0.1575	0	3.5906	INCHES
43466	30.8418	-97.7220	0.7205	0.0354	1.0866	0.3386	1.5866	0.0984	2.2008	0.0591	0.2362	0.0197	6.3819	INCHES
43523	30.9150	-97.7519	0.8622	0.2402	1.7677	0.6299	0.7913	0.3701	1.3543	0.122	0.2087	0	6.3464	INCHES
59326	30.9362	-97.6262	0.8071	0.1024	1.2795	0.063	0.6535	0.0315	0.7992	0.0354	0.2402	0.0236	4.0354	INCHES
61929	30.8461	-97.7621	0.6693	0.0433	1.3032	0.4685	1.0591	0.1693	2.4803	0.1575	0.2362	0	6.5867	INCHES
63885	30.8373	-97.6819	0.563	0.1339	0.7205	0.5945	1.2402	0.0709	1.811	0.0394	0.2165	0.1299	5.5198	INCHES
73302	30.9662	-97.5808	0.3543	0.0945	1.2835	0.3346	0.5866	0.0236	0.5118	0.0315	0.189	0	3.4094	INCHES
98720	30.8973	-97.5913	0.9291	0.1535	1.4724	0.1339	0.811	0	1.1417	0.0354	0.1575	0.0394	4.8739	INCHES
122207	30.8762	-97.7169	0.7913	0.3268	1.2756	0.6299	1.2323	0.1299	1.9291	0.1496	0.3346	0	6.7991	INCHES
154077	30.8029	-97.6870	0.1732	0.0157	0.9764	0.4252	1.122	0.0512	1.8307	0.0236	0.1969	0	4.8149	INCHES
165670	30.9617	-97.5406	0.311	0.0315	1.4567	0.5039	0.5315	0.0433	0.4961	0.0394	0.1732	0.0157	3.6023	INCHES
195800	30.9407	-97.6664	1.2992	0.3583	1.3189	0.189	0.7087	0.0787	0.8386	0.0433	0.2598	0	5.0945	INCHES
206081	30.8806	-97.7570	0.6693	0.1378	1.0866	0.4055	0.9291	0.2874	1.9094	0.1772	0.1772	0	5.7795	INCHES
219192	31.0007	-97.5756	0.2953	0.2717	1.0984	0.2953	0.6929	0.0236	0.4764	0.0315	0.1614	0.0039	3.3504	INCHES
233427	30.7641	-97.6521	0.3898	0.0157	1.1024	0.685	0.7126	0.0354	1.4528	0.0315	0.189	0	4.6142	INCHES
234955	30.7729	-97.7322	0.7638	0.0157	0.9291	0.3504	1.3032	0.063	1.9094	0.0433	0.1929	0	5.5708	INCHES
235217	30.9917	-97.4951	0.4961	0	1.8032	0.1929	0.5276	0.063	0.5472	0.0354	0.1575	0.0315	3.8544	INCHES
241487	30.8673	-97.6366	1.3189	0.3307	1.1339	0.3071	1.2323	0.0512	1.5354	0.0315	0.1496	0.0157	6.1063	INCHES
253562	30.7985	-97.6470	0.2913	0.0118	0.8661	0.6142	0.6811	0.0394	1.4488	0.0315	0.0512	0	4.0354	INCHES
265023	30.7341	-97.6973	0.4094	0.0157	0.5866	0.4646	0.6693	0.0394	1.4331	0.0354	0.1496	0.0118	3.8149	INCHES
265067	30.8505	-97.8022	0.5157	0.2362	1.5984	0.2598	0.9291	0.4528	2.5906	0.1496	0.3661	0	7.0983	INCHES

Table A.1. Rain totals for the 88D grid points for the September 4-13, 2018 event—Continued

GEO_ID	LAT	LON	9/4/18	9/5/18	9/6/18	9/7/18	9/8/18	9/9/18	9/10/18	9/11/18	9/12/18	9/13/18	TOTAL	UNITS
268852	30.8850	-97.7972	0.9449	0.4567	1.5472	0.2126	0.685	0.5315	1.6339	0.1378	0.2323	0	6.3819	INCHES
277204	30.8893	-97.8373	1.2992	0.5039	1.9252	0.1299	0.5512	0.1929	1.4685	0.0787	0.1811	0	6.3306	INCHES
279978	30.9062	-97.6716	1.2992	0.252	1.4134	0.5866	0.9449	0.0827	1.0787	0.1693	0.2283	0.0551	6.1102	INCHES
307593	30.9018	-97.6314	1.2205	0.1339	1.4173	0.2008	0.8465	0.0591	1.0354	0.0591	0.1772	0.0827	5.2325	INCHES
312628	30.8629	-97.5965	0.9606	0.063	1.6457	0.2717	1.1575	0.0354	1.3504	0.0354	0.1772	0.0394	5.7363	INCHES
354401	30.8117	-97.7672	0.7992	0.0433	1.1929	0.4449	1.3032	0.1811	2.6693	0.0591	0.3346	0	7.0276	INCHES
372021	30.7685	-97.6922	0.2677	0.0197	1.0433	0.5354	0.811	0.0433	1.6496	0.0236	0.1339	0	4.5275	INCHES
378309	30.8718	-97.6767	1.0591	0.4173	1.1969	0.685	1.063	0.0787	1.6181	0.0945	0.2402	0	6.4528	INCHES
387424	30.9707	-97.6210	0.4724	0.0551	1.2008	0.122	0.5433	0.0591	0.6457	0.0315	0.0906	0	3.2205	INCHES
388864	30.9107	-97.7117	1.0433	0.315	1.7283	0.7008	0.8819	0.2677	1.2756	0.1969	0.2913	0.0197	6.7205	INCHES
389640	30.9451	-97.7066	1.2047	0.2953	1.6142	0.3583	0.5748	0.1969	0.8386	0.0512	0.2913	0	5.4253	INCHES
399079	30.8548	-97.8424	0.3543	0.2598	1.2441	0.1378	0.8268	0.2992	1.9646	0.1378	0.2205	0	5.4449	INCHES
422041	31.0307	-97.5301	0.2205	0.0906	1.9331	0.1811	0.8622	0.0787	0.5354	0.0394	0.1772	0.0197	4.1379	INCHES
424218	30.8247	-97.8875	0.2795	0.0394	1.3228	0.1339	0.8858	0.2559	1.9134	0.0827	0.1496	0	5.063	INCHES
478026	30.9962	-97.5354	0.315	0.0787	1.626	0.2008	0.5433	0.0709	0.4291	0.0394	0.0984	0.0118	3.4134	INCHES
507289	30.8329	-97.6418	0.7205	0.2402	0.6496	0.5354	1.1732	0.0433	1.4134	0.0197	0.1378	0	4.9331	INCHES
513543	30.7903	-97.8925	0.1614	0.0315	1.4685	0.5827	0.9094	0.1929	2.1457	0.0906	0.189	0	5.7717	INCHES
514429	30.9318	-97.5861	0.5315	0.437	1.2795	0.374	0.5709	0.0433	0.6102	0.0354	0.189	0	4.0708	INCHES
538879	30.8161	-97.8073	0.4528	0.1693	1.0472	0.3701	0.9291	0.4488	3.6732	0.1181	0.4488	0	7.6574	INCHES
539561	31.0052	-97.6158	0.3189	0.0709	1.1063	0.2087	0.4843	0.0945	0.5039	0.0236	0.2087	0	3.0198	INCHES
544185	30.7860	-97.8524	0.1339	0.1614	1.1929	0.4134	0.8386	0.2992	2.378	0.0591	0.2126	0	5.6891	INCHES
556304	30.8592	-97.8825	0.6024	0.1969	1.4606	0.0984	0.6339	0.0984	1.6181	0.0906	0.1024	0	4.9017	INCHES
559170	30.8204	-97.8474	0.3661	0.1142	1.0945	0.252	0.9764	0.3307	2.5118	0.0591	0.2795	0	5.9843	INCHES
560097	30.7816	-97.8124	0.1535	0.1929	1.126	0.3465	1.1654	0.1969	2.6496	0.063	0.2953	0	6.1891	INCHES
564547	30.7773	-97.7723	0.6654	0.1024	1.0079	0.3543	1.5276	0.1575	2.2441	0.0591	0.3504	0	6.4687	INCHES
565744	30.9572	-97.5004	0.3386	0	1.6299	0.374	0.4291	0.0551	0.6693	0.0354	0.2362	0.0039	3.7715	INCHES

Table A.1. Rain totals for the 88D grid points for the September 4-13, 2018 event—Continued

GEO_ID	LAT	LON	9/4/18	9/5/18	9/6/18	9/7/18	9/8/18	9/9/18	9/10/18	9/11/18	9/12/18	9/13/18	TOTAL	UNITS
581938	30.8073	-97.7271	0.3976	0.0236	1.1339	0.2756	1.3701	0.0827	2.1575	0.0394	0.2717	0	5.7521	INCHES
609938	30.9273	-97.5459	0.4449	0.248	1.3307	1.1142	0.7283	0.0433	0.6732	0.0315	0.1417	0.0039	4.7597	INCHES

Table A.2. Rain totals for the 88D grid points for the October 13-20, 2018 event.

GEO_ID	LAT	LON	10/13/18	10/14/18	10/15/18	10/16/18	10/17/18	10/18/18	10/19/18	10/20/18	TOTAL	UNITS
8443	30.7385	-97.7373	0.122	0.1339	0.0433	3.6417	0.2008	0.2559	0.2008	0.622	5.2204	INCHES
30536	30.9752	-97.6612	0.1535	0.0118	0.1339	3.5591	0.3465	0.1024	0.1732	1.063	5.5434	INCHES
43466	30.8418	-97.7220	0.1811	0.0748	0.0157	3.6339	0.2677	0.252	0.0787	0.9803	5.4842	INCHES
43523	30.9150	-97.7519	0.1969	0.0354	0.0157	3.6575	0.378	0.2283	0.0315	0.9094	5.4527	INCHES
59326	30.9362	-97.6262	0.1024	0.0354	0.0945	3.4252	0.2598	0.0512	0.248	1.1811	5.3976	INCHES
61929	30.8461	-97.7621	0.2008	0.0787	0.0315	3.6772	0.3071	0.2913	0.0984	0.9252	5.6102	INCHES
63885	30.8373	-97.6819	0.1181	0.0551	0.0157	3.437	0.2008	0.1575	0.1378	0.878	5	INCHES
73302	30.9662	-97.5808	0.1102	0.0118	0.0591	3.2913	0.2677	0.0433	0.1024	1.2756	5.1614	INCHES
98720	30.8973	-97.5913	0.1417	0.0394	0.0354	3.5079	0.2283	0.0827	0.1693	1.0591	5.2638	INCHES
122207	30.8762	-97.7169	0.1378	0.063	0.0315	3.5591	0.2677	0.1929	0.0591	1.0354	5.3465	INCHES
154077	30.8029	-97.6870	0.1142	0.0591	0.0197	3.563	0.1929	0.1614	0.0945	0.7283	4.9331	INCHES
165670	30.9617	-97.5406	0.0984	0.0118	0.0591	3.252	0.2717	0.0354	0.0433	1.2717	5.0434	INCHES
195800	30.9407	-97.6664	0.1024	0.0551	0.1024	3.5591	0.2874	0.1102	0.1929	1.1142	5.5237	INCHES
206081	30.8806	-97.7570	0.1929	0.0945	0.0157	3.4843	0.3268	0.2598	0.0787	0.9488	5.4015	INCHES
219192	31.0007	-97.5756	0.1142	0.0118	0.1811	3.3386	0.3268	0.0512	0.1102	1.378	5.5119	INCHES
233427	30.7641	-97.6521	0.1024	0.0984	0.0236	3.8032	0.1772	0.1024	0.1732	0.6417	5.1221	INCHES
234955	30.7729	-97.7322	0.122	0.0748	0.0394	3.5748	0.2283	0.2756	0.1535	0.752	5.2204	INCHES
235217	30.9917	-97.4951	0.0827	0.0236	0.0906	2.9685	0.248	0.0236	0.0039	1.2165	4.6574	INCHES
241487	30.8673	-97.6366	0.1299	0.0512	0.1102	3.4016	0.2087	0.1142	0.2126	0.9882	5.2166	INCHES
253562	30.7985	-97.6470	0.1299	0.063	0.0197	3.626	0.1969	0.0906	0.1969	0.626	4.949	INCHES
265023	30.7341	-97.6973	0.0787	0.1339	0.0315	3.6417	0.1772	0.1496	0.1811	0.5945	4.9882	INCHES
265067	30.8505	-97.8022	0.2323	0.0827	0.0354	3.874	0.3583	0.3346	0.1142	0.9567	5.9882	INCHES
268852	30.8850	-97.7972	0.2165	0.0551	0.0236	3.9291	0.3898	0.2874	0.0827	0.9213	5.9055	INCHES
277204	30.8893	-97.8373	0.1693	0.0551	0.063	4.0984	0.5433	0.3346	0.063	0.811	6.1377	INCHES
279978	30.9062	-97.6716	0.1181	0.0433	0.0945	3.5669	0.2913	0.1378	0.1772	1.122	5.5511	INCHES
307593	30.9018	-97.6314	0.1535	0.0709	0.1299	3.5551	0.2559	0.0709	0.2598	1.1063	5.6023	INCHES

Table A.2. Rain totals for the 88D grid points for the October 13-20, 2018 event—Continued

GEO_ID	LAT	LON	10/13/18	10/14/18	10/15/18	10/16/18	10/17/18	10/18/18	10/19/18	10/20/18	TOTAL	UNITS
312628	30.8629	-97.5965	0.122	0.0709	0.0551	3.6929	0.2402	0.0945	0.2795	1.0157	5.5708	INCHES
354401	30.8117	-97.7672	0.189	0.0748	0.0394	3.622	0.2874	0.311	0.122	0.9213	5.5669	INCHES
372021	30.7685	-97.6922	0.1575	0.0709	0.0236	3.6654	0.1772	0.1772	0.1339	0.6417	5.0474	INCHES
378309	30.8718	-97.6767	0.122	0.0512	0.0591	3.3701	0.252	0.1378	0.1693	0.9803	5.1418	INCHES
387424	30.9707	-97.6210	0.1181	0.0118	0.1102	3.4173	0.2795	0.0512	0.2008	1.1024	5.2913	INCHES
388864	30.9107	-97.7117	0.1024	0.0433	0.0709	3.5472	0.311	0.1732	0.0551	1.0236	5.3267	INCHES
389640	30.9451	-97.7066	0.1772	0.0315	0.1024	3.7323	0.378	0.1496	0.0551	1.0827	5.7088	INCHES
399079	30.8548	-97.8424	0.189	0.0945	0.0827	4.0118	0.4646	0.3504	0.1024	0.8504	6.1458	INCHES
422041	31.0307	-97.5301	0.0906	0	0.063	2.9252	0.3071	0.0315	0.0118	1.4606	4.8898	INCHES
424218	30.8247	-97.8875	0.1969	0.0945	0.0827	3.9528	0.4449	0.2795	0.1575	0.6693	5.8781	INCHES
478026	30.9962	-97.5354	0.1102	0.0118	0.0827	3.1339	0.2874	0.0315	0.0118	1.3701	5.0394	INCHES
507289	30.8329	-97.6418	0.0945	0.0551	0.0197	3.4646	0.1811	0.1339	0.1693	0.8898	5.008	INCHES
513543	30.7903	-97.8925	0.2323	0.0984	0.1181	3.7992	0.3898	0.315	0.1575	0.6929	5.8032	INCHES
514429	30.9318	-97.5861	0.1181	0.0354	0.0157	3.2047	0.2362	0.0591	0.1535	1.1063	4.929	INCHES
538879	30.8161	-97.8073	0.2717	0.1102	0.0787	3.9961	0.3268	0.3504	0.0984	1.0197	6.252	INCHES
539561	31.0052	-97.6158	0.1811	0.0118	0.2205	3.6654	0.3583	0.0591	0.1811	1.3032	5.9805	INCHES
544185	30.7860	-97.8524	0.252	0.1299	0.0827	3.626	0.3268	0.3661	0.2008	0.7913	5.7756	INCHES
556304	30.8592	-97.8825	0.1732	0.0551	0.0906	4.2165	0.5945	0.2559	0.1378	0.7441	6.2677	INCHES
559170	30.8204	-97.8474	0.248	0.122	0.0984	3.815	0.3543	0.3465	0.1417	0.8465	5.9724	INCHES
560097	30.7816	-97.8124	0.2283	0.0984	0.0551	3.6417	0.2874	0.3346	0.1693	0.878	5.6928	INCHES
564547	30.7773	-97.7723	0.1614	0.0787	0.0354	3.5472	0.2677	0.3268	0.2008	0.8228	5.4408	INCHES
565744	30.9572	-97.5004	0.1102	0.0236	0.0433	3.063	0.2205	0.0236	0.0315	1.1811	4.6968	INCHES
581938	30.8073	-97.7271	0.1339	0.063	0.0236	3.5945	0.2402	0.2362	0.1142	0.8465	5.2521	INCHES
609938	30.9273	-97.5459	0.1024	0.0354	0.0197	3.2717	0.2559	0.0394	0.0433	1.1614	4.9292	INCHES

Table A.3. Rain totals for the 88D grid points for the December 7-9, 2018 event.

GEO_ID	LAT	LON	12/7/18	12/8/18	12/9/18	TOTAL	UNITS
8443	30.7385	-97.7373	0.2756	2.0669	0.0197	2.3622	INCHES
30536	30.9752	-97.6612	0.2756	1.9843	0	2.2599	INCHES
43466	30.8418	-97.7220	0.2598	2.0709	0.0197	2.3504	INCHES
43523	30.9150	-97.7519	0.2598	1.9055	0.0236	2.1889	INCHES
59326	30.9362	-97.6262	0.248	2.0394	0	2.2874	INCHES
61929	30.8461	-97.7621	0.2953	2.0472	0.0236	2.3661	INCHES
63885	30.8373	-97.6819	0.2559	2.126	0.0354	2.4173	INCHES
73302	30.9662	-97.5808	0.2992	2.189	0	2.4882	INCHES
98720	30.8973	-97.5913	0.2756	2.0709	0.0315	2.378	INCHES
122207	30.8762	-97.7169	0.2323	1.9882	0.0394	2.2599	INCHES
154077	30.8029	-97.6870	0.2756	2.2165	0.0197	2.5118	INCHES
165670	30.9617	-97.5406	0.3189	2.315	0	2.6339	INCHES
195800	30.9407	-97.6664	0.2559	2.0472	0	2.3031	INCHES
206081	30.8806	-97.7570	0.2598	1.9252	0.0354	2.2204	INCHES
219192	31.0007	-97.5756	0.3307	2.1181	0	2.4488	INCHES
233427	30.7641	-97.6521	0.248	1.8937	0.0197	2.1614	INCHES
234955	30.7729	-97.7322	0.2717	2.0315	0.0157	2.3189	INCHES
235217	30.9917	-97.4951	0.2992	2.1299	0	2.4291	INCHES
241487	30.8673	-97.6366	0.2756	2.122	0.0236	2.4212	INCHES
253562	30.7985	-97.6470	0.2559	1.9606	0.0197	2.2362	INCHES
265023	30.7341	-97.6973	0.2756	1.9882	0.0236	2.2874	INCHES
265067	30.8505	-97.8022	0.3071	2.0315	0.0236	2.3622	INCHES
268852	30.8850	-97.7972	0.2795	1.9409	0.0354	2.2558	INCHES
277204	30.8893	-97.8373	0.2362	2.1024	0.0197	2.3583	INCHES
279978	30.9062	-97.6716	0.2677	2.0591	0.0197	2.3465	INCHES
307593	30.9018	-97.6314	0.2717	2.1811	0.0157	2.4685	INCHES

Table A.3. Rain totals for the 88D grid points for the December 7-9, 2018 event—Continued

GEO_ID	LAT	LON	12/7/18	12/8/18	12/9/18	TOTAL	UNITS
312628	30.8629	-97.5965	0.2953	2.1417	0.0236	2.4606	INCHES
354401	30.8117	-97.7672	0.3071	1.9803	0.0197	2.3071	INCHES
372021	30.7685	-97.6922	0.2874	2.1181	0.0197	2.4252	INCHES
378309	30.8718	-97.6767	0.2402	2.0591	0.0236	2.3229	INCHES
387424	30.9707	-97.6210	0.2598	1.9331	0	2.1929	INCHES
388864	30.9107	-97.7117	0.2795	1.9331	0.0236	2.2362	INCHES
389640	30.9451	-97.7066	0.2559	2.0197	0	2.2756	INCHES
399079	30.8548	-97.8424	0.2756	2.0709	0.0236	2.3701	INCHES
422041	31.0307	-97.5301	0.374	1.9606	0	2.3346	INCHES
424218	30.8247	-97.8875	0.252	2.0276	0.0197	2.2993	INCHES
478026	30.9962	-97.5354	0.3346	2.1654	0	2.5	INCHES
507289	30.8329	-97.6418	0.2795	2.1024	0.0315	2.4134	INCHES
513543	30.7903	-97.8925	0.2402	2.063	0.0197	2.3229	INCHES
514429	30.9318	-97.5861	0.2795	2.0906	0	2.3701	INCHES
538879	30.8161	-97.8073	0.3937	1.9213	0.0197	2.3347	INCHES
539561	31.0052	-97.6158	0.315	2.0906	0	2.4056	INCHES
544185	30.7860	-97.8524	0.2795	1.9409	0.0197	2.2401	INCHES
556304	30.8592	-97.8825	0.2165	2.1575	0.0236	2.3976	INCHES
559170	30.8204	-97.8474	0.2913	1.9055	0.0197	2.2165	INCHES
560097	30.7816	-97.8124	0.3189	2.0039	0.0197	2.3425	INCHES
564547	30.7773	-97.7723	0.3071	2.0118	0.0197	2.3386	INCHES
565744	30.9572	-97.5004	0.3268	2.1496	0	2.4764	INCHES
581938	30.8073	-97.7271	0.2913	2.0984	0.0197	2.4094	INCHES
609938	30.9273	-97.5459	0.315	2.3071	0.0157	2.6378	INCHES

Table A.4. Rain totals for the 88D grid points for the April 24-25, 2019 event.

GEO_ID	LAT	LON	4/24/19	4/25/19	TOTAL	UNITS
8443	30.7385	-97.7373	0.3937	2.1378	2.5315	INCHES
30536	30.9752	-97.6612	0.5709	2.0236	2.5945	INCHES
43466	30.8418	-97.7220	0.7795	2	2.7795	INCHES
43523	30.9150	-97.7519	0.626	1.5984	2.2244	INCHES
59326	30.9362	-97.6262	0.5748	2.2205	2.7953	INCHES
61929	30.8461	-97.7621	0.8386	1.8465	2.6851	INCHES
63885	30.8373	-97.6819	0.7638	2.3189	3.0827	INCHES
73302	30.9662	-97.5808	0.4882	2.4409	2.9291	INCHES
98720	30.8973	-97.5913	0.7677	2.3976	3.1653	INCHES
122207	30.8762	-97.7169	0.6654	2.063	2.7284	INCHES
154077	30.8029	-97.6870	0.5906	2.2559	2.8465	INCHES
165670	30.9617	-97.5406	0.5236	2.622	3.1456	INCHES
195800	30.9407	-97.6664	0.6142	2.3819	2.9961	INCHES
206081	30.8806	-97.7570	0.6614	1.815	2.4764	INCHES
219192	31.0007	-97.5756	0.4173	2.2559	2.6732	INCHES
233427	30.7641	-97.6521	0.3504	2.1417	2.4921	INCHES
234955	30.7729	-97.7322	0.6142	2.2362	2.8504	INCHES
235217	30.9917	-97.4951	0.4724	2.374	2.8464	INCHES
241487	30.8673	-97.6366	0.7008	2.4016	3.1024	INCHES
253562	30.7985	-97.6470	0.4134	2.2008	2.6142	INCHES
265023	30.7341	-97.6973	0.3189	2.0472	2.3661	INCHES
265067	30.8505	-97.8022	0.9055	1.7323	2.6378	INCHES
268852	30.8850	-97.7972	0.7992	1.5551	2.3543	INCHES
277204	30.8893	-97.8373	0.7126	1.6063	2.3189	INCHES
279978	30.9062	-97.6716	0.6142	2.315	2.9292	INCHES
307593	30.9018	-97.6314	0.7008	2.6181	3.3189	INCHES

Table A.4. Rain totals for the 88D grid points for the April 24-25, 2019 event—Continued

GEO_ID	LAT	LON	4/24/19	4/25/19	TOTAL	UNITS
312628	30.8629	-97.5965	0.6142	2.5591	3.1733	INCHES
354401	30.8117	-97.7672	0.8504	1.9724	2.8228	INCHES
372021	30.7685	-97.6922	0.4291	2.3386	2.7677	INCHES
378309	30.8718	-97.6767	0.6535	2.1614	2.8149	INCHES
387424	30.9707	-97.6210	0.5354	2.185	2.7204	INCHES
388864	30.9107	-97.7117	0.5551	1.9134	2.4685	INCHES
389640	30.9451	-97.7066	0.6063	1.9488	2.5551	INCHES
399079	30.8548	-97.8424	0.8425	1.7126	2.5551	INCHES
422041	31.0307	-97.5301	0.3386	2.1575	2.4961	INCHES
424218	30.8247	-97.8875	0.8189	1.7244	2.5433	INCHES
478026	30.9962	-97.5354	0.4488	2.4449	2.8937	INCHES
507289	30.8329	-97.6418	0.5827	2.4055	2.9882	INCHES
513543	30.7903	-97.8925	0.7677	1.6496	2.4173	INCHES
514429	30.9318	-97.5861	0.5906	2.5236	3.1142	INCHES
538879	30.8161	-97.8073	0.9803	1.748	2.7283	INCHES
539561	31.0052	-97.6158	0.4646	2.2992	2.7638	INCHES
544185	30.7860	-97.8524	0.7638	1.7677	2.5315	INCHES
556304	30.8592	-97.8825	0.6693	1.7244	2.3937	INCHES
559170	30.8204	-97.8474	0.8386	1.7047	2.5433	INCHES
560097	30.7816	-97.8124	0.7795	1.8937	2.6732	INCHES
564547	30.7773	-97.7723	0.748	2.0591	2.8071	INCHES
565744	30.9572	-97.5004	0.4843	2.378	2.8623	INCHES
581938	30.8073	-97.7271	0.7402	2.2953	3.0355	INCHES
609938	30.9273	-97.5459	0.622	2.5591	3.1811	INCHES

Table A.5. Rain totals for the 88D grid points for the May 2-4, 2019 event.

GEO_ID	LAT	LON	5/2/19	5/3/19	5/4/19	TOTAL	UNITS
8443	30.7385	-97.7373	0.1811	2.1102	1.1535	3.4448	INCHES
30536	30.9752	-97.6612	0.2559	2.7717	1.8465	4.8741	INCHES
43466	30.8418	-97.7220	0.3307	3.1654	1.8543	5.3504	INCHES
43523	30.9150	-97.7519	0.2992	2.5197	1.3543	4.1732	INCHES
59326	30.9362	-97.6262	0.2559	3.8701	1.5472	5.6732	INCHES
61929	30.8461	-97.7621	0.3465	2.8346	1.9134	5.0945	INCHES
63885	30.8373	-97.6819	0.2874	3.3386	1.2638	4.8898	INCHES
73302	30.9662	-97.5808	0.2165	4.0276	1.4016	5.6457	INCHES
98720	30.8973	-97.5913	0.3189	4.2047	1.1339	5.6575	INCHES
122207	30.8762	-97.7169	0.311	2.8307	1.4685	4.6102	INCHES
154077	30.8029	-97.6870	0.2362	3.1024	1.1732	4.5118	INCHES
165670	30.9617	-97.5406	0.374	4.1969	1.1181	5.689	INCHES
195800	30.9407	-97.6664	0.2362	3.0157	1.7047	4.9566	INCHES
206081	30.8806	-97.7570	0.2992	2.6732	1.4803	4.4527	INCHES
219192	31.0007	-97.5756	0.1693	3.1811	1.4213	4.7717	INCHES
233427	30.7641	-97.6521	0.2126	2.2205	1.1142	3.5473	INCHES
234955	30.7729	-97.7322	0.1339	2.6299	1.1063	3.8701	INCHES
235217	30.9917	-97.4951	0.2874	3.3819	1.1142	4.7835	INCHES
241487	30.8673	-97.6366	0.3268	3.811	1.122	5.2598	INCHES
253562	30.7985	-97.6470	0.2126	2.9921	1.0866	4.2913	INCHES
265023	30.7341	-97.6973	0.189	1.9724	1.0551	3.2165	INCHES
265067	30.8505	-97.8022	0.311	2.7362	1.7677	4.8149	INCHES
268852	30.8850	-97.7972	0.378	2.4764	1.4528	4.3072	INCHES
277204	30.8893	-97.8373	0.4173	2.4606	1.437	4.3149	INCHES
279978	30.9062	-97.6716	0.3307	3.1063	1.685	5.122	INCHES
307593	30.9018	-97.6314	0.3976	3.8622	1.5354	5.7952	INCHES

Table A.5. Rain totals for the 88D grid points for the May 2-4, 2019 event—Continued

GEO_ID	LAT	LON	5/2/19	5/3/19	5/4/19	TOTAL	UNITS
312628	30.8629	-97.5965	0.189	3.8425	0.9764	5.0079	INCHES
354401	30.8117	-97.7672	0.2756	2.689	1.5197	4.4843	INCHES
372021	30.7685	-97.6922	0.1693	2.3937	1.2362	3.7992	INCHES
378309	30.8718	-97.6767	0.3386	3.3189	1.3976	5.0551	INCHES
387424	30.9707	-97.6210	0.2008	3.0906	1.8346	5.126	INCHES
388864	30.9107	-97.7117	0.2992	2.5748	1.4685	4.3425	INCHES
389640	30.9451	-97.7066	0.3307	2.7717	1.437	4.5394	INCHES
399079	30.8548	-97.8424	0.4173	2.7559	1.5709	4.7441	INCHES
422041	31.0307	-97.5301	0.0984	3.2402	1.3543	4.6929	INCHES
424218	30.8247	-97.8875	0.2717	2.315	1.0984	3.6851	INCHES
478026	30.9962	-97.5354	0.1732	3.311	1.3189	4.8031	INCHES
507289	30.8329	-97.6418	0.1969	3.3465	1.1339	4.6773	INCHES
513543	30.7903	-97.8925	0.2362	2.437	1.2165	3.8897	INCHES
514429	30.9318	-97.5861	0.2992	4.4921	1.2047	5.996	INCHES
538879	30.8161	-97.8073	0.3189	2.9646	1.8661	5.1496	INCHES
539561	31.0052	-97.6158	0.2598	2.9488	1.9409	5.1495	INCHES
544185	30.7860	-97.8524	0.2559	2.5512	1.5	4.3071	INCHES
556304	30.8592	-97.8825	0.3701	2.185	1.1181	3.6732	INCHES
559170	30.8204	-97.8474	0.2874	2.6811	1.5945	4.563	INCHES
560097	30.7816	-97.8124	0.2362	2.5945	1.5984	4.4291	INCHES
564547	30.7773	-97.7723	0.1929	2.6614	1.378	4.2323	INCHES
565744	30.9572	-97.5004	0.2677	3.9724	1.0039	5.244	INCHES
581938	30.8073	-97.7271	0.1929	2.8898	1.2598	4.3425	INCHES
609938	30.9273	-97.5459	0.2913	4.8583	1.0236	6.1732	INCHES

Table A.6. Rain totals for the 88D grid points for the February 10-13, 2020 event.

GEO_ID	LAT	LON	2/10/20	2/11/20	2/12/20	2/13/20	TOTAL	UNITS
8443	30.7385	-97.7373	0.0315	0.0787	2.0906	0.1339	2.3347	INCHES
30536	30.9752	-97.6612	0.0354	0.0709	1.8937	0.1102	2.1102	INCHES
43466	30.8418	-97.7220	0.0236	0.374	2.3228	0.1575	2.8779	INCHES
43523	30.9150	-97.7519	0	0.1299	2.2559	0.1299	2.5157	INCHES
59326	30.9362	-97.6262	0	0.2283	2.0591	0.1339	2.4213	INCHES
61929	30.8461	-97.7621	0.0197	0.2953	2.5315	0.1496	2.9961	INCHES
63885	30.8373	-97.6819	0.0236	0.3937	2.2441	0.1496	2.811	INCHES
73302	30.9662	-97.5808	0	0.1339	2.0512	0.122	2.3071	INCHES
98720	30.8973	-97.5913	0.0709	0.3543	2.2638	0.1142	2.8032	INCHES
122207	30.8762	-97.7169	0.0197	0.3543	2.2283	0.1535	2.7558	INCHES
154077	30.8029	-97.6870	0.0394	0.1693	2.1693	0.1299	2.5079	INCHES
165670	30.9617	-97.5406	0.0039	0.2008	2.1811	0.1496	2.5354	INCHES
195800	30.9407	-97.6664	0.0157	0.1575	2.0472	0.1181	2.3385	INCHES
206081	30.8806	-97.7570	0.0157	0.189	2.3976	0.1575	2.7598	INCHES
219192	31.0007	-97.5756	0.0039	0.0827	1.9843	0.1417	2.2126	INCHES
233427	30.7641	-97.6521	0.0315	0.0433	1.7559	0.1102	1.9409	INCHES
234955	30.7729	-97.7322	0.0197	0.1496	2.2165	0.1378	2.5236	INCHES
235217	30.9917	-97.4951	0.0157	0.122	2.2559	0.1575	2.5511	INCHES
241487	30.8673	-97.6366	0.0354	0.3583	2.2047	0.1181	2.7165	INCHES
253562	30.7985	-97.6470	0.0197	0.0433	1.7953	0.1142	1.9725	INCHES
265023	30.7341	-97.6973	0.0315	0.063	1.8071	0.122	2.0236	INCHES
265067	30.8505	-97.8022	0.0039	0.1496	2.6299	0.1614	2.9448	INCHES
268852	30.8850	-97.7972	0	0.0945	2.4173	0.1496	2.6614	INCHES
277204	30.8893	-97.8373	0	0.1181	2.2992	0.1417	2.559	INCHES
279978	30.9062	-97.6716	0.0157	0.2992	2.0827	0.122	2.5196	INCHES
307593	30.9018	-97.6314	0.0157	0.248	2.1693	0.1299	2.5629	INCHES

Table A.6. Rain totals for the 88D grid points for the February 10-13, 2020 event—Continued

GEO_ID	LAT	LON	2/10/20	2/11/20	2/12/20	2/13/20	TOTAL	UNITS
312628	30.8629	-97.5965	0	0.1693	2.1299	0.1142	2.4134	INCHES
354401	30.8117	-97.7672	0.0236	0.3465	2.5512	0.1535	3.0748	INCHES
372021	30.7685	-97.6922	0.0354	0.0748	2.1378	0.1378	2.3858	INCHES
378309	30.8718	-97.6767	0.0157	0.3307	2.2087	0.1535	2.7086	INCHES
387424	30.9707	-97.6210	0	0.1339	1.8858	0.1339	2.1536	INCHES
388864	30.9107	-97.7117	0.0197	0.2362	2.1772	0.1181	2.5512	INCHES
389640	30.9451	-97.7066	0.0197	0.1417	2.122	0.1142	2.3976	INCHES
399079	30.8548	-97.8424	0.0157	0.1339	2.5	0.1496	2.7992	INCHES
422041	31.0307	-97.5301	0.0118	0.0906	2.2165	0.1693	2.4882	INCHES
424218	30.8247	-97.8875	0.0394	0.1929	2.4921	0.1378	2.8622	INCHES
478026	30.9962	-97.5354	0.0039	0.1142	2.2244	0.1496	2.4921	INCHES
507289	30.8329	-97.6418	0.0315	0.2795	2.0866	0.1339	2.5315	INCHES
513543	30.7903	-97.8925	0	0.2205	2.5354	0.1339	2.8898	INCHES
514429	30.9318	-97.5861	0.0394	0.3307	2.1969	0.1181	2.6851	INCHES
538879	30.8161	-97.8073	0.0197	0.2677	2.874	0.189	3.3504	INCHES
539561	31.0052	-97.6158	0.0197	0.0748	1.8898	0.1299	2.1142	INCHES
544185	30.7860	-97.8524	0	0.2953	2.5827	0.2008	3.0788	INCHES
556304	30.8592	-97.8825	0.0236	0.1772	2.3622	0.1299	2.6929	INCHES
559170	30.8204	-97.8474	0.0039	0.2323	2.6614	0.1575	3.0551	INCHES
560097	30.7816	-97.8124	0.0157	0.3386	2.6024	0.2165	3.1732	INCHES
564547	30.7773	-97.7723	0.0236	0.248	2.4331	0.1772	2.8819	INCHES
565744	30.9572	-97.5004	0.0039	0.3583	2.063	0.1614	2.5866	INCHES
581938	30.8073	-97.7271	0.0236	0.3071	2.3032	0.1496	2.7835	INCHES
609938	30.9273	-97.5459	0	0.4449	2.0984	0.1378	2.6811	INCHES

Table A.7. Rain totals for the 88D grid points for the March 18-23, 2020 event.

GEO_ID	LAT	LON	3/18/20	3/19/20	3/20/20	3/21/20	3/22/20	3/23/20	TOTAL	UNITS
8443	30.7385	-97.7373	0.0236	0.0157	0.5079	0.3937	0.7992	0.0039	1.744	INCHES
30536	30.9752	-97.6612	0.0236	0.0157	0.3346	0.3937	1.3032	0.0039	2.0747	INCHES
43466	30.8418	-97.7220	0	0.0157	0.315	0.3661	1.2638	0.0039	1.9645	INCHES
43523	30.9150	-97.7519	0	0.0315	0.2953	0.311	1.5	0	2.1378	INCHES
59326	30.9362	-97.6262	0.0433	0.0236	0.3504	0.2756	1.7717	0.0039	2.4685	INCHES
61929	30.8461	-97.7621	0.0039	0.0197	0.2283	0.311	1.3543	0	1.9172	INCHES
63885	30.8373	-97.6819	0.0787	0.0354	0.4567	0.4055	1.0276	0.0039	2.0078	INCHES
73302	30.9662	-97.5808	0.0157	0.0157	0.4488	0.3071	1.5866	0	2.3739	INCHES
98720	30.8973	-97.5913	0.0315	0.0236	0.5945	0.378	1.2047	0	2.2323	INCHES
122207	30.8762	-97.7169	0.0157	0.0197	0.2598	0.315	1.5472	0.0039	2.1613	INCHES
154077	30.8029	-97.6870	0.1142	0.0315	0.5157	0.3898	0.811	0	1.8622	INCHES
165670	30.9617	-97.5406	0.0157	0.0118	0.4961	0.378	1.5591	0	2.4607	INCHES
195800	30.9407	-97.6664	0.0236	0.0118	0.252	0.2953	1.6181	0.0039	2.2047	INCHES
206081	30.8806	-97.7570	0	0.0236	0.2559	0.2953	1.6654	0	2.2402	INCHES
219192	31.0007	-97.5756	0	0.0039	0.3346	0.3307	1.3425	0.0118	2.0235	INCHES
233427	30.7641	-97.6521	0.0906	0.0236	0.5079	0.3465	0.7008	0	1.6694	INCHES
234955	30.7729	-97.7322	0.0157	0.0315	0.5157	0.378	0.8228	0.0039	1.7676	INCHES
235217	30.9917	-97.4951	0.0748	0.0197	0.4173	0.4291	1.4134	0.0157	2.37	INCHES
241487	30.8673	-97.6366	0.063	0.0157	0.5551	0.3661	1.0787	0.0157	2.0943	INCHES
253562	30.7985	-97.6470	0.1024	0.0315	0.5354	0.3504	0.6614	0	1.6811	INCHES
265023	30.7341	-97.6973	0.0748	0.0157	0.4843	0.4528	0.7874	0	1.815	INCHES
265067	30.8505	-97.8022	0.0039	0.0236	0.2756	0.3346	1.4291	0	2.0668	INCHES
268852	30.8850	-97.7972	0	0.0394	0.2992	0.3543	1.6102	0	2.3031	INCHES
277204	30.8893	-97.8373	0	0.0354	0.3346	0.4173	1.374	0	2.1613	INCHES
279978	30.9062	-97.6716	0.0591	0.0118	0.311	0.2795	1.7717	0.0039	2.437	INCHES
307593	30.9018	-97.6314	0.0512	0.0236	0.4173	0.3465	1.6142	0.0157	2.4685	INCHES

Table A.7. Rain totals for the 88D grid points for the March 18-23, 2020 event—Continued

GEO_ID	LAT	LON	3/18/20	3/19/20	3/20/20	3/21/20	3/22/20	3/23/20	TOTAL	UNITS
312628	30.8629	-97.5965	0.0748	0.0315	0.6102	0.4094	0.7913	0	1.9172	INCHES
354401	30.8117	-97.7672	0.0039	0.0157	0.3071	0.3504	1.1024	0	1.7795	INCHES
372021	30.7685	-97.6922	0.1102	0.0236	0.5079	0.3976	0.7638	0	1.8031	INCHES
378309	30.8718	-97.6767	0.0512	0.0236	0.3858	0.3583	1.374	0.0039	2.1968	INCHES
387424	30.9707	-97.6210	0.0354	0.0157	0.3071	0.3189	1.5276	0.0039	2.2086	INCHES
388864	30.9107	-97.7117	0.0197	0.0197	0.2598	0.2756	1.6929	0.0039	2.2716	INCHES
389640	30.9451	-97.7066	0.0236	0.0197	0.2992	0.3465	1.4528	0.0039	2.1457	INCHES
399079	30.8548	-97.8424	0.0039	0.0354	0.3307	0.4173	1.4409	0	2.2282	INCHES
422041	31.0307	-97.5301	0	0.0118	0.4094	0.3543	1.3425	0.0118	2.1298	INCHES
424218	30.8247	-97.8875	0.0118	0.0433	0.3465	0.3386	1.5276	0.0039	2.2717	INCHES
478026	30.9962	-97.5354	0.0039	0.0118	0.4173	0.3858	1.4488	0.0118	2.2794	INCHES
507289	30.8329	-97.6418	0.0984	0.0236	0.5669	0.4252	0.7992	0	1.9133	INCHES
513543	30.7903	-97.8925	0.0118	0.0236	0.3504	0.2953	1.3228	0.0039	2.0078	INCHES
514429	30.9318	-97.5861	0.0197	0.0039	0.563	0.3071	1.6772	0	2.5709	INCHES
538879	30.8161	-97.8073	0.0118	0.0118	0.3268	0.3543	1.1772	0	1.8819	INCHES
539561	31.0052	-97.6158	0.0118	0.0197	0.3189	0.374	1.2047	0.0039	1.933	INCHES
544185	30.7860	-97.8524	0.0236	0.0236	0.3504	0.3189	1.0787	0	1.7952	INCHES
556304	30.8592	-97.8825	0.0157	0.0591	0.4055	0.4449	1.5472	0	2.4724	INCHES
559170	30.8204	-97.8474	0.0118	0.0315	0.3071	0.3346	1.2756	0	1.9606	INCHES
560097	30.7816	-97.8124	0.0197	0.0157	0.3661	0.3504	1.063	0	1.8149	INCHES
564547	30.7773	-97.7723	0.0197	0.0039	0.4488	0.3858	0.9961	0.0039	1.8582	INCHES
565744	30.9572	-97.5004	0.122	0.0039	0.4449	0.437	1.4567	0	2.4645	INCHES
581938	30.8073	-97.7271	0	0.0236	0.4646	0.3976	1.0394	0.0039	1.9291	INCHES
609938	30.9273	-97.5459	0.0197	0	0.563	0.3976	1.3543	0	2.3346	INCHES

Table A.8. Rain totals for the 88D grid points for the April 10-13, 2020 event.

GEO_ID	LAT	LON	4/10/20	4/12/20	4/13/20	TOTAL	UNITS
8443	30.7385	-97.7373	0.4291	0.8898	0.0197	1.3386	INCHES
30536	30.9752	-97.6612	0.5118	1.1457	0.0039	1.6614	INCHES
43466	30.8418	-97.7220	0.9016	1.1929	0.0039	2.0984	INCHES
43523	30.9150	-97.7519	0.6929	1.1457	0	1.8386	INCHES
59326	30.9362	-97.6262	0.5906	1.2717	0	1.8623	INCHES
61929	30.8461	-97.7621	0.8622	1.2008	0.0039	2.0669	INCHES
63885	30.8373	-97.6819	0.8228	1.2992	0	2.122	INCHES
73302	30.9662	-97.5808	0.5709	1.252	0.0039	1.8268	INCHES
98720	30.8973	-97.5913	0.7638	1.4882	0	2.252	INCHES
122207	30.8762	-97.7169	0.8386	1.2165	0	2.0551	INCHES
154077	30.8029	-97.6870	0.6654	1.0551	0.0157	1.7362	INCHES
165670	30.9617	-97.5406	0.5669	1.2992	0.0039	1.87	INCHES
195800	30.9407	-97.6664	0.5354	1.2165	0	1.7519	INCHES
206081	30.8806	-97.7570	0.8858	1.2126	0	2.0984	INCHES
219192	31.0007	-97.5756	0.3858	1.2402	0.0039	1.6299	INCHES
233427	30.7641	-97.6521	0.4724	0.9606	0.0157	1.4487	INCHES
234955	30.7729	-97.7322	0.5433	0.9567	0.0157	1.5157	INCHES
235217	30.9917	-97.4951	0.4961	1.3386	0.0039	1.8386	INCHES
241487	30.8673	-97.6366	0.7598	1.4606	0	2.2204	INCHES
253562	30.7985	-97.6470	0.5945	1.0354	0	1.6299	INCHES
265023	30.7341	-97.6973	0.4134	0.8701	0.0157	1.2992	INCHES
265067	30.8505	-97.8022	0.7283	1.2165	0.0039	1.9487	INCHES
268852	30.8850	-97.7972	0.8189	1.2126	0.0157	2.0472	INCHES
277204	30.8893	-97.8373	1	1.2244	0	2.2244	INCHES
279978	30.9062	-97.6716	0.6142	1.2402	0	1.8544	INCHES
307593	30.9018	-97.6314	0.6614	1.4134	0	2.0748	INCHES

Table A.8. Rain totals for the 88D grid points for the April 10-13, 2020 event—Continued

GEO_ID	LAT	LON	4/10/20	4/12/20	4/13/20	TOTAL	UNITS
312628	30.8629	-97.5965	0.6339	1.3583	0	1.9922	INCHES
354401	30.8117	-97.7672	0.7323	1.126	0.0039	1.8622	INCHES
372021	30.7685	-97.6922	0.4882	0.9606	0.0197	1.4685	INCHES
378309	30.8718	-97.6767	0.748	1.3346	0	2.0826	INCHES
387424	30.9707	-97.6210	0.5551	1.2244	0.0039	1.7834	INCHES
388864	30.9107	-97.7117	0.6693	1.2047	0	1.874	INCHES
389640	30.9451	-97.7066	0.5354	1.1969	0	1.7323	INCHES
399079	30.8548	-97.8424	0.8661	1.185	0.0236	2.0747	INCHES
422041	31.0307	-97.5301	0.2677	1.3504	0.0118	1.6299	INCHES
424218	30.8247	-97.8875	0.7205	1.1378	0.0157	1.874	INCHES
478026	30.9962	-97.5354	0.374	1.2795	0.0039	1.6574	INCHES
507289	30.8329	-97.6418	0.748	1.2165	0	1.9645	INCHES
513543	30.7903	-97.8925	0.6024	1.0827	0	1.6851	INCHES
514429	30.9318	-97.5861	0.6732	1.3937	0.0039	2.0708	INCHES
538879	30.8161	-97.8073	0.6693	1.3032	0.0118	1.9843	INCHES
539561	31.0052	-97.6158	0.3937	1.1614	0.0039	1.559	INCHES
544185	30.7860	-97.8524	0.5709	1.1339	0.0039	1.7087	INCHES
556304	30.8592	-97.8825	0.9449	1.3189	0.0118	2.2756	INCHES
559170	30.8204	-97.8474	0.6654	1.185	0.0157	1.8661	INCHES
560097	30.7816	-97.8124	0.5945	1.1024	0.0039	1.7008	INCHES
564547	30.7773	-97.7723	0.626	1.0354	0.0039	1.6653	INCHES
565744	30.9572	-97.5004	0.6339	1.4921	0.0039	2.1299	INCHES
581938	30.8073	-97.7271	0.7441	1.1378	0.0039	1.8858	INCHES
609938	30.9273	-97.5459	0.7323	1.4803	0	2.2126	INCHES

Table A.9. Rain totals for the 88D grid points for the May 25-29, 2020 event.

GEO_ID	LAT	LON	5/25/20	5/26/20	5/27/20	5/28/20	5/29/20	TOTAL	UNITS
8443	30.7385	-97.7373	1.1614	0	0.0551	1.8622	0	3.0787	INCHES
30536	30.9752	-97.6612	1.6457	0.0039	0	0.1929	0.0118	1.8543	INCHES
43466	30.8418	-97.7220	0.9409	0	0.0197	0.5512	0	1.5118	INCHES
43523	30.9150	-97.7519	1.185	0	0	0.5039	0.0394	1.7283	INCHES
59326	30.9362	-97.6262	1.1969	0.0236	0	0.437	0.0039	1.6614	INCHES
61929	30.8461	-97.7621	0.9803	0	0.0118	0.7126	0.0197	1.7244	INCHES
63885	30.8373	-97.6819	0.7874	0	0.0236	0.4882	0.0118	1.311	INCHES
73302	30.9662	-97.5808	0.9016	0.0039	0	0.315	0.0039	1.2244	INCHES
98720	30.8973	-97.5913	1.7441	0.0039	0	0.9646	0.0039	2.7165	INCHES
122207	30.8762	-97.7169	0.9252	0	0.0118	0.626	0.0039	1.5669	INCHES
154077	30.8029	-97.6870	0.9252	0	0.0394	0.311	0	1.2756	INCHES
165670	30.9617	-97.5406	0.6654	0.0118	0.0039	0.2598	0	0.9409	INCHES
195800	30.9407	-97.6664	1.4016	0.0315	0	0.5118	0.0118	1.9567	INCHES
206081	30.8806	-97.7570	1.0276	0	0.0039	0.6142	0.0315	1.6772	INCHES
219192	31.0007	-97.5756	0.8386	0.0118	0.0039	0.1378	0.0039	0.996	INCHES
233427	30.7641	-97.6521	0.9094	0	0.1575	0.7835	0	1.8504	INCHES
234955	30.7729	-97.7322	1.1181	0	0.0433	1.6181	0	2.7795	INCHES
235217	30.9917	-97.4951	0.8307	0.0354	0.0039	0.1496	0	1.0196	INCHES
241487	30.8673	-97.6366	0.8976	0	0.0197	0.878	0	1.7953	INCHES
253562	30.7985	-97.6470	0.8228	0	0.0984	0.2717	0	1.1929	INCHES
265023	30.7341	-97.6973	1.0945	0	0.0984	1.8071	0	3	INCHES
265067	30.8505	-97.8022	0.9055	0	0	0.8504	0.0236	1.7795	INCHES
268852	30.8850	-97.7972	0.9606	0	0	0.4173	0.0354	1.4133	INCHES
277204	30.8893	-97.8373	0.9173	0	0	0.3504	0.0512	1.3189	INCHES
279978	30.9062	-97.6716	1.0079	0	0	0.8268	0.0039	1.8386	INCHES
307593	30.9018	-97.6314	1.1535	0.0039	0	0.9173	0.0039	2.0786	INCHES

Table A.9. Rain totals for the 88D grid points for the May 25-29, 2020 event—Continued

GEO_ID	LAT	LON	5/25/20	5/26/20	5/27/20	5/28/20	5/29/20	TOTAL	UNITS
312628	30.8629	-97.5965	1.4134	0	0.0197	0.8819	0	2.315	INCHES
354401	30.8117	-97.7672	1.0276	0	0.0197	0.6693	0	1.7166	INCHES
372021	30.7685	-97.6922	0.9606	0	0.0709	1.2795	0	2.311	INCHES
378309	30.8718	-97.6767	0.752	0	0.0157	0.6732	0	1.4409	INCHES
387424	30.9707	-97.6210	1.3386	0.0039	0	0.3307	0.0118	1.685	INCHES
388864	30.9107	-97.7117	1.1181	0	0	0.7795	0.0394	1.937	INCHES
389640	30.9451	-97.7066	1.5157	0.0315	0	0.6614	0.0354	2.244	INCHES
399079	30.8548	-97.8424	1.0157	0	0	1.1024	0.0354	2.1535	INCHES
422041	31.0307	-97.5301	0.8031	0.0197	0.0118	0.0591	0	0.8937	INCHES
424218	30.8247	-97.8875	1.1457	0	0	1.3307	0	2.4764	INCHES
478026	30.9962	-97.5354	0.6654	0.0197	0.0039	0.1024	0.0039	0.7953	INCHES
507289	30.8329	-97.6418	0.7874	0	0.0315	0.4567	0	1.2756	INCHES
513543	30.7903	-97.8925	1.4291	0	0.0039	0.5079	0	1.9409	INCHES
514429	30.9318	-97.5861	1.3898	0.0039	0	0.685	0.0039	2.0826	INCHES
538879	30.8161	-97.8073	1.063	0	0	1.9134	0.0157	2.9921	INCHES
539561	31.0052	-97.6158	1.185	0.0039	0	0.2087	0.0118	1.4094	INCHES
544185	30.7860	-97.8524	1.1772	0	0.0039	1.0945	0	2.2756	INCHES
556304	30.8592	-97.8825	1.1142	0	0	1.3583	0	2.4725	INCHES
559170	30.8204	-97.8474	1.0276	0	0	1.9488	0	2.9764	INCHES
560097	30.7816	-97.8124	1.0669	0	0.0157	1.7283	0	2.8109	INCHES
564547	30.7773	-97.7723	1.1024	0	0.0315	2.1575	0	3.2914	INCHES
565744	30.9572	-97.5004	0.7047	0.0236	0	0.2323	0	0.9606	INCHES
581938	30.8073	-97.7271	0.9409	0	0.0315	0.3858	0	1.3582	INCHES
609938	30.9273	-97.5459	1.1969	0.0118	0	0.7992	0	2.0079	INCHES

Table A.10. Rain totals for the 88D grid points for the July 26-27, 2020 event.

GEO_ID	LAT	LON	7/26/20	7/27/20	TOTAL	UNITS
8443	30.7385	-97.7373	0.0787	0.0512	0.1299	INCHES
30536	30.9752	-97.6612	0.0512	1.1142	1.1654	INCHES
43466	30.8418	-97.7220	0.0787	0.0591	0.1378	INCHES
43523	30.9150	-97.7519	0.1575	0.2795	0.437	INCHES
59326	30.9362	-97.6262	0.1142	0.9488	1.063	INCHES
61929	30.8461	-97.7621	0.1142	0.0433	0.1575	INCHES
63885	30.8373	-97.6819	0.0709	0.0827	0.1536	INCHES
73302	30.9662	-97.5808	0.0197	0.878	0.8977	INCHES
98720	30.8973	-97.5913	0.0945	0.748	0.8425	INCHES
122207	30.8762	-97.7169	0.1772	0.189	0.3662	INCHES
154077	30.8029	-97.6870	0.0787	0.063	0.1417	INCHES
165670	30.9617	-97.5406	0.0197	1.2362	1.2559	INCHES
195800	30.9407	-97.6664	0.1299	0.9094	1.0393	INCHES
206081	30.8806	-97.7570	0.2323	0.0787	0.311	INCHES
219192	31.0007	-97.5756	0.0354	0.9016	0.937	INCHES
233427	30.7641	-97.6521	0.0512	0.0591	0.1103	INCHES
234955	30.7729	-97.7322	0.0748	0.0591	0.1339	INCHES
235217	30.9917	-97.4951	0.0433	1.5709	1.6142	INCHES
241487	30.8673	-97.6366	0.1142	0.3504	0.4646	INCHES
253562	30.7985	-97.6470	0.0551	0.0827	0.1378	INCHES
265023	30.7341	-97.6973	0.063	0.0906	0.1536	INCHES
265067	30.8505	-97.8022	0.1102	0.0236	0.1338	INCHES
268852	30.8850	-97.7972	0.2756	0.0827	0.3583	INCHES
277204	30.8893	-97.8373	0.3583	0.063	0.4213	INCHES
279978	30.9062	-97.6716	0.1142	0.5276	0.6418	INCHES
307593	30.9018	-97.6314	0.0945	0.6614	0.7559	INCHES

Table A.10. Rain totals for the 88D grid points for the July 26-27, 2020 event—Continued

GEO_ID	LAT	LON	7/26/20	7/27/20	TOTAL	UNITS
312628	30.8629	-97.5965	0.0945	0.2992	0.3937	INCHES
354401	30.8117	-97.7672	0.1496	0.0394	0.189	INCHES
372021	30.7685	-97.6922	0.0551	0.0551	0.1102	INCHES
378309	30.8718	-97.6767	0.1378	0.248	0.3858	INCHES
387424	30.9707	-97.6210	0.0354	1.0787	1.1141	INCHES
388864	30.9107	-97.7117	0.2087	0.315	0.5237	INCHES
389640	30.9451	-97.7066	0.0906	0.8898	0.9804	INCHES
399079	30.8548	-97.8424	0.0906	0.0354	0.126	INCHES
422041	31.0307	-97.5301	0.0315	0.9409	0.9724	INCHES
424218	30.8247	-97.8875	0.1378	0.0236	0.1614	INCHES
478026	30.9962	-97.5354	0.0394	1.0276	1.067	INCHES
507289	30.8329	-97.6418	0.1024	0.189	0.2914	INCHES
513543	30.7903	-97.8925	0.2283	0.0354	0.2637	INCHES
514429	30.9318	-97.5861	0.0748	1.1811	1.2559	INCHES
538879	30.8161	-97.8073	0.2205	0	0.2205	INCHES
539561	31.0052	-97.6158	0.0591	0.811	0.8701	INCHES
544185	30.7860	-97.8524	0.1772	0.0354	0.2126	INCHES
556304	30.8592	-97.8825	0.0827	0.0354	0.1181	INCHES
559170	30.8204	-97.8474	0.1575	0.0197	0.1772	INCHES
560097	30.7816	-97.8124	0.1535	0.0354	0.1889	INCHES
564547	30.7773	-97.7723	0.1181	0.0512	0.1693	INCHES
565744	30.9572	-97.5004	0.0197	1.3504	1.3701	INCHES
581938	30.8073	-97.7271	0.1024	0.0512	0.1536	INCHES
609938	30.9273	-97.5459	0.1024	1.3307	1.4331	INCHES

Table A.11. Rain totals for the 88D grid points for the September 2-6, 2020 event.

GEO_ID	LAT	LON	9/2/20	9/3/20	9/4/20	9/5/20	9/6/20	TOTAL	UNITS
8443	30.7385	-97.7373	0	0.3858	0.8976	0.311	0.6063	2.2007	INCHES
30536	30.9752	-97.6612	1.6181	1.5079	0.3583	0.6417	0	4.126	INCHES
43466	30.8418	-97.7220	0.5866	0.8268	1.1378	0.4764	0.5945	3.6221	INCHES
43523	30.9150	-97.7519	1.3622	0.9488	0.8661	0.1929	0.1732	3.5432	INCHES
59326	30.9362	-97.6262	1.7244	1.4685	0.4882	0.7598	0.0236	4.4645	INCHES
61929	30.8461	-97.7621	0.437	0.9409	1.2717	0.2362	0.8701	3.7559	INCHES
63885	30.8373	-97.6819	0.622	0.8071	1.3622	0.4843	0.5669	3.8425	INCHES
73302	30.9662	-97.5808	1.9646	1.3622	0.4567	0.2126	0.0157	4.0118	INCHES
98720	30.8973	-97.5913	1.4528	0.7717	0.9291	1.0472	0.0984	4.2992	INCHES
122207	30.8762	-97.7169	1	1.0984	0.8976	0.3268	0.752	4.0748	INCHES
154077	30.8029	-97.6870	0.2992	0.6102	1.1929	0.6811	0.6654	3.4488	INCHES
165670	30.9617	-97.5406	2.2205	1.1024	0.626	0.3465	0.0236	4.319	INCHES
195800	30.9407	-97.6664	1.626	1.4173	0.4173	1.063	0.0433	4.5669	INCHES
206081	30.8806	-97.7570	0.7402	1	1.1457	0.2402	0.5906	3.7167	INCHES
219192	31.0007	-97.5756	2.2244	1.5394	0.3976	0.3189	0	4.4803	INCHES
233427	30.7641	-97.6521	0.1614	0.311	0.5906	0.7638	0.5276	2.3544	INCHES
234955	30.7729	-97.7322	0.1535	0.4252	0.9961	0.4882	0.6811	2.7441	INCHES
235217	30.9917	-97.4951	2.8307	1.0984	0.563	1.2008	0	5.6929	INCHES
241487	30.8673	-97.6366	0.9961	0.8701	1.1378	0.6929	0.6496	4.3465	INCHES
253562	30.7985	-97.6470	0.311	0.3976	0.8228	0.689	0.8268	3.0472	INCHES
265023	30.7341	-97.6973	0.0591	0.315	0.6693	0.6063	0.5748	2.2245	INCHES
265067	30.8505	-97.8022	0.311	0.6732	0.9016	0.1496	0.9882	3.0236	INCHES
268852	30.8850	-97.7972	0.7874	0.7244	0.8504	0.122	0.5906	3.0748	INCHES
277204	30.8893	-97.8373	0.6063	0.6417	0.8386	0.1299	0.6299	2.8464	INCHES
279978	30.9062	-97.6716	1.311	1.2992	0.5748	0.7913	0.3268	4.3031	INCHES
307593	30.9018	-97.6314	1.1772	1.1417	0.7323	1.0748	0.1969	4.3229	INCHES

Table A.11. Rain totals for the 88D grid points for the September 2-6, 2020 event—Continued

GEO_ID	LAT	LON	9/2/20	9/3/20	9/4/20	9/5/20	9/6/20	TOTAL	UNITS
312628	30.8629	-97.5965	1.2008	0.5512	1.1614	0.9764	0.4173	4.3071	INCHES
354401	30.8117	-97.7672	0.4921	0.7402	1.1063	0.2559	0.7677	3.3622	INCHES
372021	30.7685	-97.6922	0.0591	0.5236	0.7598	0.7047	0.5118	2.559	INCHES
378309	30.8718	-97.6767	0.8976	0.9685	0.7835	0.4449	0.8622	3.9567	INCHES
387424	30.9707	-97.6210	1.7953	1.5118	0.4252	0.2992	0	4.0315	INCHES
388864	30.9107	-97.7117	1.0394	1.2913	0.8307	0.2913	0.2992	3.7519	INCHES
389640	30.9451	-97.7066	1.5157	1.4016	0.5157	0.8386	0.0236	4.2952	INCHES
399079	30.8548	-97.8424	0.2677	0.5827	0.622	0.0551	0.9055	2.433	INCHES
422041	31.0307	-97.5301	2.7795	1.4094	0.374	1.0197	0	5.5826	INCHES
424218	30.8247	-97.8875	0.0787	0.437	0.5748	0.0354	0.5157	1.6416	INCHES
478026	30.9962	-97.5354	2.6929	1.2598	0.5118	0.6063	0	5.0708	INCHES
507289	30.8329	-97.6418	0.7244	0.7008	1.6181	0.4291	0.7047	4.1771	INCHES
513543	30.7903	-97.8925	0	0.374	0.8858	0.0512	0.1811	1.4921	INCHES
514429	30.9318	-97.5861	1.5354	1.0945	0.5866	0.5669	0.0433	3.8267	INCHES
538879	30.8161	-97.8073	0.1693	0.6929	1.2756	0.1024	0.689	2.9292	INCHES
539561	31.0052	-97.6158	1.7323	1.5276	0.4094	0.1969	0	3.8662	INCHES
544185	30.7860	-97.8524	0.0118	0.5709	0.9409	0.0906	0.248	1.8622	INCHES
556304	30.8592	-97.8825	0.2205	0.5354	0.6693	0.0157	0.8661	2.307	INCHES
559170	30.8204	-97.8474	0.0591	0.5945	0.9016	0.0827	0.7717	2.4096	INCHES
560097	30.7816	-97.8124	0.1142	0.4646	1.0157	0.1142	0.1969	1.9056	INCHES
564547	30.7773	-97.7723	0.1535	0.4921	1.3189	0.1772	0.4724	2.6141	INCHES
565744	30.9572	-97.5004	2.5787	0.9409	0.8228	1.0157	0.0157	5.3738	INCHES
581938	30.8073	-97.7271	0.4528	0.5866	1.2638	0.7795	0.5039	3.5866	INCHES
609938	30.9273	-97.5459	1.8504	0.9606	0.8189	0.6614	0.0551	4.3464	INCHES

Table A.12. Rain totals for the 88D grid points for the September 9-11, 2020 event.

GEO_ID	LAT	LON	9/9/20	9/10/20	9/11/20	TOTAL	UNITS
8443	30.7385	-97.7373	0.0236	1.1535	0.0315	1.2086	INCHES
30536	30.9752	-97.6612	0.122	1.1024	0	1.2244	INCHES
43466	30.8418	-97.7220	0.0236	1.0748	0.1102	1.2086	INCHES
43523	30.9150	-97.7519	0.0157	1.0984	0.063	1.1771	INCHES
59326	30.9362	-97.6262	0.0827	1.2717	0	1.3544	INCHES
61929	30.8461	-97.7621	0.0236	1.2244	0.0433	1.2913	INCHES
63885	30.8373	-97.6819	0.0315	1.2992	0.0236	1.3543	INCHES
73302	30.9662	-97.5808	0.1811	1.0591	0	1.2402	INCHES
98720	30.8973	-97.5913	0.1339	1.2559	0	1.3898	INCHES
122207	30.8762	-97.7169	0.0197	1.1339	0	1.1536	INCHES
154077	30.8029	-97.6870	0.0039	1.2756	0.0591	1.3386	INCHES
165670	30.9617	-97.5406	0.5827	1.0354	0	1.6181	INCHES
195800	30.9407	-97.6664	0.0787	1.0866	0	1.1653	INCHES
206081	30.8806	-97.7570	0.0197	1.1732	0.0551	1.248	INCHES
219192	31.0007	-97.5756	0.3976	1.0354	0	1.433	INCHES
233427	30.7641	-97.6521	0.0197	1.2992	0.189	1.5079	INCHES
234955	30.7729	-97.7322	0.0157	1.1772	0.0197	1.2126	INCHES
235217	30.9917	-97.4951	0.3898	1.0039	0	1.3937	INCHES
241487	30.8673	-97.6366	0.0551	1.315	0	1.3701	INCHES
253562	30.7985	-97.6470	0.0039	1.3386	0.0236	1.3661	INCHES
265023	30.7341	-97.6973	0.0236	1.3543	0.2165	1.5944	INCHES
265067	30.8505	-97.8022	0.0236	1.378	0.0236	1.4252	INCHES
268852	30.8850	-97.7972	0.0315	1.3346	0.0394	1.4055	INCHES
277204	30.8893	-97.8373	0.063	1.4606	0.0394	1.563	INCHES
279978	30.9062	-97.6716	0.0551	1.1181	0	1.1732	INCHES
307593	30.9018	-97.6314	0.0551	1.2953	0	1.3504	INCHES

Table A.12. Rain totals for the 88D grid points for the September 9-11, 2020 event—Continued

GEO_ID	LAT	LON	9/9/20	9/10/20	9/11/20	TOTAL	UNITS
312628	30.8629	-97.5965	0.0512	1.2402	0	1.2914	INCHES
354401	30.8117	-97.7672	0.0197	1.2244	0.0197	1.2638	INCHES
372021	30.7685	-97.6922	0.0197	1.2402	0.1693	1.4292	INCHES
378309	30.8718	-97.6767	0.0039	1.1535	0.0157	1.1731	INCHES
387424	30.9707	-97.6210	0.0906	1.2323	0	1.3229	INCHES
388864	30.9107	-97.7117	0.0039	1.0591	0	1.063	INCHES
389640	30.9451	-97.7066	0.0906	1.0276	0	1.1182	INCHES
399079	30.8548	-97.8424	0.0354	1.5512	0.0512	1.6378	INCHES
422041	31.0307	-97.5301	0.622	0.9173	0.0354	1.5747	INCHES
424218	30.8247	-97.8875	0.0906	1.7283	0.0512	1.8701	INCHES
478026	30.9962	-97.5354	0.5512	0.9882	0	1.5394	INCHES
507289	30.8329	-97.6418	0.0039	1.2559	0	1.2598	INCHES
513543	30.7903	-97.8925	0.0827	1.6457	0.0394	1.7678	INCHES
514429	30.9318	-97.5861	0.2087	1.2047	0	1.4134	INCHES
538879	30.8161	-97.8073	0.0197	1.5551	0.0591	1.6339	INCHES
539561	31.0052	-97.6158	0.1732	1.311	0.0157	1.4999	INCHES
544185	30.7860	-97.8524	0.0236	1.6772	0.0551	1.7559	INCHES
556304	30.8592	-97.8825	0.0709	1.7874	0	1.8583	INCHES
559170	30.8204	-97.8474	0.0157	1.5866	0.0709	1.6732	INCHES
560097	30.7816	-97.8124	0.0118	1.3898	0.0433	1.4449	INCHES
564547	30.7773	-97.7723	0.0197	1.1929	0.0157	1.2283	INCHES
565744	30.9572	-97.5004	0.6142	0.9843	0	1.5985	INCHES
581938	30.8073	-97.7271	0.0197	1.1417	0.0984	1.2598	INCHES
609938	30.9273	-97.5459	0.6654	1.1378	0	1.8032	INCHES

Table A.13. Rain totals for the 88D grid points for the September 18-23, 2020 event.

GEO_ID	LAT	LON	9/18/20	9/21/20	9/22/20	9/23/20	TOTAL	UNITS
8443	30.7385	-97.7373	0.0945	0.0551	1.626	0.1614	1.937	INCHES
30536	30.9752	-97.6612	0.0827	0.0118	0.9055	0.4331	1.4331	INCHES
43466	30.8418	-97.7220	0.0748	0.0433	1.1614	0.315	1.5945	INCHES
43523	30.9150	-97.7519	0.0236	0.0236	0.8268	0.3386	1.2126	INCHES
59326	30.9362	-97.6262	0.4252	0.0157	1.0079	0.2874	1.7362	INCHES
61929	30.8461	-97.7621	0.0157	0.0512	0.9882	0.2953	1.3504	INCHES
63885	30.8373	-97.6819	0.1181	0.0748	1.3189	0.2598	1.7716	INCHES
73302	30.9662	-97.5808	0.5945	0.063	1	0.3386	1.9961	INCHES
98720	30.8973	-97.5913	0.1417	0.0039	1.2559	0.1772	1.5787	INCHES
122207	30.8762	-97.7169	0.1024	0.0354	1.0472	0.3346	1.5196	INCHES
154077	30.8029	-97.6870	0.1142	0.0709	1.4764	0.1969	1.8584	INCHES
165670	30.9617	-97.5406	0.6614	0.0787	1.0472	0.2992	2.0865	INCHES
195800	30.9407	-97.6664	0.1811	0	0.9252	0.2795	1.3858	INCHES
206081	30.8806	-97.7570	0	0.0433	0.8858	0.374	1.3031	INCHES
219192	31.0007	-97.5756	0.5079	0.0748	1.063	0.4882	2.1339	INCHES
233427	30.7641	-97.6521	0.1181	0.0591	1.9291	0.1102	2.2165	INCHES
234955	30.7729	-97.7322	0.122	0.0827	1.3189	0.1929	1.7165	INCHES
235217	30.9917	-97.4951	0.6614	0.0394	1.0787	0.3465	2.126	INCHES
241487	30.8673	-97.6366	0.1378	0.0118	1.2913	0.2165	1.6574	INCHES
253562	30.7985	-97.6470	0.1575	0.0709	1.1811	0.0906	1.5001	INCHES
265023	30.7341	-97.6973	0.252	0.0748	2.0906	0.1181	2.5355	INCHES
265067	30.8505	-97.8022	0.0157	0.0433	0.8307	0.2362	1.1259	INCHES
268852	30.8850	-97.7972	0.0433	0.0433	0.7008	0.2953	1.0827	INCHES
277204	30.8893	-97.8373	0.063	0.0551	0.5827	0.2874	0.9882	INCHES
279978	30.9062	-97.6716	0.1535	0.0394	1.0591	0.2756	1.5276	INCHES
307593	30.9018	-97.6314	0.3189	0.0236	1.1339	0.252	1.7284	INCHES

Table A.13. Rain totals for the 88D grid points for the September 18-23, 2020 event—Continued

GEO_ID	LAT	LON	9/18/20	9/21/20	9/22/20	9/23/20	TOTAL	UNITS
312628	30.8629	-97.5965	0.189	0.0118	1.2559	0.1339	1.5906	INCHES
354401	30.8117	-97.7672	0.0197	0.0433	1.0079	0.2913	1.3622	INCHES
372021	30.7685	-97.6922	0.0984	0.0591	1.7244	0.1772	2.0591	INCHES
378309	30.8718	-97.6767	0.2126	0.0354	1.2047	0.2913	1.744	INCHES
387424	30.9707	-97.6210	0.252	0	0.9016	0.3937	1.5473	INCHES
388864	30.9107	-97.7117	0.0394	0.0197	0.9173	0.2874	1.2638	INCHES
389640	30.9451	-97.7066	0.0433	0	0.8701	0.3386	1.252	INCHES
399079	30.8548	-97.8424	0.0236	0.0748	0.7047	0.2402	1.0433	INCHES
422041	31.0307	-97.5301	0.752	0.0315	1.1535	0.5079	2.4449	INCHES
424218	30.8247	-97.8875	0.0945	0.0354	0.6693	0.2205	1.0197	INCHES
478026	30.9962	-97.5354	0.6929	0.0512	1.0827	0.4528	2.2796	INCHES
507289	30.8329	-97.6418	0.1339	0.0236	1.3898	0.1693	1.7166	INCHES
513543	30.7903	-97.8925	0.0591	0.0433	0.752	0.1929	1.0473	INCHES
514429	30.9318	-97.5861	0.3071	0.0433	1.1535	0.2362	1.7401	INCHES
538879	30.8161	-97.8073	0	0.0394	0.7913	0.2283	1.059	INCHES
539561	31.0052	-97.6158	0.1378	0.0512	1.0039	0.4724	1.6653	INCHES
544185	30.7860	-97.8524	0.0157	0.0512	0.8465	0.189	1.1024	INCHES
556304	30.8592	-97.8825	0.1575	0.0709	0.5315	0.2362	0.9961	INCHES
559170	30.8204	-97.8474	0.0354	0.0394	0.7283	0.2165	1.0196	INCHES
560097	30.7816	-97.8124	0.0433	0.063	0.9567	0.1969	1.2599	INCHES
564547	30.7773	-97.7723	0.1378	0.0551	1.1024	0.1811	1.4764	INCHES
565744	30.9572	-97.5004	0.5315	0.063	1.1142	0.2362	1.9449	INCHES
581938	30.8073	-97.7271	0.0709	0.0551	1.2638	0.3268	1.7166	INCHES
609938	30.9273	-97.5459	0.5315	0.0433	1.3189	0.1929	2.0866	INCHES

Table A.14. Rain totals for the 88D grid points for the October 24-29, 2020 event.

GEO_ID	LAT	LON	10/24/20	10/26/20	10/27/20	10/28/20	10/29/20	TOTAL	UNITS
8443	30.7385	-97.7373	0.3071	0.0709	0.0118	0.1732	0.0157	0.5787	INCHES
30536	30.9752	-97.6612	0.0827	0.1535	0.1339	0.1535	0.0157	0.5393	INCHES
43466	30.8418	-97.7220	0.1339	0.0591	0.0197	0.1417	0.0118	0.3662	INCHES
43523	30.9150	-97.7519	0.1417	0.0787	0.0906	0.1811	0.0236	0.5157	INCHES
59326	30.9362	-97.6262	0.0748	0.0827	0.1575	0.1929	0.0394	0.5473	INCHES
61929	30.8461	-97.7621	0.1772	0.063	0.0512	0.1772	0.0118	0.4804	INCHES
63885	30.8373	-97.6819	0.1024	0.0709	0.0197	0.1496	0.0197	0.3623	INCHES
73302	30.9662	-97.5808	0.0945	0.0591	0.1496	0.2559	0.0394	0.5985	INCHES
98720	30.8973	-97.5913	0.0906	0.0433	0.1181	0.2126	0.0591	0.5237	INCHES
122207	30.8762	-97.7169	0.1181	0.0591	0.0433	0.1339	0.0039	0.3583	INCHES
154077	30.8029	-97.6870	0.0984	0.0591	0	0.1496	0.0197	0.3268	INCHES
165670	30.9617	-97.5406	0.122	0.0984	0.122	0.2126	0.0433	0.5983	INCHES
195800	30.9407	-97.6664	0.0827	0.1142	0.0945	0.1417	0.0236	0.4567	INCHES
206081	30.8806	-97.7570	0.1811	0.0591	0.063	0.1417	0.0197	0.4646	INCHES
219192	31.0007	-97.5756	0.1417	0.1102	0.1693	0.2756	0.0394	0.7362	INCHES
233427	30.7641	-97.6521	0.1102	0.0315	0.0197	0.1417	0.0236	0.3267	INCHES
234955	30.7729	-97.7322	0.2008	0.0551	0.0118	0.1772	0.0118	0.4567	INCHES
235217	30.9917	-97.4951	0.1417	0.1732	0.1299	0.1811	0.0591	0.685	INCHES
241487	30.8673	-97.6366	0.0945	0.063	0.0748	0.1614	0.0433	0.437	INCHES
253562	30.7985	-97.6470	0.0394	0.0315	0.0236	0.1535	0.0512	0.2992	INCHES
265023	30.7341	-97.6973	0.189	0.1024	0	0.122	0.0236	0.437	INCHES
265067	30.8505	-97.8022	0.189	0.0709	0.0551	0.2126	0.0157	0.5433	INCHES
268852	30.8850	-97.7972	0.1614	0.0984	0.0709	0.1732	0.0236	0.5275	INCHES
277204	30.8893	-97.8373	0.1693	0.122	0.0512	0.2402	0.0236	0.6063	INCHES
279978	30.9062	-97.6716	0.1142	0.0984	0.063	0.1575	0.0039	0.437	INCHES
307593	30.9018	-97.6314	0.1024	0.0709	0.1102	0.1929	0.0394	0.5158	INCHES

Table A.14. Rain totals for the 88D grid points for the October 24-29, 2020 event—Continued

GEO_ID	LAT	LON	10/24/20	10/26/20	10/27/20	10/28/20	10/29/20	TOTAL	UNITS
312628	30.8629	-97.5965	0.0709	0.0433	0.0906	0.2598	0.0709	0.5355	INCHES
354401	30.8117	-97.7672	0.1181	0.0748	0.0236	0.189	0.0157	0.4212	INCHES
372021	30.7685	-97.6922	0.1929	0.0551	0	0.1417	0.0197	0.4094	INCHES
378309	30.8718	-97.6767	0.0827	0.0906	0.0433	0.1575	0.0197	0.3938	INCHES
387424	30.9707	-97.6210	0.0827	0.1142	0.1575	0.2323	0.0197	0.6064	INCHES
388864	30.9107	-97.7117	0.1299	0.0748	0.0433	0.1339	0.0039	0.3858	INCHES
389640	30.9451	-97.7066	0.1142	0.1024	0.0906	0.0984	0.0157	0.4213	INCHES
399079	30.8548	-97.8424	0.2559	0.1024	0.0591	0.2283	0.0118	0.6575	INCHES
422041	31.0307	-97.5301	0.1693	0.1496	0.1575	0.2559	0.0394	0.7717	INCHES
424218	30.8247	-97.8875	0.252	0.0551	0.0906	0.3504	0.0118	0.7599	INCHES
478026	30.9962	-97.5354	0.1614	0.1535	0.1575	0.2362	0.0433	0.7519	INCHES
507289	30.8329	-97.6418	0.0748	0.0433	0.0551	0.1772	0.0394	0.3898	INCHES
513543	30.7903	-97.8925	0.1614	0.0157	0.1024	0.3386	0.0118	0.6299	INCHES
514429	30.9318	-97.5861	0.0748	0.0512	0.1535	0.2559	0.0433	0.5787	INCHES
538879	30.8161	-97.8073	0.0709	0.0787	0.0512	0.2362	0.0315	0.4685	INCHES
539561	31.0052	-97.6158	0.1181	0.1142	0.1496	0.1811	0.0315	0.5945	INCHES
544185	30.7860	-97.8524	0.2008	0.063	0.0551	0.252	0.0118	0.5827	INCHES
556304	30.8592	-97.8825	0.3858	0.0512	0.0945	0.3583	0.0118	0.9016	INCHES
559170	30.8204	-97.8474	0.1811	0.0945	0.0512	0.2205	0.0157	0.563	INCHES
560097	30.7816	-97.8124	0.1969	0.063	0.0433	0.2283	0.0157	0.5472	INCHES
564547	30.7773	-97.7723	0.2126	0.0787	0.0394	0.2165	0.0118	0.559	INCHES
565744	30.9572	-97.5004	0.1496	0.1339	0.1102	0.1614	0.063	0.6181	INCHES
581938	30.8073	-97.7271	0.1142	0.0551	0.0236	0.1772	0.0118	0.3819	INCHES
609938	30.9273	-97.5459	0.1496	0.0748	0.1024	0.2402	0.0591	0.6261	INCHES

APPENDIX B

Modeling Base Flow and Stream Flow by Dr. Jane L. Harvill

Introduction

The primary goal of our analysis is to quantify the effect of rainfall at each of the 50 stations on each of stream flow and base flow at USGS~Gage #08104300, located in the Salado Creek Basin and determine the importance of each station to the measured stream flow and base flow. Figure B.1 contains a time plot of the average rainfall across all stations in the basin from February 1, 2020 through May 6, 2020 with stream flow and base flow superimposed. In this plot, it was noted that the response of stream flow and base flow is not solely influenced by the total rainfall. For example, the rainfall event that occurs between Feb. 11-13, 2020 is one with the largest amount of rainfall for the time considered in this plot. However, base flow and stream flow responded very little, relative to their response to the rainfall event on March 5, 2020 – a rainfall event with much less rainfall. Based on this observation, we attempted to find a proxy measure that could be used to model this phenomenon.

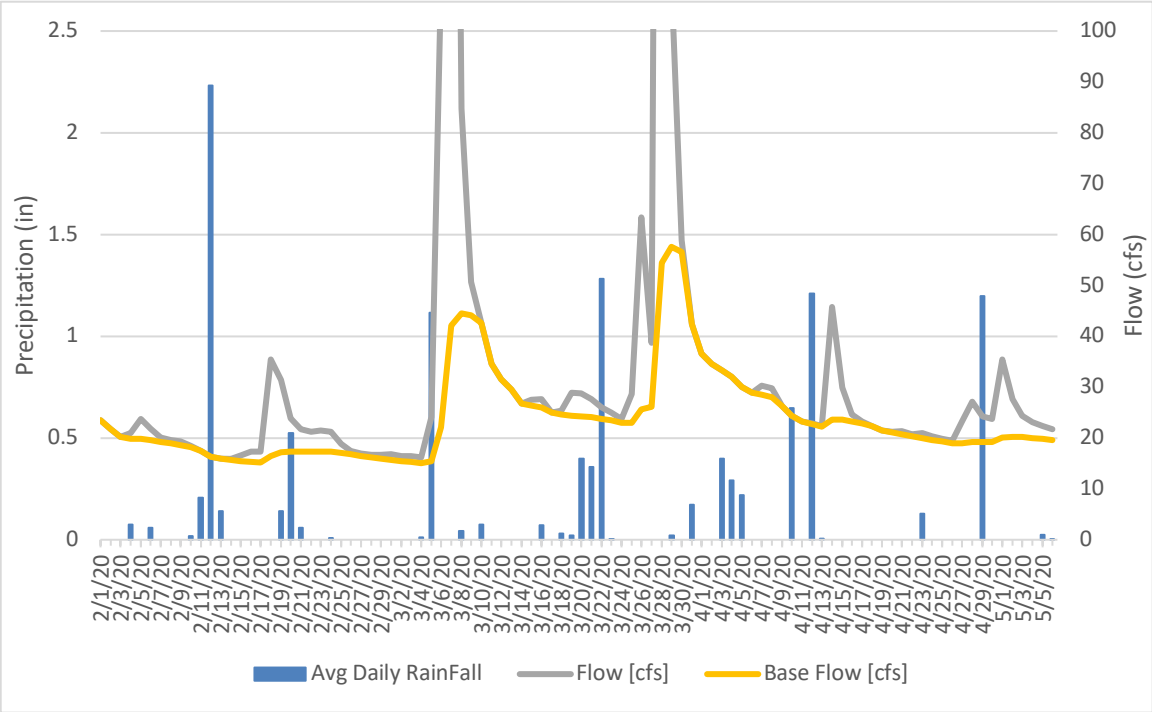

Figure B.1. Plot of average rainfall for rain events (vertical bars) from February 1, 2020 through May 6, 2020 at Salado Creek Basin. The gray line is the measured stream flow, and the yellow line is the measured base flow.

Stillhouse Hollow Surface Elevation

Stillhouse Hollow Lake is a U.S. Army Corp of Engineers reservoir on the Lampasas River in the Brazos River Basin, about five miles from Belton, Texas, and is close to the Salado Creek Basin. Figure B.2 is a graph of the surface elevation (in feet) for the same dates as shown in Figure B.1. A comparison of these two graphs seems to indicate that higher surface elevations correspond to more extreme responses in stream flow and base flow. In an attempt to numerically account for the larger system that is contributing to this behavior in stream flow and base flow, Stillhouse Hollow Lake surface elevation was used as a proxy.

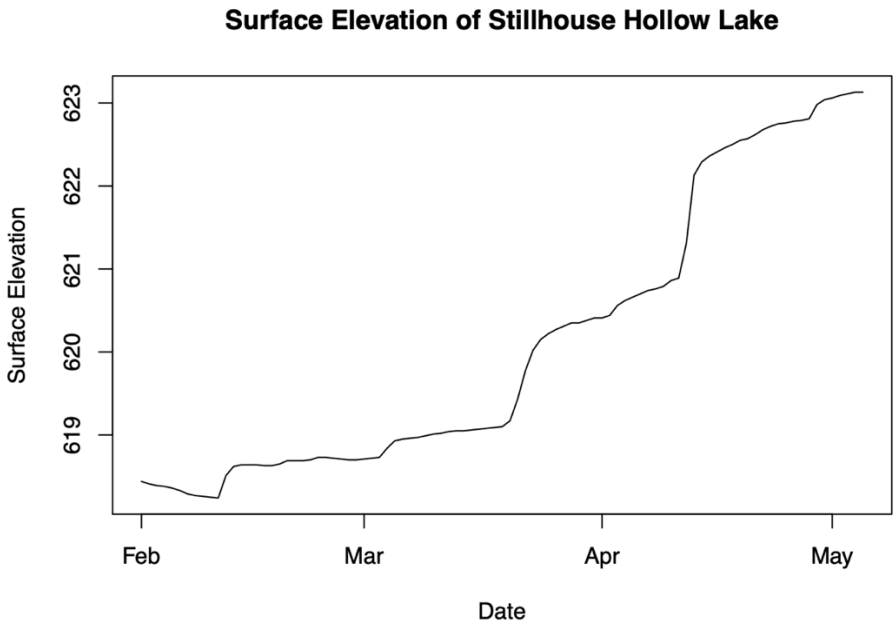

Figure B.2. Plot daily surface elevation of Stillhouse Hollow Lake from February 1, 2020 through May 6, 2020.

Baseflow and Surface Elevation

A preliminary analysis of the relationship between surface elevation and base flow indicated that a transformation of base flow to the natural logarithm of base flow would provide better statistical properties. A simple linear regression was used to model that relationship. The first day in this analysis is September 1, 2019 and the last day is January 25, 2021. We note that the correlation between the two variables r = 0.5927 is a moderately strong correlation.

```
#
#  Correlation between the natural logarithm of base flow and surface elevation.
#
cor(log(Base_Flow), Surface_Elevation)
```

```
## [1] 0.5926546
```

```
#
#  Summary of regression of natural logarithm of base flow on surface elevation
#
summary(fit_baseflow)
```

```
##
## Call:
## lm(formula = log(Base_flow) ~ Surface_Elevation, data = data_step1)
##
## Residuals:
##      Min       1Q   Median       3Q      Max
## -1.64275 -0.60934  0.08339  0.48140  2.95744
##
## Coefficients:
##                     Estimate Std. Error t value Pr(>|t|)
## (Intercept)       -68.378570   3.299446  -20.72   <2e-16 ***
## Surface_Elevation   0.114765   0.005297   21.67   <2e-16 ***
## ---
## Signif. codes:  0 '***' 0.001 '**' 0.01 '*' 0.05 '.' 0.1 ' ' 1
##
## Residual standard error: 0.7198 on 867 degrees of freedom
## Multiple R-squared:  0.3512, Adjusted R-squared:  0.3505
## F-statistic: 469.4 on 1 and 867 DF,  p-value: < 2.2e-16
```

The extremely small p-value for Surface_Elevation (of $< 2 \times 10^{-16}$) implies a very significant relationship between the surface elevation of Stillhouse Hollow Lake and the natural logarithm of base flow. The value of $R^2 = 0.3512$ can be interpreted as "35.12% of the variation in the natural logarithm of base flow from its mean is explained by the regression on the surface elevation of Stillhouse Hollow Lake."

Because of the strong numerical relationship between the lake's surface elevation and base flow, the re-scaled residuals from the regression are used in the remainder of the analysis for the effect of rainfall on base flow. The idea of considering residuals from the regression is a way of removing the effect of the (proxy) surface level on base flow, allowing us to more directly explore the effect of rainfall on base flow. The graph in Figure B.1 also suggests that the impact on base flow of rainfall changes for several days after the rain event. For each of the 50 sensors, the model in equation (1) was fit:

$$e_d = \beta_0 + \beta_1 x_d + \beta_2 x_{d-1} + \beta_2 x_{d-2} + \cdots + \beta_7 x_{d-6} + \varepsilon_d, \quad d = 7, \ldots, 869, \tag{1}$$

where d is the day (beginning on September 7, 2019 through January 25, 2021), e_d is the re-scaled residual from the regression of the lake surface level on the natural logarithm of

base flow, each x_{d-k} is the rainfall at the sensor on day $d - k$, k referred to as the "lag," and the εd are random error terms. For each station, stepwise regression was used to determine the best subset model for describing the residual base flow as a function of lagged values of rainfall for that station. Models could be as small as containing only one x_{d-k}, or could be the full model given in equation (1).

Below the first table contains for each lagged day the number of stations that included that day in the optimal model. We note that day four x_{d-4} is in none of the models. The second table contains the ten stations (of the 50) with the largest multiple correlation coefficient R^2 computed based on the optimal fitted model.

```
#
# Number of stations for which each lagged day was included in the final model.
#
```

```
## .
## Lag_0 Lag_1 Lag_2 Lag_3 Lag_5 Lag_6
##    50    50    45    21    45    37
```

```
## # A tibble: 50 x 2
##    stations r_squared_baseflow
##    <chr>                 <dbl>
##  1 514429                0.385
##  2 73302                 0.382
##  3 539561                0.375
##  4 59326                 0.373
##  5 307593                0.373
##  6 253562                0.370
##  7 387424                0.364
##  8 165670                0.362
##  9 609938                0.361
## 10 98720                 0.359
## # ... with 40 more rows
```

Figure B.3 is a bar chart. For each station (represented on the horizontal axis), the value of R^2 from regressing the re-scaled residuals on the optimal number of lagged days is plotted from order of largest R^2 to smallest R^2 for all fifty stations.

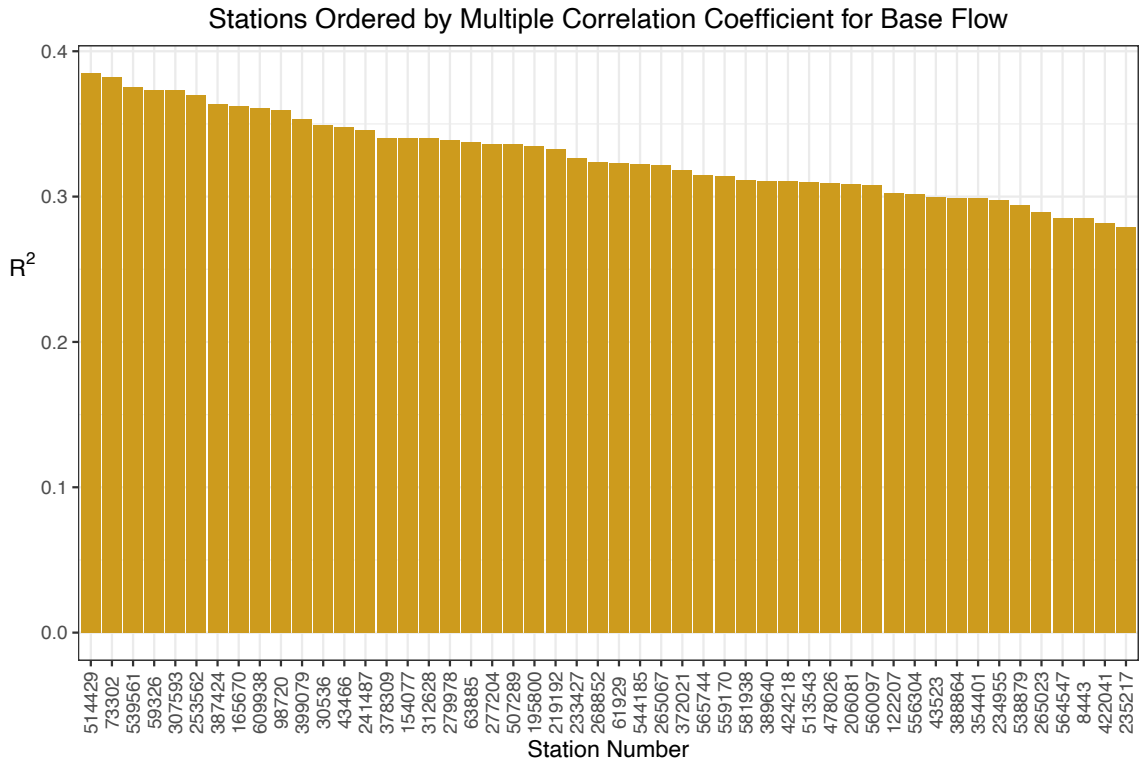

Figure B.3. Stations plotted by decreasing values of R^2 for regression of re-scaled residuals based on base flow for optimal model of lagged days of rainfall for each station.

Streamflow and Surface Elevation

A similar analysis for stream flow was conducted. A preliminary analysis of the relationship between surface elevation and stream flow indicated that a natural logarithm transformation of stream flow would provide better statistical properties. A simple linear regression was used to model that relationship. The first day in this analysis is September 1, 2019 and the last day is January 25, 2021. We note that the correlation between the two variables r = 0.5203 is a moderately strong correlation.

```
#
#  Correlation between the natural logarithm of stream flow and surface elevation.
#
cor(log(Stream_Flow), Surface_Elevation)
```

```
## [1] 0.5202961
```

```
#
#  Summary of regression of natural logarithm of stream flow on surface elevation
#
summary(fit_streamflow)
```

```
##
## Call:
## lm(formula = log(Stream_flow) ~ Surface_Elevation, data = data_step1)
##
## Residuals:
##     Min      1Q  Median      3Q     Max
## -1.8396 -0.6201  0.0216  0.4493  5.1336
##
## Coefficients:
##                     Estimate Std. Error t value Pr(>|t|)
## (Intercept)       -63.474375   3.722514  -17.05   <2e-16 ***
## Surface_Elevation   0.107213   0.005976   17.94   <2e-16 ***
## ---
## Signif. codes:  0 '***' 0.001 '**' 0.01 '*' 0.05 '.' 0.1 ' ' 1
##
## Residual standard error: 0.8121 on 867 degrees of freedom
## Multiple R-squared:  0.2707, Adjusted R-squared:  0.2699
## F-statistic: 321.8 on 1 and 867 DF,  p-value: < 2.2e-16
```

The extremely small p-value for Surface_Elevation (of $< 2 \times 10^{-16}$) implies a very significant relationship between the surface elevation of Stillhouse Hollow Lake and the natural logarithm of stream flow. The value of $R^2 = 0.2707$ can be interpreted as "27.07% of the variation in the natural logarithm of stream flow from its mean is explained by the regression on the surface elevation of Stillhouse Hollow Lake."

Because of the strong numerical relationship between the lake's surface elevation and stream flow, the re-scaled residuals from the regression are used in the remainder of the analysis for the effect of rainfall on stream flow. As with base flow, we note that the graph in Figure B.1 suggests that the impact on stream flow of rainfall changes for several days after the rain event. For each of the 50 sensors, the model in equation (1) was fit. The

variables in the model are similarly defined, with the exception that e_d is now the re-scaled residual from the regression of the lake surface level on the natural logarithm of stream flow. The table below gives the number of stations having that lag as being included in a model to describe the residual stream flow and rainfall. Then for each station, stepwise regression was used to determine the best subset model for describing stream flow as a function of lagged values of rainfall for that station. Models could be as small as containing only one x_{d-k}, or could be the full model given in equation (1).

Below the first table contains for each lagged day the number of stations that included that day in the optimal model. We note that days three x_{d-3} and six x_{d-6} are in none of the models. The second table contains the ten stations (of the 50) with the largest the multiple correlation coefficient R^2 was computed based on the optimal fitted model.

```
#
# Number of stations for which each lagged day was included in the final model.
#
```

```
## .
## Lag_0 Lag_1 Lag_2 Lag_4 Lag_5
##    50     8    28    29    42
```

```
## # A tibble: 50 x 2
##    stations r_squared_streamflow
##    <chr>                   <dbl>
##  1 514429                  0.565
##  2 253562                  0.565
##  3 59326                   0.559
##  4 73302                   0.557
##  5 98720                   0.557
##  6 609938                  0.555
##  7 307593                  0.555
##  8 312628                  0.549
##  9 241487                  0.548
## 10 378309                  0.536
## # ... with 40 more rows
```

Figure B.4 is a bar chart. For each station (represented on the horizontal axis), the value of R^2 from regressing the re-scaled residuals on the optimal number of lagged days is plotted from order of largest R^2 to smallest R^2 for all fifty stations.

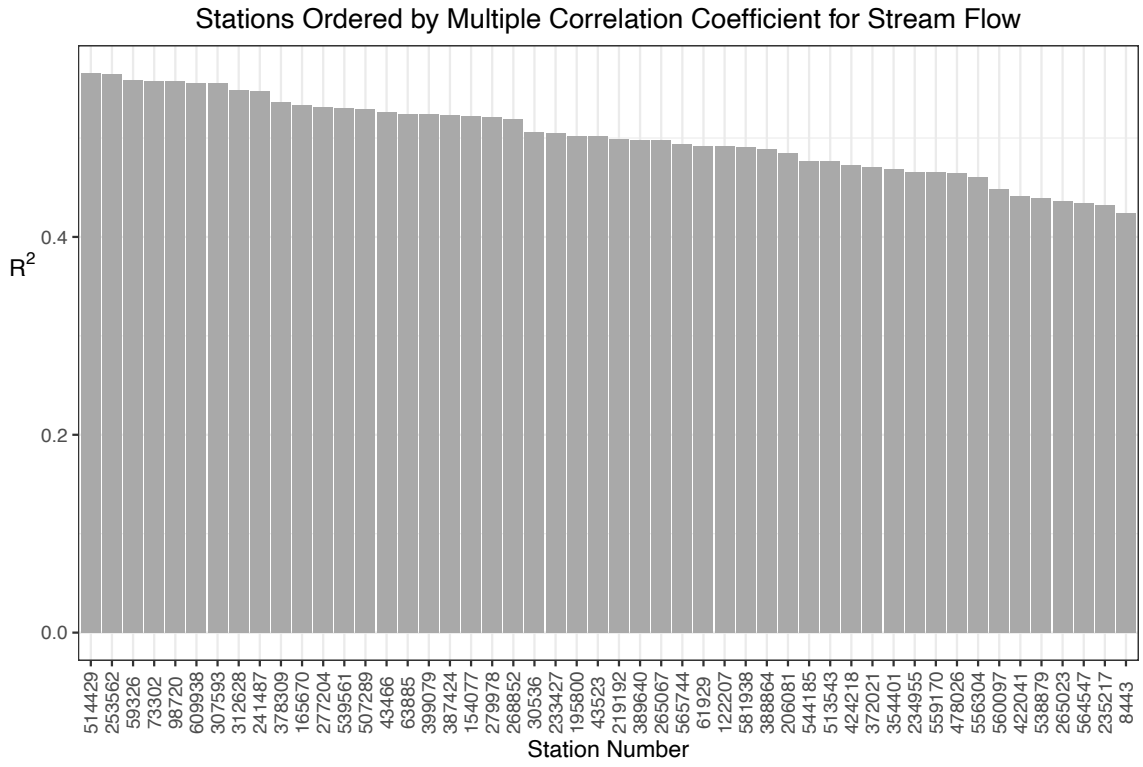

Figure B.4. Stations plotted by decreasing values of R^2 for regression of re-scaled residuals based on streamflow for optimal model of lagged days of rainfall for each station.

APPENDIX C

Isotopic Composition During Precipitation Events

Table C.1. Isotopic composition of Salado Creek, Big Boiling Spring, and precipitation samples from July 2020 to January 2021.

Sample ID	Date	Sample	$\delta^{18}O$ VSMOW	δD VSMOW
20200720 scr 1412	7/20/20	Salado Creek	-4.42	-30.69
20200720 big 1419	7/20/20	Big Boiling	-4.66	-32.05
20200724 scr 1607	7/24/20	Salado Creek	-4.24	-29.02
20200724 big 1611	7/24/20	Big Boiling	-4.61	-28.12
20200726 rain 1518	7/26/20	Precipitation	-1.62	-2.93
20200728 scr 1043	7/28/20	Salado Creek	-3.68	-24.30
20200728 big 1046	7/28/20	Big Boiling	-4.26	-26.18
20200825 scr 1700	8/25/20	Salado Creek	-4.01	-23.85
20200825 big 1707	8/25/20	Big Boiling	-4.20	-23.31
20200901 scr 1645	9/1/20	Salado Creek	-4.15	-24.42
20200901 big 1650	9/1/20	Big Boiling	-4.30	-25.36
20200902 rain 0800	9/2/20	Precipitation	-6.12	-35.62
20200905 rain 0855	9/5/20	Precipitation	-4.31	-20.54
20200905 rain 1600	9/5/20	Precipitation	-5.79	-32.14
20200907 scr 1110	9/7/20	Salado Creek	-4.01	-22.25
20200907 big 1115	9/7/20	Big Boiling	-4.42	-25.52
20200910 rain 0805	9/10/20	Precipitation	-3.29	-9.58
20200912 big 1610	9/12/20	Big Boiling	-4.18	-23.98
20200912 scr 1605	9/12/20	Salado Creek	-2.82	-22.22
20200919 scr 1920	9/19/20	Salado Creek	-3.87	-22.22
20200919 big 1927	9/19/20	Big Boiling	-4.34	-26.64
20200922 rain 1525	9/22/20	Precipitation	-5.95	-33.47
20200924 scr 1832	9/24/20	Salado Creek	-3.32	-21.19
20200924 big 1838	9/24/20	Big Boiling	-4.21	-23.57
20200928 big 0800	9/28/20	Big Boiling	-4.14	-27.00
20200928 scr 0805	9/28/20	Salado Creek	-3.19	-20.10
20201012 big 1140	10/12/20	Big Boiling	-4.18	-26.11
20201023 big	10/23/20	Big Boiling	-4.67	-24.41
20201023 scr	10/23/20	Salado Creek	-3.85	-18.08

Table C.1. Isotopic composition of Salado Creek, Big Boiling Spring, and precipitation samples from July 2020 to January 2021—Continued

Sample ID	Date	Sample	$\delta^{18}O$ VSMOW	δD VSMOW
20201026 rain	10/26/20	Precipitation	-2.57	0.24
20201027 rain	10/27/20	Precipitation	-4.95	-16.59
20201101 big	11/1/20	Big Boiling	-4.76	-25.76
20201101 scr	11/1/20	Salado Creek	-3.29	-18.87
20201228 bb-1	12/28/20	Big Boiling	-3.29	-18.18
20201228 sc-1	12/28/20	Salado Creek	-4.46	-21.41
20201230 pre-1	12/30/20	Precipitation	-1.71	3.67
20201230 pre-2	12/30/20	Precipitation	-3.16	-11.87
20201231 pre-3	12/31/20	Precipitation	-8.10	-52.07
20201231 pre-4	12/31/20	Precipitation	-7.29	-42.53
20210101 pre-5	1/1/21	Precipitation	-7.51	-42.92
20210104 bb-2	1/4/21	Big Boiling	-4.17	-26.68
20210104 sc-2	1/4/21	Salado Creek	-3.37	-21.91

BIBLIOGRAPHY

Abbott, P. L. (1975). On the hydrology of the Edwards Limestone, south-central Texas. *Journal of Hydrology*. v. 24. p. 251-269.

Alexander, S.C., Luhmann, A.J., Alexander Jr, E.C., Green, J.A., and Peters, A.J. (2008). Spring Characterization Methods & Springshed Mapping. 11th Multidisicplinary Conference on Sinkholes and the Engineering and Environmental Impact of Karst. *American Society of Civil Engineers*.

Baker, E.T., Jr., Slade, R.M., Jr., Dorsey, M.E., Ruiz, L.M., and Duffin, G.L. (1986). Geohydrology of the Edwards Aquifer in the Austin area, Texas. Texas Water Development Board, Report 293.

Boghici, R. (2003). A Field Manual for Groundwater Sampling. *Texas Water Development Board*. User Manual 51.

Brune, G. M. (1981). *Springs of Texas* (Vol. 1): Fort Worth, Branch-Smith.

Brune, G., and Duffin, G. L. (1983). Occurrence, availability, and quality of groundwater in Travis County, Texas. *Texas Department of Water Resources*. Report 276. p. 219.

Budge, T. J. (2008). Delineating contributing areas for karst springs using NEXRAD data and cross-correlation analysis. Ph.D. Dissertation. Jackson School of Geosciences, University of Texas at Austin.

Cooper, H.H., and Jacob, C.E. (1946). A generalized graphical method for evaluating formation constants and summarizing well history: *Transactions of the American Geophysical Union*. v. 2. p. 526-534.

Dahl, S.L. (1990). Hydrogeology and Stream Interactions of the Edwards Aquifer in the Salado Creek Basin, Bell and Williamson Counties, Central Texas. Unpublished Masters Thesis, Baylor University, Waco, Texas.

Dansgaard, W. (1964). Stable isotopes in precipitation: Tellus. v. 16. p. 436-468.

De La Garza, L. and Slade, R.M., Jr. (1987). Relations between areas of high transmissivity and lineaments for part of the northern Edwards aquifer – a preliminary study, *in* Yelderman, Joe C., Jr., Slade, Raymond M., Jr., Sharp, John M., Jr., and Woodruff, Charles M., Jr., coordinators, Hydrogeology of the Edwards aquifer in the Northern Balcones and Washita Prairie Segments, South Central G.S.A, Baylor Univ., Waco, Texas.

Duffin, G., and Musick, S. P. (1991). Evaluation of Water Resources in Bell, Burnet, Travis, Williamson and parts of adjacent counties, Texas. *Texas Water Development Board*, Report 326.

Eckhoff, I. J. (2016). Geologic and Geochemical Characterization of Cross-Communication Potential within the Northern Edwards Aquifer System, Texas. Electronic Theses and Dissertations. 59.

Fetter, C.W. (2001). Applied Hydrogeology, 4th ed. Waveland Press.

Fulton, R.A., Breidenbach, J.P., Seo, D., Miller, D.A., and O'Bannon, T. (1998). The WSR- 88D rainfall algorithm: Weather and Forecasting. v. 13, p. 377–395.

Gary, M.O., Hunt, B.B., Smith, B.A., Watson, J.A., and Wierman, D.A. (2019) Evaluation for the Development of a Jacob's Well Groundwater Management Zone Hays County, Texas. Technical Report prepared for the Hays Trinity Groundwater Conservation District, Hays County, Texas. Meadows Center for Water and the Environment, Texas State University at San Marcos, TX. Report: 2019-05. July 2019. 58 p.

Hovorka, S., Mace, R., and Collins, E. (1998). Permeability structure of the Edwards Aquifer, south Texas—Implications for aquifer management: Texas Bureau of Economic Geology Report of Investigations 250, Austin. p. 55.

Ingraham, N.L. (1998). Isotopic variations in precipitation. In: Kendall, C., McDonnell, J. (Eds.). Isotope Tracers in Catchment Hydrology. Elsevier. Amsterdam. p. 87–118.

Interstate 35 Corridor Advisory Committee (I-35 CAC). (2011). I-35 Corridor Advisory Committee Plan. *http://ftp.dot.state.tx.us/pub/txdot-info/my35/advisory_plan.pdf*

IAEA/WMO. (2021). Global Network of Isotopes in Precipitation. The GNIP Database. Accessible at: *http://www.iaea.org/water*

Jones, I. C. (2003). Groundwater Availability Model: Northern Segment of the Edwards Aquifer, Texas. *Texas Water Development Board*.

Jones, I.C. (2019). The Northern Segment of the Edwards (Balcones Fault Zone) Aquifer, in Sharp, J.M., Jr., Green, R.T., and Schindel, G.M., eds. The Edwards Aquifer: The Past, Present, and Future of a Vital Water Resource: Geological Society of America Memoir 215. p. 119-130.

Jones, I. C. (2020). Conceptual Model: Northern Segment of the Edwards (Balcones Fault Zone) and Associated Trinity Aquifers of Texas. *Texas Water Development Board*. Draft.

Keester, M.R. and Konetchy, B. (2017). Statistical Evaluation of Edwards Aquifer Water Levels, Pumping, and Springflow. LBG-Guyton Associates, report prepared for Clearwater Underground Water Conservation District.

Kovacs, J. (1983). Practical application of continuum approach to characterize the porosity of carbonate rocks, *in* methods and instrumentation for the investigation of groundwater systems. Committee for hydrological research. TNO.

Kreitler, C. W., Senger, R. K., and Collins, E. W. (1987). Geology and hydrology of the northern segment of the Edwards aquifer with an emphasis on the recharge zone in the Georgetown, Texas area: *Bureau of Economic Geology*. Unpublished report, contract number IAC (86-87)-1046.

Lim, K. J., Engel, B. A., Tang, Z., Choi, J., Kim, K. S., Muthukrishnan, S., and Tripathy, D. (2005). Automated web GIS based hydrograph analysis tool, WHAT 1. *JAWRA Journal of the American Water Resources Association*, 41(6), 1407-1416.

Mahler, B. J., Bennett, P. C., and Zimmerman, M. (1998). Lanthanide-labeled clay: A new method for tracing sediment transport in karst. *Groundwater*. Vol. 36, No. 5. p. 835-843.

Meinikmann, K., Lewandowski, J., and Nützmann, G. (2013). Lacustrine groundwater discharge: Combined determination of volumes and spatial patterns. *Journal of Hydrology*, *502*, 202-211.

Mook, W. G., and Rozanski, K. (2000). Environmental isotopes in the hydrological cycle. *IAEA Publish*. v. IV, no. 39.

Rose, P.R. (1972). Edwards Ground, surface and subsurface, Central Texas: The University of Texas at Austin, Bureau of Economic Geology Report of Investigations No. 74. p. 198.

Schwartz, F., and Zhang, H. (2003). Fundamentals of Groundwater. Chichester: J. Wiley.

Senger, R.K., Collins, E.W., and Kreitler, C.W. (1990). Hydrogeology of the northern segment of the Edwards aquifer, Austin region: The University of Texas at Austin, Bureau of Economic Geology, Report of Investigations No. 192.

Sharp, Z. (2017). Principles of stable isotope geochemistry.

Smith, B.A., and Hunt. B.B. (2010). A comparison of the 1950s drought of record and the 2009 drought, Barton Springs segment of the Edwards Aquifer, Central Texas. Gulf Coast Association of Geological Societies Transactions. v. 60. p. 611-622.

Smith, B.A., Hunt, B.B., and Johnson, S.B. (2012). Revisiting the Hydrologic Divide Between the San Antonio and Barton Springs Segments of the Edwards Aquifer: Insights from Recent Studies: *Gulf Coast Association of Geological Societies Journal*. Vol. 1, 62nd Annual Convention, October 21-24, 2012, Austin, TX. https://bseacd.org/uploads/Smith_2012-GCAGS-Journal.pdf

Stamm, J. F., Poteet, M. F., Symstad, A. J., Musgrove, M., Long, A. J., Mahler, B., and Norton, P. A. (2014). Historical and projected climate (1901–2050) and hydrologic response of karst aquifers, and species vulnerability in south-central Texas and western South Dakota. *US Geological Survey*. No. 2014-5089.

Texas Water Development Board. Groundwater Conservation District Facts: TWDB. Accessed March 2021.

Tucker, D.R. (1962). Subsurface Lower Cretaceous stratigraphy, Central Texas: University of Texas, Austin. Ph.D. dissertation.

United States Census Bureau. (2021). State and County QuickFacts. *https://www.census.gov/quickfacts/fact/table/TX,bellcountytexas,US/PST120219*. *Last accessed 16 March 2021.*

Wong, S. and Yelderman, J.C., Jr. (2015, 2016, 2017). An Investigation into the Recharge Pathways and Mechanisms in the Northern Segment of the Edwards Aquifer, Bell County, Texas (Phase I, Phase II, Phase III): Waco, Texas. Baylor University, Department of Geology, research report prepared for Clearwater Underground Water Conservation District.

Woodruff, C. M., Jr., and Abbott, P. L. (1979). Drainage-basin evolutation and aquifer development in a karstic limestone terrain, south – central Texas, U.S.A.: *Earth Surface Processes*. v. 4, p. 319-334.

Woodruff, C. M., Jr., Snyder, F., De La Garza, L., and Slade, R. M., Jr., (eds.). (1985). Edwards Aquifer – Northern segment, Travis, Williamson, and Bell Counties, Texas: *Austin Geological Society*. Guidebook 8.

Yelderman, J.C., Jr. (2013). Hydrogeology of the Northern Segment of the Edwards Balcones Fault Zone Aquifer in the Salado Creek Basin and Environs; a current understanding. Baylor University, Department of Geology.

Yelderman, J.C., Jr. Slade, R.M., Jr., Sharp, J.M., Jr., and Woodruff, C.M., Jr. (1987). Hydrogeology of the Edwards Aquifer, northern Balcones and Washita Prairie segments: *Austin Geological Society*. Guidebook 11.

Young, K., Grunig, D., Jordan, M. A., Parker, D. F., and Williams, B. (1977). Guidebook to the Geology of Travis County: Student Geological Society. *The University of Texas, Austin*.